IONIC LIQUIDS WITH AND WITHOUT TRANSITION METAL NANOPARTICLES FOR ADVANCED HEAT TRANSFER FLUIDS AND CATALYSIS APPLICATIONS.

Virendra Sudam Patil

Dipòsit Legal: T 1459-2015

VIRENDRA SUDAM PATIL

IONIC LIQUIDS WITH AND WITHOUT TRANSITION METAL NANOPARTICLES FOR ADVANCED HEAT TRANSFER FLUIDS AND CATALYSIS APPLICATIONS

DOCTORAL THESIS

SUPERVISED BY

Dr. Chandrashekhar V. Rode

Chemical Engineering and Process Development

CSIR-National Chemical Laboratory, Pune, India.

Dr. Alberto Coronas

Mechanical Engineering Departament

Universitat Rovira i Virgili, Tarragona, Spain

UNIVERSITAT ROVIRA I VIRGILI

Tarragona, Spain. June 2015

UNIVERSITAT
ROVIRA I VIRGILI
DEPARTAMENT D'ENGINYERIA MECÀNICA
Escola Tècnica Superior d'Enginyeria Química (ETSEQ).
Av. Països Catalans 26. 43007 Tarragona (Spain)

We state that the present study entitled "Ionic liquids with and without transition metal nanoparticles for advanced heat transfer fluids and catalysis applications" presented by Mr Virendra Sudam Patil for the award of the Degree of Doctor has been carried out under our supervision at the Mechanical Engineering Department of the Rovira I Virgili University and it fulfills all the requirements to be eligible for the International Doctorate Award

Tarragona, June 5, 2015

Doctoral Thesis Supervisors

Dr. Chandrashekhar V. Rode

Dr. Alberto Coronas

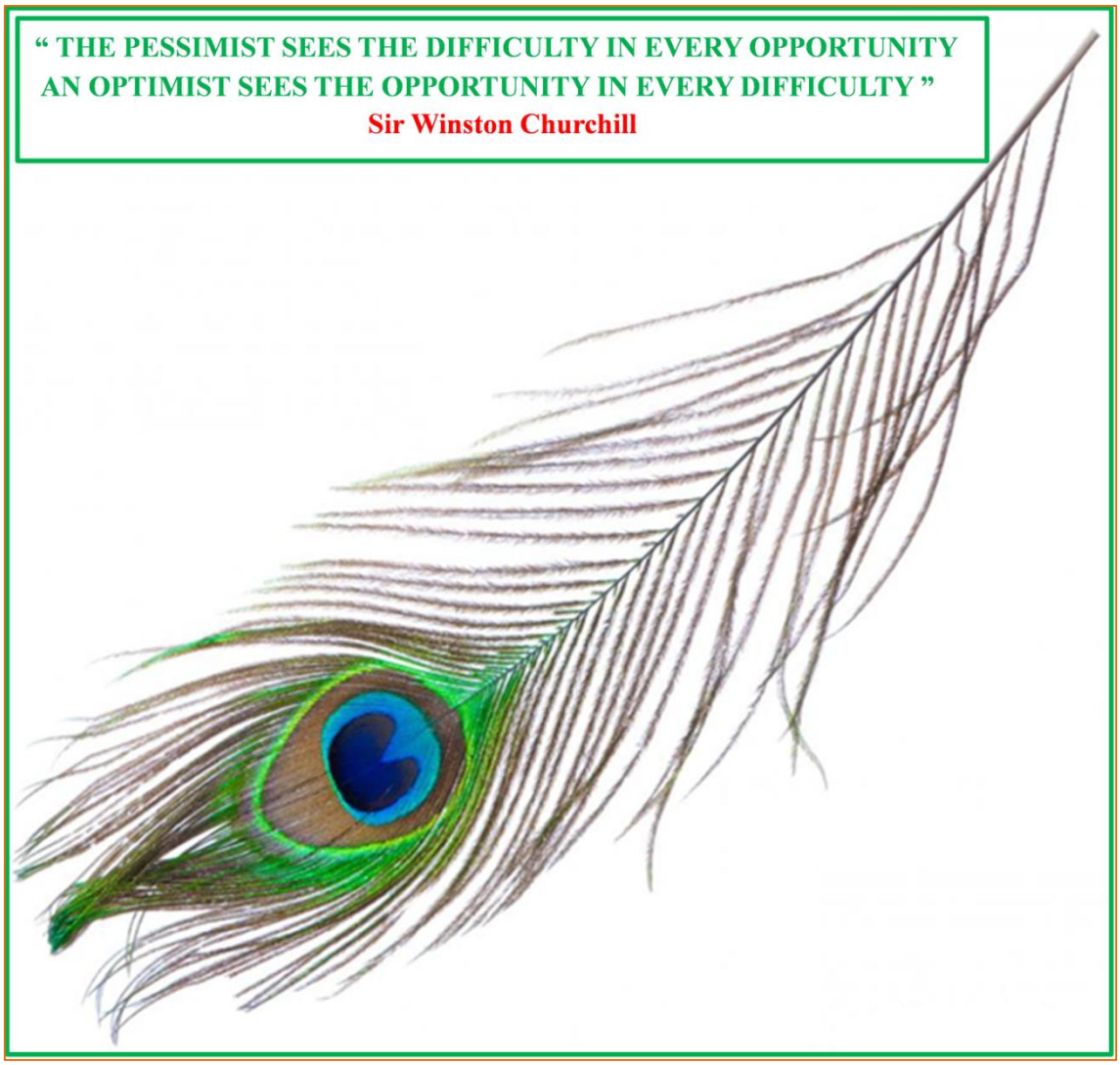

Dedicated to my beloved Parents

ABSTRACT

New generation heat transfer technologies with less energy consumption and improved economy are needed for welfare of the society. In this regard, ionic liquids (ILs) are most investigated fluids due to their higher thermal stability and non-volatile nature which make them more advantageous than the conventional fluids. In addition, dispersion of metal nanoparticles in conventional fluids are also being investigated in recent times due to their higher thermal conductivity, easy flow, which reduce pumping cost as well as no salt sedimentation. These fascinating features make NFs as a good alternative to the conventional salt solutions for heat transfer applications. In this work, imidazolium cation based ILs were prepared with variation in anions such as chloride, bromide, iodide and tetrafluroborate. Thermal properties as well as density and viscosity of these fluids were investigated in detail.

Nevertheless, in case of such fluids mainly, thermal conductivity and heat capacities have been studied while it is also necessary to study other fluid properties such as density and viscosity which dramatically influence fluid flow through pipes of heat transfer equipment. As there are only a very few reports available on transition metal NPs in ILs for heat transfer applications, this thesis work is focused on first designing the desired ILs and then developing composites of transition metal NPs with the prepared ionic ILs. For this purpose, NPs of ruthenium (Ru) and silver (Ag) were used. Thermal properties of these ILs were improved by in-situ preparation of composites of ILs with ruthenium nanoparticles without using capping agents or surfactants at room temperature. For preparing Ag containing INFs, readily available NPs of Ag with variable morphologies, of 1D, 2 D and 3 D were used. These ionanofluids reduced the viscosity of base ILs along with the enhancement in their thermal conductivity.

Another important aspect of this thesis work comprises the evaluation of the prepared ILs and their composites with transition metal NPs for catalytic applications. As development of new heat transfer fluids contribute to minimizing energy requirement similarly, new materials as catalysts also make the chemical process less energy intensive. From this perspective, carbon supported 5% ruthenium catalyst with Bronsted acidic IL [Hmim][HSO_4] as a co-catalyst was developed for selective hydrogenolysis of bio-derived levulinic acid (LA) to γ-valerolactone (GVL) which is fuel additive. Variation in catalyst activity was successfully correlated with the acidities of ILs studied by Hammet acidity function.

Acknowledgements

I would like to take this opportunity to express a token of gratitude and unimaginable appreciations for the known and unknown support and guidance to achieve one of the goals of my life. It is excellent quoted by *Bo Bennett* about goal. The discipline you learn and character you build from setting and achieving a goal can be more valuable than the achievement of the goal itself. I would like to extend my gratitude and love to all those people who have contributed directly and indirectly for the successful completion of doctoral thesis.

Education is the key to success in life, and teachers make a lasting impact in the lives of their students. I can't express my gratitude towards **Dr. Alberto Coronas** for great opportunity to register a PhD in his group. His undying inspiration, supporting nature, motivation, positive attitude and valuable advices keeps me active. His expertise, guidance valuable comments and knowledge he shared for data analysis, research funds and giving endless help lead to finish my thesis.

I would like acknowledge **Dr. Chandrashekhar Rode** for accepting me as PhD student. His scientific expertise, constructive suggestions, continuous encouragement in the field of catalysis and green chemistry helped me a lot. Friendly atmosphere during the course of my research study developed me to do multiple tasks and make my like more joyful.

As deep respect and love to **Dr. Kashinath Patil** for his undying help available every time. His moral and financial support, multiple opportunities given to me to learn new scientific things has extended my knowledge. His expertise in the field of nanomaterial's synthesis and characterization, important and valuable suggestions during my research, discussions and his kindness and best teaching in innovative way developed me as good student as Albert Einstein said it is the supreme art of the teacher to awaken joy in creative expression and knowledge.

Indeed I appreciate **Dr. Daniel Salavera** for his help in measurements of thermophysical properties, data analysis and his valuable suggestions in need. Not only on professional front but also his help in personal things like accommodation, travelling and medical help shows his kindness. I will never forget his kind and helping nature and pleasant attitude during my PhD tenure.

I am very thankful to **Dr. Carlos Nieto de Castro** for his constant support, deep sense of gratitude, scientific teaching and valuable scientific discussions always provides good direction. His help during my tenure in Lisboa, Portugal is inexpressible.

I would like to thank Dr. Sourav Pal, Director CSIR- NCL, Pune for allow me to carried out part of my doctoral research in CSIR- NCL and providing all infrastructure and facilities of CSIR- NCL. I would like to acknowledge Dr. V. V. Ranade, Chair of CEPD division CSIR-NCL, Pune for divisional facilities required to complete my doctorate research.

I would like to thank scientists belonging to various groups in India, Spain and Portugal. Dr. S. D. Sathaye, Dr. Anil Kumar, Dr. P. N. Joshi, Dr. R. C. Chikate, Dr. Ranjit Hawaldar**,** Dr. Amol Hengne, Dr. Rasika Mane, Dr. Maria Soledad Larrechi, Dr Maria Jose, Dr. Fernando J. V. Santos and Dr. Sohel Murshed, who help me indirectly to complete my thesis.

I have learned silence from the talkative, toleration from the intolerant, and kindness from the unkind; still, strange, I am grateful to those teachers. My immense pleasure to acknowledge Sagar Patil, Babasaheb Waghmode, Narayan Biradar, Suhas Shinde, Sumit Kamble, Sharda Kondawar, Sachin Sakate, Rajan Pandya, Bhanu Singh, Tejansh Chandole, Atul Malawadkar, Rameshwar Swami, Shobha Birajadar, Sagar More, Harish Joshi, Aparna potdar, Sachin Jadkar, Aarti Jadhav, Abhijit Kshirsagar, Andry Cera-manjarres, Maria Isabel Barba, Faisal Asfand, Salome Vieira, Carla Queiros, who are my friends and colleagues worked with me in CSIR-NCL India, CREVER Spain and FCUL Portugal.

I owe my special thanks to all scientist and experts in CMC department CSIR-NCL India, technical staff of facility lab from URV Spain, I would like to specially acknowledge Mr. A. B. Gaikwad for providing me first opportunity to work with him in CMC department CSIR-NCL where I began journey towards my research. I would like to thank Mr. H. M. Raheja and Mrs. Maria Jose Duran for help in document related work from CEPD division CSIR-NCL and Mechanical Engineering Department, URV Spain respectively.

I would like to thank Mr. David Soloman for his technical guidance to work with reactors and the very pleasant person Mr. S. Chinadurai for his time to time help during my tenure in CEPD division CSIR-NCL. I would like to acknowledge all the members and friends from CREVER group URV Spain, Marathi@NCL group from CSIR-NCL India,

Vasundhara Swachata Abhiyan Group Pune, India, for filling my research journey with joy and happiness.

This doctoral thesis work was supported by the FP7-People-2010-IRSES Program (NARILAR -New Working Fluids based on Natural Refrigerants and Ionic Liquids for Absorption Refrigeration, Grant Number 269321).

I can’t even express my love and gratitude in few words towards my parents and my younger brother Mr. Pramod. It was impossible for me to complete my degree without their motivation, help in every situation of my life. Lot of patience to wait for my degree, their unconditional support over these years expresses their deep love and affections towards me.

The completion of this undertaking could not been possible without the participation and assistance of so many people, friends and well-wishers whose names may not all the enumerated. Their contributions are sincerely appreciated and gratefully acknowledged.

CONTRIBUTIONS BY THE AUTHOR

ARTICLES IN PEER REVIEWED ACADEMIC JOURNALS

V. Patil, A. Cera-Manjarres, D. Salavera, C. Rode, K. Patil, C. Nieto di Castro, A. Coronas. Ru-Imidazolium Halide IoNanofluids: Synthesis, structural, morphological and thermophysical properties [Communicated to Journal of Nanofluids 2015]

V. Patil, S. Shinde, A. Coronas, K. Patil, C. Rode. Selective hydrogenation of levulinic acid to γ-valerolactone over ionic liquid assisted Ru/C catalyst [revised Manuscript ID: ie-2015-00894u.R1submitted to I&EC research 2015]

V. Patil, A. Cera-Manjarres, D. Salavera, C. Rode, K. Patil, A. Coronas. Structural and morphological influence of nanoparticles on heat transport properties of silver nanofluids and silver ionanofluids [manuscript under preparation]

PAPERS IN CONGRESSES, CONFERENCES AND WORKSHOPS

V. Patil, K. Patil, C. Rode, A. Coronas. Preparation and characterization of gold nanofluids 2nd International Workshop on Ionic Liquids: Alternative Benign Materials for Renewable Energy and its Applications (WILS 2013). CSIR-NCL Pune, India. 16-17 January 2013. ISBN 84-616-7541-X.

S. Murshed, **V. Patil**, K. Patil, C. Nieto de Castro and A. Coronas. Morphological and structural characterization of ZnO and TiO_2 nanoparticles. Nano Spain Conference, Bilbao Spain. 23-26 April, 2013.

V. Patil, D. Salavera, C. Rode, A. Coronas. Ruthenium-Ionanofluids: density, viscosity and thermal conductivity studies. Congress on Ionic Liquids (COIL-5). Vilamoura, Algarve, Portugal. 21-25 April, 2013.

V. Patil, S. Patil, K. Patil, C. Rode, A. Coronas, C. Nieto de Castro. Study of anion effect and heat trasfer properties of Ru-Ionanofluids. Solar Absorption Refrigeration Systems Operating with Ionic Liquids an Indo-Spanish Workshop. IIT Madras, Chennai, India. 21-22 February, 2014.

V. Patil, A. Cera-Manjarres, A. Coronas, K. Patil, C. Rode. Pt and Ru based ionanofluids for catalytic hydrogenation of furfuryl alcohol. GPE-4th International Congress on Green Process Engineering. Sevilla Spain. 7-10 April 2014.

V. Patil, S. Shinde, K. Patil, A. Coronas and C. Rode. Acidic Brønsted ionic liquid (ABIL) over Ru/C catalyst for highly selective hydrogenation of levulinic acid to gamma-valerolactone. 4th International Workshop *on* Ionic Liquids Advanced Energy Applications (WILS 2015). Universitat Rovira I Virgili, Tarragona, Spain. 15-16 January, 2015. ISBN 84-617-3875-6.

MOBILITY VISIT

PLACE: Centro de Química Estrutural, Departamento de Química e Bioquímica, Faculdade de Ciências da Universidade de Lisboa Campo Grande, Ed. C8, 1749-016 Lisboa, Portugal.

RESEARCH ADVISOR: Dr. Carlos Nieto de Castro

DURATION: 4th April 2013 to 1st May 2013

SPONSER PROJECT: New Working Fluids based on Natural Refrigerant and Ionic liquids for Absorption Refrigeration (NARILAR)

TASK: Measurements of thermal conductivity of phosphonium ionic liquids and their ionanofluids with carbon nanotubes.

PARTICIPATION IN PROJECTS

RESEARCH PROJECT: New Working Fluids based on Natural Refrigerant and Ionic liquids for Absorption Refrigeration (NARILAR)

PLACE: Department of Mechanical Engineering University Rovira i Virgili Escola Technica Superior d' Enginyeria Quimica (ETSEQ), Tarragona, Spain.

RESEARCH ADVISOR: Dr. Alberto Coronas

DURATION: 4th February 2013- 3rd April 2013 and 2nd December 2014 to 31st March 2015.

RESEARCH PROJECT: Scale up NCL process for selective hydrogenolysis of glycerol to 1,2 propanidiol

PLACE: Chemical Engineering and Process Development Division CSIR-National Chemical Laboratory Pune, Maharashtra, India.

RESEARCH ADVISOR: Dr. Chandrashekhar V. Rode

DURATION: 10th May 2013- 25th September 2014.

CONTENTS

LIST OF TABLES

LIST OF FIGURES

CHAPTER 3

CHAPTER 4

CHAPTER 5

ABBREVIATIONS

IL	Ionic liquid
RTIL	Room temperature ionic liquid
PIIL	Protic acid ionic liquid
NHC	N-Hetrocyclic carbene
INF	IoNanofluid
NEIL	Nanoparticle enhanced ionic liquid
NP	Nanoparticles
TB	Tribiological property
K	Thermal conductivity
P	Density
η	Viscosity
Cp	Specific Heat Capacity
n	Refractive index
Re	Reynolds number
[C4mim][Cl]	1-butyl-3-methyl imidazolium chloride
[C4mim][Br]	1-butyl-3-methyl imidazolium bromide
[C4mim][I]	1-butyl-3-methyl imidazolium iodide
$[C_4mim][BF_4]$	1-Butyl-3-methyl imidazolium terrafluroborate
Phen	Phenanthroline
TBAB	Tetrabutylammonium bromide
SILP	Supported ionic liquid phase
TC	Thermal conductivity
[Hmim][HCOO]	1-methyl imidazolium formate
$[Hmim][CH_3COO]$	1-methyl imidazolium acetate
$[Hmim][CH_3CH_2COO]$	1-methyl imidazolium propionate
$[Hmim][HSO_4]$	1-methyl imidazolium hydrogen sulfate
UV-Visible	Ultraviolet-Visible spectroscopy
IR	Infrared spectroscopy
NMR	Nuclear magnetic Resonance spectroscopy
XPS	X-ray photoelectron spectroscopy
SEM	Scanning electron microscopy
EDAX	Energy Dispersive analysis by X-rays
TEM	Trasmission electron microscopy
XRD	X-ray diffraction Study
TGA	Thermogravimetric analysis
SDS	Sodium dodeycyl sulphate
Ru-INFs	Ruthenium ionanofluids
HR-TEM	High resolution transmission electron microscopy
1D	One dimentional
2D	Two dimentional
3D	Three dimentional
Choline [NTf2]	Choline bis(trifluromethylsulfonyl)imide ionic liquid
LSPR	Localized surface plasmon resonance
Ag-nanospheres-NF	Silver nanospheres nanofluid
Ag-nanowires-NF	Silver nanowires nanofluid
Ag-nanoplates-NF	Silver nanoplates nanofluids
Ag-nanospheres-INF	Silver nanospheres ionanofluid
Ag-nanowires-INF	Silver nanowires ionanofluid
Ag-nanoplates-INF	silver nanoplates ionanofluids

LA	Levulinic acid
GVL	γ-valerolactone
TPPTS	tris(3-sulfonatophenyl) phosphine

Chapter 1

Introduction, justification and objective

Chapter 1 gives general introduction about ionic liquids their properties, synthesis protocols and applications. This chapter also provides general idea about transition metal nanoparticles in ionic liquids, their advanced applications in catalysis and heat transfer technologies along with literature search on ionic liquid based nanofluids. Justification, objectives of the present study and structure of the thesis are presentented at the end of this chapter.

1.1 IONIC LIQUID

Ionic liquids (ILs) are salts with melting point below 100 ^{o}C. When these salts are in a liquid state at room temperature, those are called as room temperature ionic liquids (RTILs). These salts in liquid phase are also decribed with other names as molten salt, liquid organic salt, non-aqueous ionic liquid and fused salt as well [1]. Conventional crystalline salts have symmetrical packing of anions and cations leading to a higher packing efficiency, while in case of ILs with unsymmetrical packing of ions leads to lower packing efficiency (Fig. 1.1). The melting point of an ionic compound depends on the lattice enthalpy which in turn depends on the size and charge of the ions. For larger ions and small charge, the energy requirement is less to break the ionic bond. So, organic cations with quaternary ammonium groups (R_4N^+) have low lattice energies and much lower melting points than their alkali metal analogues. For example, 1-Ethyl-3-methylimidazolium chloride melts at ~70 °C where as NaCl melts at 801 °C [2].

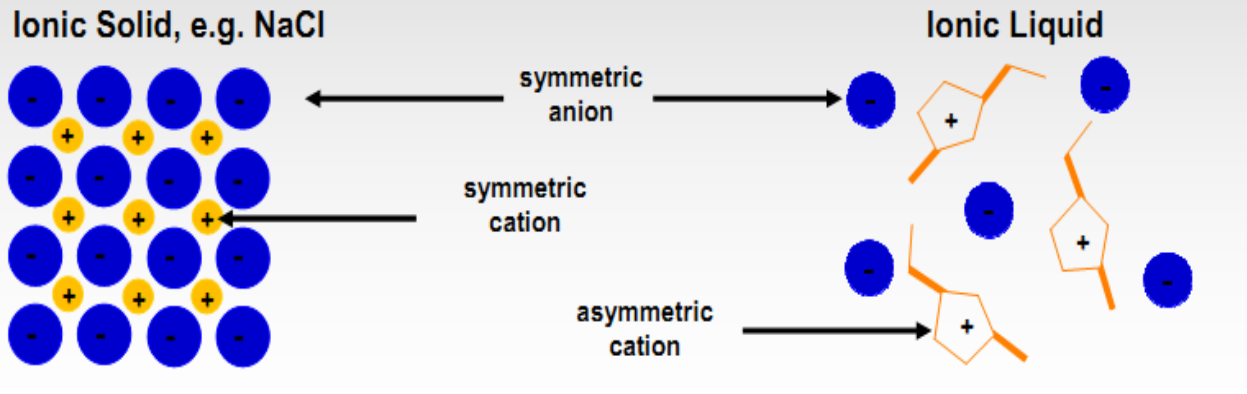

Figure 1.1 *Structure of ionic solid and ionic liquid (Figure adapted from site ref.[3])*

1.1.1 Structures of ionic liquids

IL is a combination of cation and anion. Usually IL cation is an organic structure. Cations reported are ammonium, sulphonium, phosponium, imidazolium, pyridinium, pyrrolidinium, thiazolium, oxazolium and pyrazolium. Anions structures are either organic (CH_3COO^-, $CH_3SO_3^-$ etc.) or inorganic anions (Cl^-, Br^-, I^-, BF_4^-, PF_6^-, NTF_2^-, DCA^- etc.). The structure and related properties of ILs depend on how cations and anions get blended. Consequently, there are

innumerable possible structures that may form ILs. The conceivable cation-anion combinations to be evaluated can be as high as 10^{18} [4]. Some of the examples are shown in Fig.s 1.2 and 1.3.

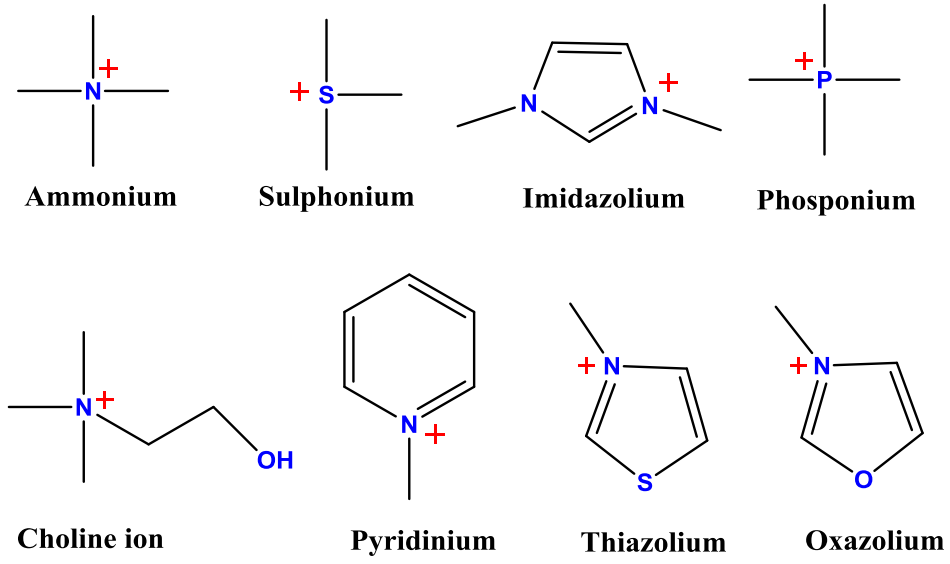

Figure 1.2 *Some common cations used for synthesis of ionic liquids*

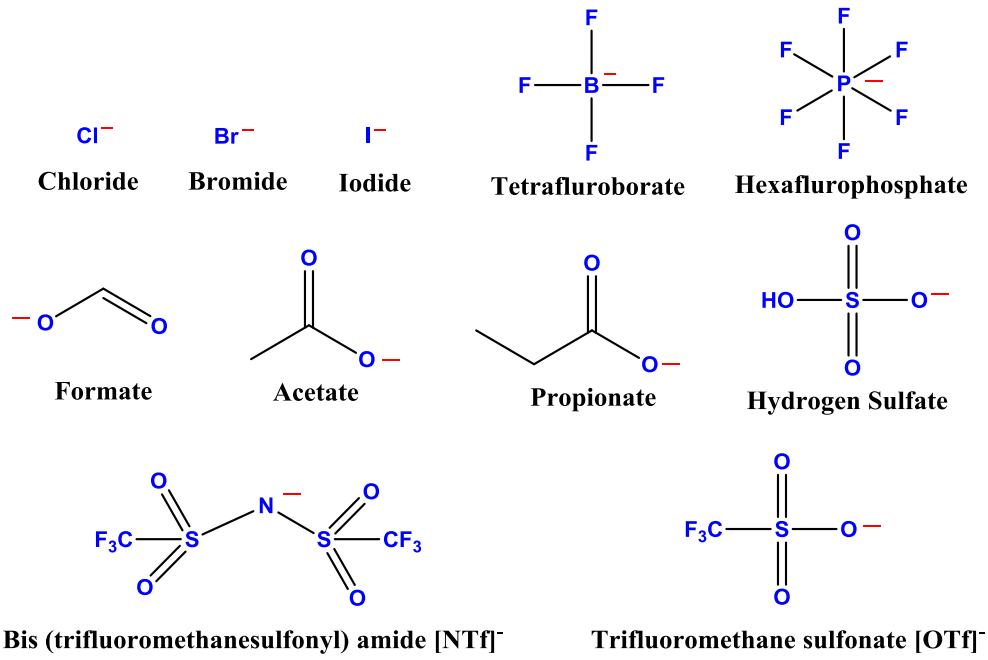

Figure 1.3 *Some common anions used for synthesis of ionic liquids*

1.1.2 Properties of ionic liquids

ILs possess an unique array of physicochemical properties which shifted them from laboratory curiosity to task-specific applications. Many ILs have desirable properties for such uses, including low volatility, thermal stability, good electrical and thermal conductivity, wide electrochemical windows, and the miscibility with other organic, inorganic, ionic and molecular compounds including polymers and biopolymers. Those properties made these ILs as ideal media for various transformations in solution [5]. General physico-chemical properties of an ionic liquid are mentioned in Table 1.1. A large number of ILs can be synthesized using various combinations of ions, also by modifying the length, branching and/or the number of substituents in the cation and anion. Because of this reason, ILs are often referred to as tailor-made designer solvents [6-7].

Table 1.1 *General physico chemical properties of Ionic liquids (Table adapted from ref. [8])*

Entry	Property	Measure of property
1	A salt	Cation and or anion quite large
2	Freezing point	Preferably below 100 ^{o}C
3	Liquidus range	Often > 200 ^{o}C
4	Thermal stability	Usually high
5	Viscosity	Normally < 100 cP, workable
6	Dielectric constant	Implied < 30
7	Polarity	Moderate
8	Specific conductivity	Usually < 10 $mScm^{-1}$, good
9	Molar conductivity	< 10 Scm^2 mol^{-1}
10	Electrochemical window	>2V, even 4.5 V, except for Brønsted acidic systems
11	Solvent and/or catalyst	Excellent for many organic reactions
12	Vapor pressure	Usually negligible

1.1.3 Synthesis of ionic liquids

The selection of the synthesis method for IL depends as per the convenience of user and necessity to design the aimed IL with choice of particular cation and anion. General routes for preparation of an IL are discussed below.

a) Direct alkylation reaction. In the alkylation reaction, alkyl group is taken from one molecule to another. This is a one way reaction in which the desired IL is produced directly from their

starting materials in a single step [9]. General scheme of an alkylation reaction used for preparation of IL (scheme 1.1) is as follows

$$[\text{Lewis Base}] + [R][A] \longrightarrow ([Cat]^+[A]^-)$$

$$\text{Lewis Base} \longrightarrow (NR_3, PR_3, SR_2, \text{N-alkyl pyrrolidine, N-alkyl imidazole})$$

$$\text{Cat= Cation} \qquad \text{A=(Anion)= } PF_6, BF_4, NTf_2 \text{ etc.}$$

Scheme 1.1 *General scheme for direct alkylation reaction of ionic liquids*

b) Quaternization and Metathesis of anion reaction. In this method, IL can be obtained in the following two steps: The initial step of synthesis is the quaternization of amines, phosphanes etc. with haloalkanes [2]. Reaction of quaternized product with metal salt of the desired anion generates the final product as an IL, as shown in Scheme 1.2 below.

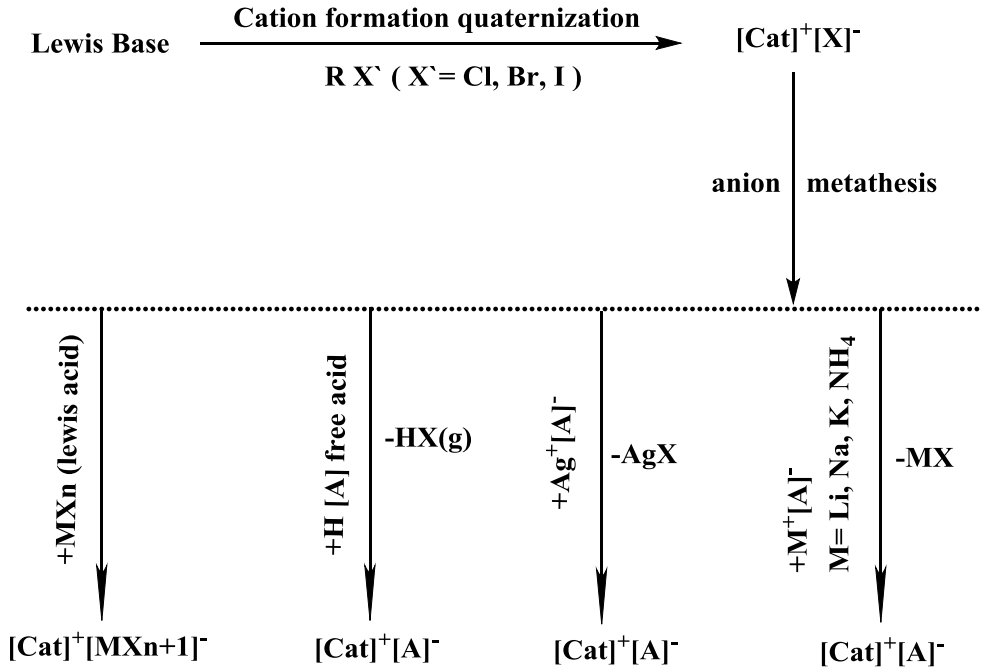

Scheme 1.2 *Quaternization and metathesis reactions of ionic liquids*

c) Synthesis of IL by neutralization of base with Brønsted acid. Protic acid ionic liquids (PIILs) can be prepared through a simple and atom economic neutralization of base as amines (e.g.

diisopropylmethylamine, diisopropylethylamine) with Brønsted acid HX where (X= $HCOO^-$, CH_3COO^-, HF_2^-, $H_2SO_4^-$ etc.). These rections are exothermic in nature and are carried out at 0 ^oC or less than this temperatures [10]. General example of neutralization reaction of amine as a base with acid is shown in Scheme 1.3.

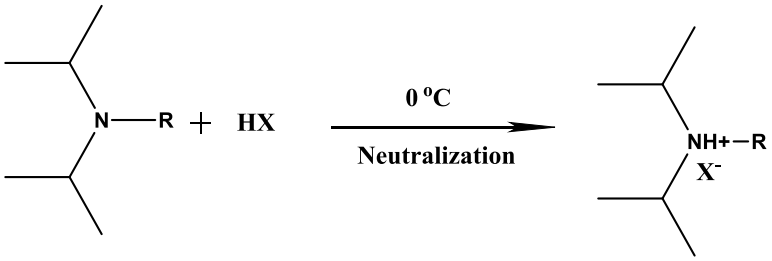

Scheme 1.3 *Neutralization reaction of amines with acids for preparation of ionic liquids*

c) Synthesis of ILs via N-Hetrocyclic carbene (NHC) intermediates.Carbenes are molecules which have lone pair of electrons on a carbon atom. This in turn renders them highly reactive. As a result, carbenes are useful intermediates in the synthesis of chemical compounds. The synthesis of ILs via carbenes can be achieved either by reaction of NHC adducts with acids or reaction of NHC organometallic intermediates with acids as shown in Scheme 1.4.

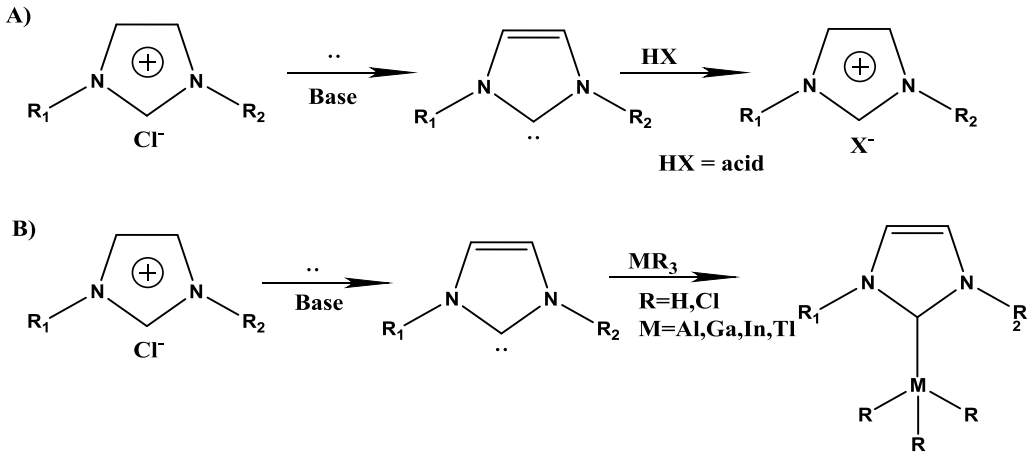

Scheme 1.4 *Synthesis of ionic liquids by N-Hetrocyclic carbene route*

d) Synthesis of ILs with ion-exchange material.Essentially, ion exchange materials are salts where, one of the ions is fixed in a stationary (solid/gel) phase and the counter ion (in solution) is exchangeable. For anion exchange, when a solution is passed through a column of ion exchange

material, the counter ion of the material $[A]^-$ will equillibriate with the corresponding ion of the solution $[B]^-$. Provided the column is of sufficient length or the equilibrium constant for exchange is sufficiently large, exchange will take place until complete exchange occurs and only species $[Cation]^+[A]^-$ is eluted as a pure solution [11]. Exchange of anions in a column of an ion-exchange material is shown in Scheme 1.5, below.

$$[resin]^+[A]^- + [Cation]^+[B]^- \longleftrightarrow [resin]^+[B]^- + [Cation]^+[A]^-$$

Scheme 1.5 *Synthesis of ionic liquids by ion-exchange in a column of ion-exchange material*

1.1.4 Applications of ionic liquids

ILs are liquid salts which allow tailor-made synthesis, having stability over a wide temperature range, high heat capacity, high density, negligible vapor pressure, and their green credential as an alternative to volatile organic solvents make them popular in the scientific community [15]. One more advantage of ILs is that they can be used to insitu generate and stabilize metallic nanoparticles [14].

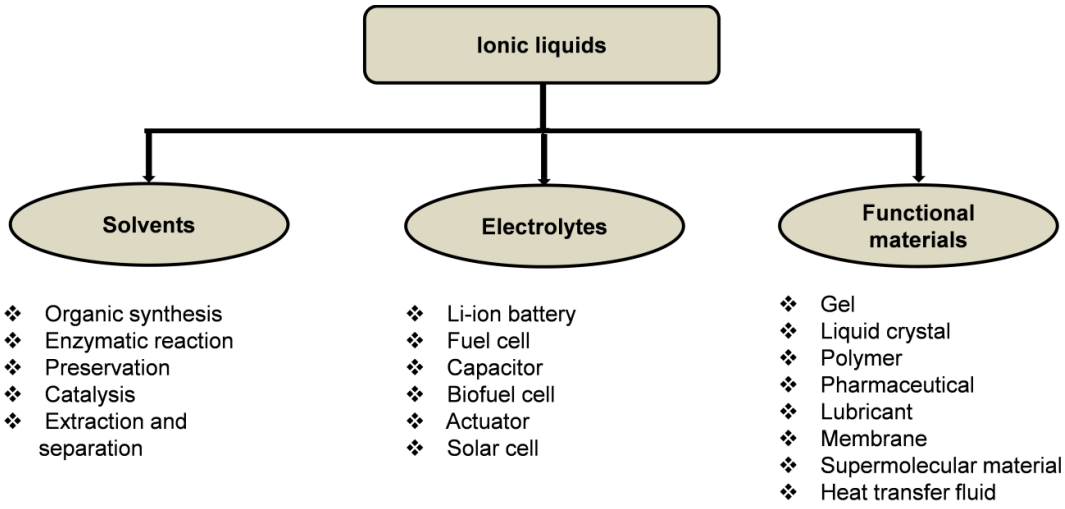

Figure 1.4 *Applications of ionic liquids (adapted from ref. [12])*

Classical salts have charge-ordered structures while ILs differ from them in a very important aspect that they possess pre-organised structures, mainly through hydrogen bonds. ILs serve both as a solvent and as a structure-directing agent. Structural organization of ILs can be used as "entropic drivers" for the spontaneous, well-defined and extended ordering of nanoscale

structures [5, 16-17]. Due to such properties, ILs have a wide range of applications as shown in Figure 1.4.

1.2 TRANSITION METAL NANOPARTICLES IN IONIC LIQUIDS

Nanoscale materials especially, transition metal nanoparticles have attracted intensive attention from scientific community, because of their unique chemical and structural properties. We can vary the properties like size, shape and surrounding chemical environment of the nanomaterials [13]. It is supposed that nanoparticles less than 100 Å in diameter will have properties intermediate between those of bulk and single atom. However, nanoparticles should be stabilized against aggregation into bulk form. The main methods used for the stabilization of nanoparticles are electrostatic or steric protection by using water-soluble polymers, quaternary ammonium salts, surfactants, or polyoxoanions [14].

1.2.1 Advantages of transition metal nanoparticles in ionic liquids

IL based nanofluids attracted extensive attention in recent years because of their enhanced thermal and catalytic performances compared to the base fluid counterpart [18-19] as IL nanofluids can overcome the shortcomings of IL itself. The scientific community refers IL based nanofluids with different names. The name “IoNanofluids” (INFs) was recently proposed by Nieto de Castro and co-workers [20], while Paul et al. pronounce these type of nanofluids as a Nanoparticle Enhanced Ionic Liquids (NEILs) [21]. Other attractive features of INFs are that they are designable and fine-tuneable through their base ILs for chosen properties and tasks. With these fascinating features including high thermal conductivity, high heat capacity, non-volatality, INFs can be used as advanced heat transfer fluids in numerous cooling, chemical engineering and green energy based applications. Noble metal nanoparticles (NPs) may constitute an alternative material for the construction of novel biosensors [23]. NPs in ILs have prominent applications in biosensors most likely due to the high conductivity of ILs arising from electron trasfer from the metal NPs [24]. Some other applications include the nonaqueous microemulsions containing the as-synthesized copper nanoparticles as high performance nanolubricants directly, which showed excellent tribological performance and high stability after

storage for 6 months at ambient conditions [25]. The dispersed metal nanoparticles stabilised in ILs are utilized as colloidal catalysts for biphasic fluid reactions or as supported catalysts on suitable solid material as a support. These multiphase frameworks allow easy product separation from the catalyst and reuse of the transition metal NPs without any appreciable loss of activity for many of reactions [26]. C-C coupling reaction is one of the most important and investigated process in catalysis. Transition metal stabilized in IL is very attractive, especially for Pd metal catalyzed C-C bond formation processes with a recycle of catalyst [27].

1.2.2 Synthesis protocols for transition metal nanoparticles in ionic liquids

It is possible to synthesize colloidal suspensions of transition metal nanoparticles into ILs by the following methods:

(1) Metal precursors in the form of [M (I-IV] are reduced and dissolved in the IL medium [14].

(2) Organometallic complexes are decomposed in the formal zero oxidation state and dissolved in ILs [28].

(3) Bombardment of metal prucursors in bulk form which generate metal NPs that are deposited in ILs [29]. Figure 1.5 shows the process of metal NPs deposition from metal foil to IL.

(4) In phase transfer method, pre-formed NPs in water or organic solvents are transfered to the IL phase (Figure 1.6) [30].

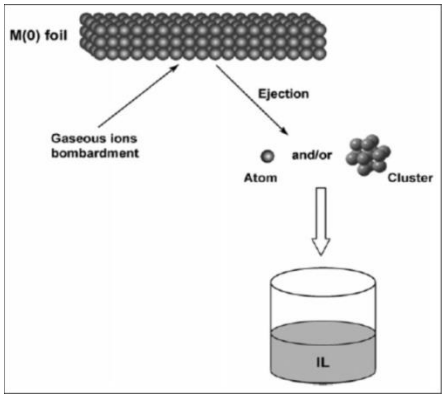

Figure 1.5 *Simplified model of metal NPs deposition in ILs by the sputtering method. (Figure adapted from ref. [26])*

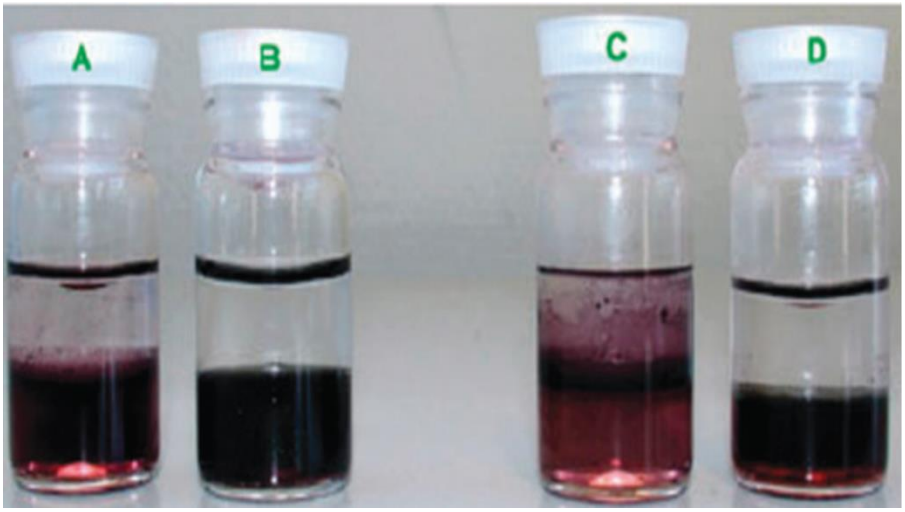

Figure 1.6 *(a) Gold NPs transferred from the aqueous phase to the BMI.PF_6 phase (b) and in the presence of HPF6; (c) [Au(0)]n NPs transferred from water to BMI.NTf_2 and (d) with $LiNTf_2$. (Figure adapted from ref. [31])*

All four methods of preparation of transition metal based nanoparticles in IL medium are shown in Scheme 1.6.

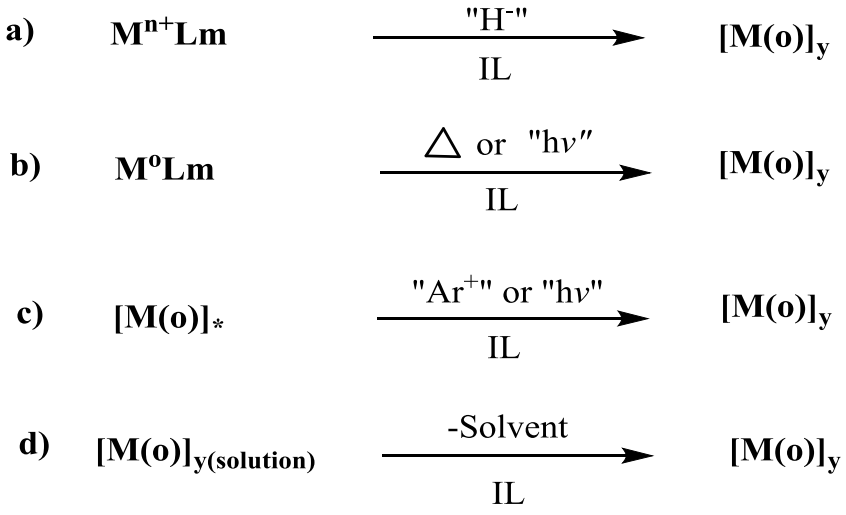

Scheme 1.6 *General methods used to prepare metal nanoparticles in ILs (Scheme adapted from reference [26])*

1.3 TRANSITION METAL NANOPARTICLES IN IONIC LIQUIDS FOR HEAT TRASFER APPLICATIONS

The suspension of nanoparticles of various morphologies (spheres, rods, tubes, plates etc.) in base liquid is commonly called as nanofluids [32]. Ceramic, metallic (Cu, Fe, Ag, Au), carbon and polymer (CNT, PVP) based nanofluids have shown improved thermal conductivity in contrast to their base liquids [33-40]. Nanofluids show higher heat conduction, more stability, microchannel cooling without clogging, reduced chances of erosion, reduction in power compared to microfluids [41-43]. In spite of the fact that nanofluids display improved heat trasfer properties, nanofluids designed with traditional base solvents (water, ethylene glycol, oil, etc.) have some drawbacks to be used as heat trasfer media.

Eventhough water is easily available, water and ethylene glycol based nanofluids can be utilized at moderately low temperatures while, synthetic oil suffers due to its higher vapor pressure. Altogether these conventional base liquids have low thermal stability. As a result, it is important to create novel nanofluids containing liquids other than these traditional liquids for designing of heat-transfer fluids [44] To design higher energy efficient heat transfer systems, heat transfer fluid properties that influence heat and mass transfer should be favorable [45]. For an ideal heat transfer fluid, it requires low vapor pressure, high heat capacity, low viscosity, high thermal stability and low or no corrosivity. Besides these, its ecological and human toxicology along with its biodegradability are further important requirements. ILs have very low vapor pressure, good heat capacity and higher thermal stability. Those unique features make them ideal media for potential heat trasfer applications. Very low vapor pressure of ILs allows them to use at very low pressure or under vaccum. Furthermore, low vapor pressure of ILs prevents them to evaporate at higher temperature unlike water. Because of this, ILs can also be used in open system to store thermal energy. One more interesting aspect in case of IL is that they are tailor made hence, we can design them as per the requirement either “hydrophilic” or “hydrophobic” which allow to dissolve or disperse other heat transfer media in ILs. It has been demonstrated that the ILs based nanofluids (INFs) show improved thermal conductivity as contrasted with the clean ILs [46]. Designing of INFs for enhanced trasport properties is the new emerging field of

research in the field of chemistry and engineering. INFs synthesis can be possible for desired application with tailored thermo-physical properties.

1.4 LITERATURE SURVEY ON STUDY OF PROPERTIES OF IONIC LIQUID BASED NANOFLUIDS

The summary of study of various properties of ILs and / or ionanofluids is presented in Table 1.2.

Table 1.2 *Literature search on IoNanofluids and their thermophysical properties*

Entry	Nanoparticles	Ionic liquid	TrasportProperty	Therotical study	Reference
1	Au	[Bmim][PF_6]	TB, K	-	[47]
2	CuO Al_2O_3 TiO_2	[C_2mim][OAc] [C_4mim][OAc] [$P_{8\,8\,8\,12}$][OAc]	*P*	-	[48]
3	AgI	[$P_{6,6,6,14}$] [Cl]	*P* , *n* , η ,Cp	-	[49]
					(Table continue)
4	Al_2O_3	[C4mim][NTf_2] [C4mpyrr][NTf_2]	K, Cp, Re	-	[50]
5	(Ni/C)	[HMIM][NTf_2]	RP	-	[51]
6	Al_2O_3 SWCNT Graphene nanofiber ZnO Fe_2O_3 SiO_2 CuO Au	[C4mmim][TN f_2]	K, η	-	[52]
7	Al_2O	[C4mpyrr][NTf_2]	K,Cp, η	-	[53]
8	Al_2O_3 Carbon black	[C4mmim][NTf_2]	*P*, Cp and Volumetric Cp	-	[54]
9	MWCNT	[C6mim][BF_4] [C4mim][CF_3SO_3]	K, Cp	-	[46]

		[C4mpyrr] [(CF_3SO_2)2N] [C4mim][PF_6] [C6mim][PF_6]			
10	Functionalised MWCNT	[Bmim][PF_6],	Rheology TB, shear η	-	[55]
11	CNT	[Cnmim][(CF_3SO_2)2N] [C4mim][BF_4]	K	-	[56]
12	carbon NP	Nmethylpiperazinium lactate	-	Molecular Dynamics Study	[57]
13	Carbon-nanotubes	[C4mim][NTf_2] [C4mim][CF_3SO_3] [C6mim][NTf_2] [C8mim][NTf_2] [C4mim][BF_4]	K, Cp	-	[58]
14	MWCNT	[C4mim]BF_4] [C4mim]PF_6]	*P*, Cp	-	[59]
15	MWCNT	[C4mim][(CF_3SO_2)2N] [C2mim][EtSO4]	K	-	[60]
16	MWCNT	[(C6)3PC14)][Phosph], [(C4)3PC1)][C1SO4], [(C6)3PC14][NTf2], [(C6)3-PC14][FAP].	K and rheology	-	[61]

(Table continue)

17	MWCNT	[C4mim][dca], [C2mim][dca] [C4mpyr][dca]	K and *P*	-	[62]
18	MWCNT	[C4mim][NTf2]	K and Cp		[63]
19	MWCNT	[Bnmim][BF_4] [Bmim][$AuCl_4$]	Imobilization and molecular rearrangement	-	[64]
20	Graphene/CNT	[HMIM][BF_4]	K, Cp, η	-	[65]
21	Graphene	[HMIM][BF_4]	K, η, Cp*P*,	-	[66]
22	Graphite Swcnt	choline benzoate choline salicylate	-	molecular dynamics simulations	[67]
23	C60 fullerene	[BMIM][BE] [BMIM][BF_4] [BMIM][LA] [BMIM][MS] [BMIM][PF_6] [BMIM][PR] [BMIM][SA] [BMIM][NTf_2] [CH][BE]	Solvation	Molecular dynamic study	[68]

[CH][BF_4]
[CH][LA]
[CH][MS]
[CH][PF_6]
[CH][PR]
[CH][SA]
[CH][NTf_2]
[MP][BE]
[MP][BF_4]
[MP][LA]
[MP][MS]
[MP][PF_6]
[MP][PR]
[MP][SA]
[MP][NTf_2]

[TB-Tribiological property, K- thermal conductivity, *P*- Density, η - Viscosity, Cp- Heat Capacity, *n*- refractive index, Re- Reynolds number]

1.5 TRANSITION METAL NANOPARTICLES IN IONIC LIQUIDS FOR CATALYSIS APPLICATIONS

Transition-metal NPs are well known for catalysis applications also. Transition-metal NPs are groups containing from a couple of tens to a few thousand metal atoms, balanced out by ligands, surfactants, polymers or dendrimers ensuring their stability in the nano size form. The utilization of transition metal nanoparticles in catalysis is for activation of the substarte molecules under milder conditions due to their nano size character which brings selectivity and efficiency in heterogeneous catalysis [69]. NPs themselves can be utilized as catalysts in homogeneous frameworks or on the other hand they can be heterogenized by fixation onto a heterogeneous base, for example, silica, alumina, different oxides or carbon, for example carbon nanotubes. It is possible to design metal nanoparticle catalyst for a particular reaction. Types of reactions catalyzed by transition metal nanoparticles in ILs are given in Table 1.3.

Table 1.3 *Examples of catalytic reactions promoted by transition metal nanoparticles in ILs*

Entry	Reaction	Metal	Ionic liquid used	Substrate	Product	Conv./sel. (%)	Ref.
1	Hydrogenation	Ru	C4mim.PF_6	1-hexene	Hexane	>99/100	[70]
2	Mizoroki-Heck	Pd	BBI.Br/BBI.BF_4	Iodobenzene/ethyl acrylate	Ethyl cinnamate	87 (isolated)	[19]
3	Suzuki-Miyuara	Pd	BMI.PF6	Bromobenzene/phenylboronic acid	Coupling product	100	[71]
4	Suzuki C-C coupling	Pd	BMI.PF6/N ligand	Bromobenzene/phenylboronic acid	Coupling product	56 (isolated)	[72]
5	Stille	Pd	THeptAB	Chlorobenzene/tributylphenylstannane	Coupling product	75	[73]
6	Ullmann	Pd	OMI.BF4	Iodobenzene	Homocoupling	99	[74]
7	Fisher-Tropsch	Ru	BMI.BF4/poly [NVP-co-VBIM.X]	CO	Hydrocarbons	75	[75]
						(Table continue)	
8	Borylation	Ir	THTdP.MS	Benzene/pinacolborane	Phenylboronic acid	47 (isolated)	[76]
9	Isotope exchange	Ru	THTdP.DBS	Decaborane	^{10}B-decaborane	90	[77]
10	Hydrosilylation	Pt	BPy.BF4	1-hexadecene/siloxane B9800	Organosilicon product	85	[78]

Generally, ionic liquid based transition metal nanoparticle catalysts are of four types:

a) Transition metal NPs in nonfunctionalized ILs,

b) Transition metal NPs in functionalized ILs,

c) Transition metal NPs with additional stabilizing ligands in ILs, and

d) Transition metal NPs on IL phase support.

a) Transition metal NPs in nonfunctionalized ILs:

Metal NPs in nonfunctionalised ILs act as catalysts for selective hydrogenation of alkenes and arenes under atmospheric reaction conditions. They behave as "single-site metal catalyst" for hydrogenation of alkenes, in solvent free conditions for reduction of arenes or in Fisher-Tropsch process. Protective layer of IL on metal NPs surface affects the catalyst activity, selectivity and stability. Metal NP surface stabilization is provided by protective layer of supramolecular ionic liquid cation aggregates, non-polar side chains, NHC carbene species, surface hydrogen atoms and an oxide layer when exist on the Metal NP surface [79], -e.g. insitu generated Rh nanoparticles in 1-Butyl-3-methyl imidazolium terrafluroborate ($[C_4mim][BF_4]$) IL efficiently catalyzed cyclohexene hydrogenation [80]. Arenes having various functional groups are hydrogenated by Ir metal NPs resulting in the reduction of the aromatic ring and subsequent hydrogenolysis of the C-O bond. The hydogenolysis is a classic reaction promoted by traditional heterogeneous catalysis [81]. Arene hydrogenation was also fruitfully employed as a probe reaction to confirm the presence of metal (0) species on the formation of Ru metal NPs from the reduction of a Ru(II) precursor in an imidazolium based IL with NTf_2 anion [82]. Some reports demonstrate that Ru(0) nanoparticles in ILs are also effective catalysts for the selective hydrogenation of biomass-derived entities [83].

b) Transition metal NPs in functionalized ILs:

Functionalized ILs provide enhanced stabilization of the metal NPs than nonfunctionalized ILs. Functionalization of an IL is an important phenomenon to necessarily improve the material ability to interact with substrates [26]. Most of the study is focused on functionalization of imidazolium cation based IL , although pyridinium and pyrrolidinum cations also have been functionalized for catalysis application study NPs [84-85]. In contrast to early reports in which only the cation was modified for a desired application, new studies have focused on the synthesis of ILs containing both fuctionalized cation and anion -e.g. Ru metal NPs dispersed in 1-butyronitrile-3-methylimidazolium NTf_2 IL exclusively hydrogenate nitrile groups instead of arenes, which are typically hydrogenated by Ru metal NPs in nonfunctionalized ILs [86]. Therefore, it is possible to modulate the selectivity of the catalyst simply by the presence of a

suitable functional group in IL. The selective hydrogenation of alkynes to (Z)-alkenes catalyzed by Pd metal NPs stabilized in (BCN)MI.NTf_2 IL was also recently reported [87].

c) Transition metal NPs with additional stabilizing ligands in ILs:

Another strategy to enhance metal NP stabilization in ILs is the use of additional stabilizing ligands. This extra protecting ligands such as N-donar ligands [88], polymers [89], or quaternary ammonium salts [90] have been utilized to improve the stability of metal NPs in ILs during the catalytic process - e.g. monofunctionalized bipyridine ligand was designed to allow good stabilization of Rh metal NPs in (BMI.PF_6) IL. The Rh nanoparticles remain stable in solution even after hydrogenation of substituted arene [91]. The role of phenanthroline (Phen) as an extra ligand was investigated during the hydrogenation of olefins using Pd metal NPs in (BMI.PF_6) IL [92]. Ligand based on tetraalkylammonium salts are commonly applied for enhanced stabilization of metal NPs in ILs. In particular, Pd metal NPs prepared in the presence of tetrabutylammonium bromide (TBAB) as a capping agent and then dispersed in (BMI.PF_6) IL displayed good efficiency and selectivity in hydrogenation reactions [90]. Polymers are another type of ligands extensively used for metal NP stabilization. These molecules give electronic stabilization by weakbinding to the NP surface, but they mainly provide steric protection against agglomeration. PVP-stabilized rhodium metal NPs give an effective and highly stable catalytic system in hydroxyl-functionalized ILs for styrene hydrogenation [93]. Bimetallic nanoparticles capped with PVP have also been used for the hydrogenation of various substrates in imidazolium ILs [94].

d) Transition metal NPs on IL phase support:

Metal NPs immobilized in supported ILs have emerged as alternative materials for catalytic reactions which combine the advantages of classical heterogeneous supports, called as SILP (supported ionic liquid phase) catalysis. ILs can be used as a simple thin film necessary to give the desired properties like stability, selectivity, etc., thus significantly reducing the mass-transfer problems usually associated with reactions performed when ILs are used as solvents and gives access to more robust/recyclable catalysts with easy catalyst separation after reactions. The SILP concept involves the use of an IL layer on the solid support or IL molecules covalently attached to the support surface to immobilize transition metal NP catalysts -e.g. Pd metal NPs synthesized

in molecular sieves containing an IL layer were successfully employed in alkene hydrogenation [95]. However, these materials showed superior catalytic activity in cyclohexene hydrogenation when compared to a biphasic system [92]. Multiwalled carbon nanotubes functionalized by ILs are other interesting supports for metal NP immobilization purpose. Indeed, the reduction of a Pd(II) precursor affords Pd metal NPs that are deposited in situ in the IL·X·MWCNTs (X is the imidazolium counterion) support. The system based on the SbF_6 anion demonstrates the best activity in trans-stilbene hydrogenation to 1,2-diphenylethane [96].

1.6 JUSTIFICATION OF THE THESIS

Previous study on most of the heat transfer properties for various nanomaterials in several ILs (as shown in Table 1.2) was mainly focused on thermal conductivity (TC) and heat capacity (Cp) of INFs. For implementation of INFs in the application of heat transfer, it becomes important to investigate other properties along with TC and Cp such as density and viscosity.

Eventhough, INFs displayed enhanced TC and Cp compared to only ILs, sometimes viscosity is not studied or occasionally INFs are more viscous in nature. Large viscosity of INFs makes the fluid unsuitable to flow easily through pipes of heat transfer system. It further increases pumping power consumption of the system, simultaneously also the cost of the instrument which creates an obstacle to apply INFs for practical utilization in heat transfer applications.

For development of new age INFs with improved transport properties it becomes essential to know the effect of nanoparticle stabilizing counterpart from ILs especially, in case of in situ generated nanoparticles in ILs. It becomes the subject of study that how the hydrogen bonding from IL, its anion size, cation size, volume of anion and cation, electrostatic stabilization affects on particle sizes and morphologies of in-situ generated metal nanoparticles. Further it is necessary to study effect of these factors on transport properties of INFs.

In general, most of the nanomaterials available in the market are stabilized with agents like PVP, thiols with unspecified thickness to overcome the agglomeration of nanoparticles. The effects of dispersing, pure and capped nanomaterials in ILs and subsequent influence on heat transport

properties would also prove an important topic of research in development of INFs for new generation heat transfer fluids.

For similar type of ILs, dispersed metal nanoparticles with altered size and shapes are possible. How this variation of nanomaterial morphology affects the transport properties of INFs is needed to be addressed. Again lack of reliable thermophysical properties data for some typical ILs and newly synthesized INFs prevents to actual utilization of INFs in heat transfer based technologies. As we have seen in Table 1.2, carbon based materials like carbon nanofibres, nanotubes and graphene show altogether enhanced TC compared to neat ILs. Also, inclusion of trasition metal nanoparticles shows the similar effect. The transport properties of combination of transition metal nanoparticles and carbon based support materials in ionic liquids have not been explored yet.

It is therefore required to explore various ILs and INFs, considering their environmentaly favorable properties and wide applicability to the industrial systems. Incorporation of transition metal nanoparticles in ILs for reactions of practical importance is a thrust area of research which is reflected by number of increasing publications in this field. Tailor made designing of transition metal nanoparticles and supported transition metal nanoparticles in ILs possessing the desired properties like acidity and/or basicity responsible for selective transformation of substrate to valuable products with high yield are not explored very well. It is also required to investigate the effect of cation and/or anion counterparts of ILs to tune the acidity and/or basicity for establishing the relationship with the catalytic activity. Extensive studies on recycling of transition metal nanoparticles and IL based catalysts are also important for successful implementation of these materials for catalytic process.

The proposed investigation in this thesis work, was to design ILs and develop ILs with transition metal nanoparticles and generate reliable data on some thermophysical properties. These data will contribute to design new generation heat transfer fluids and apply those fluids for heat transfer applications. New catalyst systems also were proposed to be developed based on ILs and transition metal nanoparticles or transition metal nanoparticles with other support materials in ILs for conversion of biomass derived platform molecules to value added chemicals with highest conversion and selectivity.

1.7 OBJECTIVES OF THE THESIS

Aim of the present study is to design ILs and subsequently, modify their structures by variation in cation or anion for enhancing their thermal and flow properties. Initially, several imidazolium cation based ILs were prepared with variation in anions such as chloride, bromide, iodide and tetrafluroborate. Then these were further modified by incorporating the NPs of transition metals such as ruthenium (Ru) and silver (Ag). It was also the objective of this work to study the catalytic properties of the prepared ILs and of the combination of IL with carbon supported NPs of Ru for hydrogenation of levulinic acid (LA) to g-valerolactone (GVL).

The specific objectives of this work are given below.

1) To review experimental and theoretical studies dealing with nanoparticles in ionic liquids for heat transfer and catalysis applications.
2) To measure thermal properties of developed fluids for heat transfer applications
3) To study the effect of variation of anions with the same cation of ionic liquids on thermal and flow properties.
4) To improve the thermal and flow properties of ionic liquids with addition of or development of new transition metal based nanoparticles in ionic liquids.
5) To screen ionic liquids for the desired fluid transport properties and further modification of these ionic liquids by incorporation of transition metal nanoparticles having various morphologies and sizes.
6) To study the catalytic activity of the prepared ILs and transition metal nanoparticles
7) To characterize in detail the above prepared transition metal based functional materials by 1H NMR, 13C NMR, XPS, SEM, ESEM, TEM, EDS, IR, UV-Visible, TGA, DTA, DSC, XRD.

1.8 STRUCTURE OF THE THESIS

The research work of this doctorate is organized in different chapters and the outline of its contents is given below.

Chapter 1 gives general introduction about ionic liquids, their properties, synthesis protocols and applications. This chapter again provides general idea about transition metal nanoparticles in

ionic liquids their advanced applications in catalysis and heat transfer technologies along with literature search on ionic liquid based nanofluids. Justification, objectives of the present study and structure of the thesis are also presented at the end in this chapter.

Chapter 2 presents materials and experimental methods used to develop transition metal and ionic liquid based heat transfer fluids and catalyst. This chapter includes characterization methods and techniques used to analyze prepared materials. Techniques used to measure thermophysical properties and to evaluate activity of the prepared IL based catalysts are also described in this chapter.

Chapter 3 includes development and preparation of imidazolium halide based ionic liquids. Study of effects of variation of anion counterparts of the ionic liquid on density, viscosity and thermal conductivity is presented here. In this chapter, ruthenium nanoparticle INFs are developed at room temperature and the effect of ruthenium nanoparticles on improvement of transport properties are also investigated. Effect of C2-(H) hydrogen atoms of the ionic liquid is correlated with the particle size of ruthenium nanoparticles.

Chapter 4 presents the study of transport properties of [Choline][NTf2] ionic liquid and silver nanoparticles of variable morphologies, such as nanospheres, nanoplates and nanowires in base ILs. INFs are developed based on the [Choline][NTf2] ionic liquid as a base fluid with silver nanospheres, nanoplates and nanowires. The effect of variation in morphology of silver nanoparticles on density, viscosity and thermal conductivity of INFs is also discussed in this chapter.

Chapter 5 deals with a new combination of 5% Ru/C and acidic Brønsted ionic liquids developed for the selective hydrogenation of bioderived levulinic acid to **γ**–valerolactone. Effect of variation in acidic anion and its chain length on acidity of ionic liquid is investigated with Hammet acidity function. Further correlation of IL Brønsted acidity and catalytic activity study is described in this chapter. Effect of process parameters is investigated for the optimization of reaction conditions.

Chapter 6 provides the conclusions of the work done in this thesis and comments for future work.

1.9 REFERENCES

[1] Welton T. Room-Temperature Ionic Liquids. Solvents for Synthesis and Catalysis Chem Rev 99 (1999) 2071-2083

[2] Wasserscheid P. And Welton T. Ionic liquids in synthesis.Weinheim: Wiley-VCH Verlag GmbH & Co. KGaAWiley-VCH Verlag, (2002) ISBNs: 3-527-30515-7 (Hardback); 3-527-60070-1 (Electronic)

[3] Salty solvents - ionic really http://www.rsc.org/education/eic/issues/2005_Jan/salty.asp (acessed 10 February 2015)

[4] Visser A. E.; Swatloski R. P.; Reichert W. M.; Mayton R.; Sheff S.; Wierzbicki A.; Davis, Jr. J. H. and Rogers R. D. Task-Specific Ionic Liquids Incorporating Novel Cations for the Coordination and Extraction of Hg^{2+} and Cd^{2+}: Synthesis, Characterization, and Extraction Studies Environ Sci Technol *36* (11) (2002) 2523-2529

[5] Dupont J. and Suarez P. A. Z. Physico-chemical processes in imidazolium ionic liquids Phys Chem Chem Phys 8 (2006) 2441-2452

[6] Anderson J. L.; Dixon J. K. and Brennecke J. F. Solubility of CO_2, CH_4, C_2H_6, C_2H_4, O_2, and N_2 in 1-Hexyl-3-methylpyridinium Bis(trifluoromethylsulfonyl)imide: Comparison to Other Ionic Liquids Acc Chem Res 40 (2007) 1208-1216

[7] Larsen A. S.; Holbrey J. D.; Tham F. S. and Reed C. A. Designing Ionic Liquids: Imidazolium Melts with Inert Carborane Anions J Am Chem Soc 122 (2000) 7264-7272

[8] The Electrochemical Society *Interface* • Spring 2007

[9] Jerry M. Advanced Organic Chemistry: Reactions, Mechanisms, and Structure (3rd ed.), New York: Wiley, (1985) ISBN 0-471-85472-7

[10] Anouti M.; Caillon-Caravanier M.; Floch C. L. and Lemordant D. Alkylammonium-Based Protic Ionic Liquids Part I: Preparation and Physicochemical Characterization, J Phys Chem B 112 (2008) 9406-9411

[11] Lee S. L. and Lee S. B. The Hildebrand solubility parameters, cohesive energy densities and internal energies of 1-alkyl-3-methylimidazolium-based room temperature ionic liquids Chem Commun (2005) 3469-3471

[12] Kohno Y. and Ohno H. Ionic liquid/water mixtures: from hostility to conciliation Chem Commun 48 (2012) 7119-7130

[13] Gajewicz A.; Puzyn T.; Rasulev B.; Leszczynska D. and Leszczynski J. Metal Oxide Nanoparticles: Size-Dependence of Quantum-Mechanical Properties Nanoscience & Nanotechnology-Asia 1 (2011) 53-58

[14] Dupont J.; Fonseca G. S.; Umpierre A. P.; Fichtner P. F. P. and Teixeira S. R. Transition-Metal Nanoparticles in Imidazolium Ionic Liquids: Recycable Catalysts for Biphasic Hydrogenation Reactions J Am Chem Soc 124 (16) (2002) 4228-4229

[15] Rooney D. W.; Jacquemin J. and Gardas R. Thermophysical properties of ionic liquids. Top Curr Chem 290 **(**2009) 185-212

[16] Tsuzuki S.; Tokuda H.; Hayamizu K. and Watanabe M. Magnitude and Directionality of Interaction in Ion Pairs of Ionic Liquids: Relationship with Ionic Conductivity J Phys Chem B 109 (34) (2005) 16474-16481

[17] Hardacre C.; Holbrey J. D.; McMath S. E. J.; Bowron D. T.; and Soper A. K. Structure of molten 1,3-dimethylimidazolium chloride using neutron diffraction J Chem Phys 118 (2003) 273-278

[18] Wang B.; Wang X.; Lou W.; Hao J. Ionic liquid-based stable nanofluids containing gold nanoparticles J Colloid Interface Sci 362 (2011) 5-14

[19] Deshmukh R. R.; Rajagopal R. and Srinivasan K. V. Ultrasound promoted C–C bond formation: Heck reaction at ambient conditions in room temperature ionic liquids Chem Commun (2001) 1544-1545

[20] Ribeiro A. P. C.; Lourenço M. J. V.; Nieto de Castro C. A.; and Hardacre C. Thermal Conductivity of "Bucky Gels". In: Proceedings of Conference on Molten Salts and Ionic Liquids (EUCHEM2008), Copenhagen, Denmark August , (2008) 24-29

[21] Paul T. C.; Morshed A. K. M. M. and Khan J. A. Nanoparticle Enhanced Ionic Liquids (NEILs) as Working Fluid for Next Generation Solar Collector Procedia Engineering 56 (2013) 631-636

[22] Murshed S. M. S.; Nieto de Castro C. A.; Lourenço M. J .V.; Lopes M. L. M. and Santos F. J. V. Current research and future applications of nano- and ionano-fluids J Phys: Conf Ser 395 (2012) 012117

[23] Fernandes S. C.; Moccelini S. K.; Scheeren C. W.; Migowski P.; Dupont J.; Heller M.; Micke A. G. and Vieira I. C. Biosensor for chlorogenic acid based on an ionic liquid containing iridium nanoparticles and polyphenol oxidase Talanta 79 (2009) 222-228

[24] Brondani D.; Scheeren C. W.; Dupont J. and Vieira I. C. Biosensor based on platinum nanoparticles dispersed in ionic liquid and laccase for determination of adrenaline, Sens Actuators B Chem 140 (2009) 252-259

[25] Wang A.; Chen F.; Xu F. and Yan Z. In situ synthesis of copper nanoparticles within ionic liquid-in-vegetable oil microemulsions and their direct use as high efficient nanolubricants RSC Adv 4 (2014) 45251-45257

[26] Dupont J. and Scholten J. D. On the structural and surface properties of transition-metal nanoparticles in ionic liquids Chem Soc Rev 39 (2010) 1780-1804

[27] Prechtl M. H. G.; Scholten J. D. and Dupont J. Carbon-Carbon Cross Coupling Reactions in Ionic Liquids Catalysed by Palladium Metal Nanoparticles Molecules 15 (2010) 3441-3461

[28] Scheeren C. W.; Machado G.; Dupont J.; Fichtner P. F. P. and Texeira S. R. Nanoscale Pt(0) Particles Prepared in Imidazolium Room Temperature Ionic Liquids: Synthesis from an Organometallic Precursor, Characterization, and Catalytic Properties in Hydrogenation Reactions Inorg Chem 42 (15) (2003) 4738-4742

[29] Meiss S. A.; Rohnke M.; Kienle L.; Zein El Abedin S.; Endres F. and Janek J. Employing Plasmas as Gaseous Electrodes at the Free Surface of Ionic Liquids: Deposition of Nanocrystalline Silver Particles, ChemPhysChem 8 (2007) 50-53

[30] Me´vellec V.; Leger B.; Mauduit M. and Roucoux A. Organic phase stabilization of rhodium nanoparticle catalyst by direct phase transfer from aqueous solution to room temperature ionic liquid based on surfactant counter anion exchange, Chem Commun (2005) 2838-2839

[31] Dongbin Z.; Zhaofu F.; Wee H. A. and Paul J. D. A Strategy for the Synthesis of Transition-Metal Nanoparticles and their Transfer between Liquid Phases Small 2 (7) (2006) 879-883

[32] Choi S. U. S. Enhancing Thermal Conductivity of Fluids with Nanoparticles, in Developments and Applications of Non-Newtonian Flows, eds. D. A. Singer and H. P. Wang, vol. FED231, American Society of Mechanical Engineers, New York, (1995), 99–105

[33] Lee S.; Choi S. U.-S.; Li S. and Eastman J. A. Measuring Thermal Conductivity of Fluids Containing Oxide Nanoparticles Transactions of ASME, J Heat Transfer 121 (1999) 280-289

[34] Murshed S. M. S.; Leong K. C.; Yang C. Enhanced thermal conductivity of TiO2—water based nanofluids Int J Therm Sci 44 (2005) 367-373

[35] Eastman J. A.; Choi S. U. S.; Li S.; Yu W. and Thompson L. J. Anomalously increased effective thermal conductivities of ethylene glycol-based nanofluids containing copper nanoparticles Appl Phys Lett 78 (6) (2001) 718-720

[36] Hong T-K. and Yanga H-S. Study of the enhanced thermal conductivity of Fe nanofluids J Appl Phys 97 (6) (2005) 064311–1-4

[37] Madhesh D.; Kalaiselvam S. Experimental study on the heat transfer and flow properties of Ag–ethylene glycol nanofluid as a coolant Heat Mass Transfer 50 (2014) 1597-1607

[38] Jime´nez-Pe´ rez J.L.; Fuentes R. G.; Alvarado E. M.; Ramo´n-Gallegos E.; Cruz-Orea A.; Ta´nori-Cordova J.; Mendoza-Alvarez J. G.; Enhancement of the thermal transport in a culture medium with Au nanoparticles Appl Surf Sci 255 (2008) 701-702

[39] Xie H.; Lee H.; Youn W. and Choi M. Nanofluids containing multiwalled carbon nanotubes and their enhanced thermal conductivities J Appl Phys 94 (8) (2003) 4967-4971

[40] Nisha M. R., Jayalakshmy M. S. and Philip J. Effective thermal conductivity of condensed polymeric nanofluids (nanosolids) controlled by diffusion and interfacial scattering, Pramana – J Phys 81(5) (2013) 849-864

[41] Chopkar M.; Das P. K. and Manna I. Synthesis and characterization of nanofluid for advanced heat transfer applications, Scripta Materialia 55 (2006) 549-552

[42] Buongiorno J.; Hu L-W.; Kim S. J.; Hannink R.; Truong B.; Forrest E. Nanofluids for Enhanced Economics and Safety of Nuclear Reactors: An Evaluation of the Potential Features

Nucl Technol 162(1) (2008) 80-91

[43] Shen B.; Shih A. J. and Tung S. C. Application of nanofluids in minimum quantity lubrication grinding Tribol T 51(6) (2008) 730-737

[44] Wang F.; Han L.; ZhangZ.; Fang X.; Shi J. and Ma W. Surfactant-free ionic liquid-based nanofluids with remarkable thermal conductivity enhancement at very low loading of graphene Nanoscale Res Lett **7**(314) (2012) 1-7

[45] International Mechanical Engineering Congress and Exposition IMECE2011, (2011), Colorado, USA.

[46] Nieto de Castro C. A.; Lourenco M. J. V.; Ribeiro A. P. C.; Langa E. and Vieira S. I. C. Thermal Properties of Ionic Liquids and IoNanofluids of Imidazolium and Pyrrolidinium Liquids J Chem Eng Data 55 (2010) 653-661

[47] Wang B.; Wang X.; Lou W. and Hao J. Gold-ionic liquid nanofluids with preferably tribological properties and thermal conductivity Nanoscale Res Lett 6(259) (2011) 1-10

[48] Swadzba-Kwa ´ sny M.; Chancelier L.; Ng S.; Manyar H. G.; Hardacre C. and Nockemann P. Facile in situ synthesis of nanofluids based on ionic liquids and copper oxide clusters and nanoparticles Dalton Trans 41 (2012) 219-227

[49] Rodrı´guez-Palmeiro I.; Rodrı´guez-CaboB.; Rodil E.; Arce A.; Saiz-Jabardo J. M.; Soto A.; Synthesis and characterization of highly concentratedAgI–[P6,6,6,14]Cl ionanofluids J Nanopart Res 15 (1881) (2013) 1-8

[50] Paul T. C.; Morshed AKM. M.; Khan J. A. Nanoparticle Enhanced Ionic Liquids (NEILS) as Working Fluid for the Next Generation Solar Collector Procedia Engineering 56 (2013) 631- 63

[51] Zhang L.; Liu J.; He G.; Ye Z.; Fang X.; Zhang Z. Radiative properties of ionic liquid-based nanofluids for medium-to-high-temperature direct absorption solar collectors, Sol Energ Mat Sol C 130 (2014) 521-528

[52] Fox E. B.; Visser A. E.; Bridges N. J. and Amoroso J. W. Thermophysical Properties of Nanoparticle-Enhanced Ionic Liquids (NEILs) Heat-Transfer Fluids Energ Fuel 27 (6) (2013) 3385-3393

[53] ASME International Mechanical Engineering Congress and Exposition, Proceedings (IMECE) Volume 7, Issue PARTS A, B, C, D (2012) 2825-2831

[54] Bridges N. J.; Visser A. E. and Fox E. B. Potential of Nanoparticle-Enhanced Ionic Liquids (NEILs) as Advanced Heat-Transfer Fluids Energ Fuel 25 (2011) 4862-4864

[55] Wang B.; Wang X.; Lou W. and Hao J. Rheological and Tribological Properties of Ionic Liquid-Based Nanofluids Containing Functionalized Multi-Walled Carbon Nanotubes J Phys Chem C 114 (2010) 8749-8754

[56] Ribeiro A. P. C.; Vieira S. I. C.; Goodrich P.; Hardacre C.; Lourenço M. J. V. and Nieto de Castro C. A. Thermal Conductivity of [C*n*mim][(CF3SO2)2N] and [C4mim][BF4] IoNanofluids with Carbon Nanotubes—Measurement, Theory and Structural Characterization J Nanofluids 2 (2013) 1-8

[57] Aparicio S. and Atilhan M. Molecular Dynamics Study of Carbon Nanostructures in N-Methylpiperazinium Lactate Ionic Liquid J Phys Chem C 117 (2013) 22046-22059

[58] Murshed S. M. S. and Nieto de Castro C. A. Superior thermal features of carbon nanotubes-based nanofluids – A review Renew Sust Energ Rev 37 (2014) 155-167

[59] Shevelyova M. P.; Paulechka Y. U.; Kabo G. J.; Blokhin A. V. and Kabo A. G. Physicochemical Properties of Imidazolium-Based Ionic Nanofluids: Density, Heat Capacity, and Enthalpy of Formation J Phys Chem C 117 (2013) 4782-4790

[60] Franca J. M. P.; Vieira S. I. C.; Lourenc¸o M. J. V.; Murshed S. M. S. and Nieto de Castro¸ C. A. Thermal Conductivity of [C4mim][(CF3SO2)2N] and [C2mim][EtSO4] and Their IoNanofluids with Carbon Nanotubes: Experiment and Theory, J Chem Eng Data 58 (2013) 467-476

[61] Ferreira A. G. M.; Simões P. N.; Ferreira A. F.; Fonseca M. A.; Oliveira M. S. A.;. Trino A. S. M Transport and thermal properties of quaternary phosphonium ionic liquids and IoNanofluids J Chem Thermodynamics 64 (2013) 80-92

[62] França J. M. P.; Reis F.; Vieira S. I. C.; Lourenço M. J. V.; Santos F. J. V.; Nieto de Castro C. A.; Pádua A. A. H. Thermophysical properties of ionic liquid dicyanamide (DCA) nanosystems J Chem Thermodynamics 79 (2014) 248-257

[63] Nieto de Castro C. A.; Murshed S. M. S.; Lourenço M. J. V.; Santos F. J. V.; Lopes M. L. M.; França J. M. P. Enhanced thermal conductivity and specific heat capacity of carbon nanotubes ionanofluids Int J Therm Sci 62 (2012) 34-39

[64] Zhao C.; Ren B.; Song Y.; Zhang J.; Wei L.; Chen S. and Zhang S. Immobilization and molecular rearrangement of ionic liquids on the surface of carbon nanotubes RSC Adv 4 (2014) 16267-16273

[65] Wang F.; Han L.; Zhang Z.; Fang X.; Shi J.and Ma W. Surfactant-free ionic liquid-based nanofluids with remarkable thermal conductivity enhancement at very low loading of grapheme, Nanoscale Res Lett 7(314) (2012) 1-7

[66] Liu J.; Wang F.; Zhang L.; Fang X.; Zhang Z. Thermodynamic properties and thermal stability of ionic liquid-based nanofluids containing graphene as advanced heat transfer fluids for medium-to-high-temperature applications, Renew Energ 63 (2014) 519-523

[67] Aparicio S. and Atilhan M. Choline-Based Ionic Liquids on Graphite Surfaces and Carbon Nanotubes Solvation: A Molecular Dynamics Study J Phys Chem C 116 (2012) 12055-12065

[68] García. G.; Atilhan M. and AparicioS.Theoretical Study on the Solvation of C60 Fullerene by Ionic Liquids J Phys Chem B 118 (2014) 11330-11340

[69] Ornelas C.; Mry D.; Blais J-C.; Cloutet E.; Aranzaes J. R. and Astruc D. Efficient Mono- and Bifunctionalization of Polyolefin Dendrimers by Olefin Metathesis Angew Chem Int Ed 44 (2005) 7399 -7404

[70] Rossi L. M.; Machado G.; Fichtner P. F. P.; Teixeira S. R. and Dupont J. On the use of ruthenium dioxide in 1-n-butyl-3-methylimidazolium ionic liquids as catalyst precursor for hydrogenation reactions J Catal Lett 92(3–4) (2004) 149-155

[71] Durand J.; Teuma E.; Malbosc F.; Kihn Y.; Go´mez M. Palladium nanoparticles immobilized in ionic liquid: An outstanding catalyst for the Suzuki C–C coupling, Catal Commun 9 (2008) 273-275

[72] Fernandez F.; Cordero B.; Durand J.; Muller G.; Malbosc F.; Kihn Y.; Teuma E. and GomezM. Palladium catalyzed Suzuki C–C couplings in an ionic liquid: nanoparticles responsible for the catalytic activity Dalton Trans (2007) 5572-5581

[73] Calo` V.; Nacci A.; Monopoli A. and Montingelli F. Pd Nanoparticles as Efficient Catalysts for Suzuki and Stille Coupling Reactions of Aryl Halides in Ionic Liquids J Org Chem 70 (2005) 6040-6044

[74] Pachn L. D.; Elsevier C. J. and Rothenberg G. Electroreductive Palladium-Catalysed Ullmann Reactions in Ionic Liquids: Scope and Mechanism Adv Synth Catal 348 (2006) 1705 -1710

[75] Xiao C-x., Cai Z-p., Wang T., Kou Y. and Yan N. Aqueous-Phase Fischer–Tropsch Synthesis with a Ruthenium Nanocluster Catalyst Angew Chem Int Ed 47 (2008) 746-749

[76] Yinghuai Z.; Chenyan K.; Peng A. T.; Emi A.; Monalisa W.; Louis L. K-J.; Hosmane N. S. and Maguire J. A. Catalytic Phenylborylation Reaction by Iridium(0) Nanoparticles Produced from HydridoiridiumCarborane Inorg Chem 47(13) (2008) 5756-5761

[77] Yinghuai Z.; Widjaja E.; Lo Pei Sia S.; Zhan W.; Carpenter K.; Maguire J. A.; Hosmane N. S. and Hawthorne M. F. Ruthenium(0) Nanoparticle-Catalyzed Isotope Exchange between ^{10}B and ^{11}B Nuclei in Decaborane(14) J Am Chem Soc 129 (2007) 6507-6512

[78] Geldbach T. J.; Zhao D.; Castillo N. C.; Laurenczy G.; Weyershausen B. and Dyson P. J. Biphasic Hydrosilylation in Ionic Liquids: A Process Set for Industrial Implementation J Am Chem Soc 128 (2006) 9773-9780

[79] Scholten J. D.; Leal B. C. and Dupont´ J. Transition Metal Nanoparticle Catalysis in Ionic Liquids ACS Catal 2 (2012) 184-200

[80] Suarez P. A. Z.; Dullius J. E. L.; Einloft S.; De souza R. F. and Dupont J. The Use of New Ionic Liquids in Two-Phase Catalytic Hydrogenation Reeaction By Rhodium Complexes J polyhedron 15 (1996) 1217-1219

[81] Fonseca G. S.; Umpierre A. P.; Fichtner P. F. P.; Teixeira S. R. and Dupont J. The Use of Imidazolium Ionic Liquids for the Formation and Stabilization of Ir0 and Rh0 Nanoparticles: Efficient Catalysts for the Hydrogenation of Arenes J Chem-Eur J 9 (2003) 3263-3269

[82] Prechtl M. H. G.; Campbell P. S.; Scholten J. D.; Fraser G. B.; Machado G.; Santini C. C.; Dupont J. and ChauvinY. Imidazolium ionic liquids as promoters and stabilising agents for the preparation of metal(0) nanoparticles by reduction and decomposition of organometallic complexes Nanoscale 2 (2010) 2601-2606

[83] Julis J.; Holscher M. and Leitner W. Selective hydrogenation of biomass derived substrates using ionic liquid-stabilized ruthenium nanoparticles Green Chem 12 (2010) 1634-1639

[84] Tatumi R. and Fujihara H. Remarkably stable gold nanoparticles functionalized with a zwitterionic liquid based on imidazolium sulfonate in a high concentration of aqueous electrolyte and ionic liquid Chem Commun (2005) 83-85

[85] Zhu W.; Yang H.; Yu Y.; Hua L.; Li H.; Feng B. and Hou Z. Amphiphilic ionic liquid stabilizing palladium nanoparticles for highly efficient catalytic hydrogenation Phys Chem Chem Phys 13 (2011) 13492-13500

[86] Prechtl M. H. G.; Scariot M.; Scholten J. D.; Machado G.; Teixeira S. R. and DupontJ. Nanoscale Ru(0) Particles: Arene Hydrogenation Catalysts in Imidazolium Ionic Liquids Inorg Chem 47 (19) (2008)

[87] Venkatesan R.; Prechtl M. H. G.; Scholten J. D.; Pezzi R. P.; Machado G. and Dupont J. Palladium nanoparticle catalysts in ionic liquids: synthesis, characterisation and selective partial hydrogenation of alkynes to Z-alkenes J Mater Chem 21 (2011) 3030-3036

[88] Dykeman R. R.; Yan N.; Scopelliti R. and Dyson P. J. Enhanced Rate of Arene Hydrogenation with Imidazolium Functionalized Bipyridine Stabilized Rhodium Nanoparticle Catalysts Inorg Chem 50 (2011) 717-719

[89] Yuan X.; Yan N.; Xiao C.; Li C.; Fei Z.; Cai Z.; Kou Y. and Dyson P. J. Highly selective hydrogenation of aromatic chloronitro compounds to aromatic chloroamines with ionic-liquid-like copolymer stabilized platinum nanocatalysts in ionic liquids Green Chem 12 (2010) 228-233

[90] Bras J. L.; Mukherjee D. K.; Gonza´lez S.; Tristany M.; Ganchegui B.; Moreno-Man˜as M.; Pleixats R.; He´nina F. and Muzart J. Palladium nanoparticles obtained from palladium salts and tributylamine in molten tetrabutylammonium bromide: their use for hydrogenolysis-free hydrogenation of olefins New J Chem 28 (2004) 1550-1553

[91] Léger B.; Denicourt-Nowicki A.; Olivier-Bourbigou H.; Roucoux A. Imidazolium-functionalized bipyridine derivatives: a promising family of ligands for catalytical Rh(0) colloids Tetrahedron Letters 50 (2009) 6531-6533

[92] Huang J.; Jiang T.; Han B.; Gao H.; Chang Y.; Zhao G. and Wu W. Hydrogenation of olefins using ligand-stabilized palladium nanoparticles in an ionic liquid Chem Commun (2003) 1654-1655

[93] Yang X.; Yan N.; Fei Z.; Crespo-Quesada R. M.; Laurenczy G.; Kiwi-Minsker L.; Kou Y.; Li Y. and Dyson P. J. Biphasic Hydrogenation over PVP Stabilized Rh Nanoparticles in Hydroxyl Functionalized Ionic Liquids Inorg Chem 47 (2008) 7444-7446

[94] Dash P.; Dehm N. A.; Scott R. W. J. Bimetallic PdAu nanoparticles as hydrogenation catalysts in imidazolium ionic liquids J Mol Catal A: Chem 286 (2008) 114-119

[95] Huang J.; Jiang T.; Gao H.; Han B.; Liu Z.; Wu W.; Chang Y. and Zhao G. Pd Nanoparticles Immobilized on Molecular Sieves by Ionic Liquids: Heterogeneous Catalysts for Solvent-Free Hydrogenation Angew Chem Int Ed 43 (2004) 1397-1399.

[96] Chun Y. S.; Shin J. Y.; Song C. E. and Lee S-g. Palladium nanoparticles supported onto ionic carbon nanotubes as robust recyclable catalysts in an ionic liquid Chem Commun (2008) 942-944.

Chapter 2

Experimental, materials and methods

Chapter 2 presents materials and experimental methods used to develop transition metal and ionic liquid based heat transfer fluids and catalyst. This chapter includes characterization methods and techniques used to analyze prepared materials. Techniques used to measure thermophysical properties and to evaluate activity of catalyst are also described in this chapter.

2.1 MATERIALS AND METHODS

This section 2.1 includes the description of chemicals and materials utilized in designing of ionic liquids and development of ionanofluids. Present section also demonstrates the reaction schemes involved in the designing of ionic liquids, their purification and procedures applied for development of transition metal based ionanofluids. In Table 2.1 all materials and chemicals used for designing of ionic liquids and development of ionanofluids are given along with their manufacturer and/or supplier.

Table 2.1 *Materials used in the preparation of ionic liquids and ionanofluids*

Entry	Chemical and materials	Company/supplier
1	1-bromobutane (98+ %)	Alfa Aesar
2	1-chlorobutane (99+ %)	Alfa Aesar
3	1-Iodobutane (99% stabilized with copper)	Alfa Aesar
4	1- methyl imidazole	Alfa Aesar
5	Sodium tetrafluroborate	Alfa Aesar
6	Methanol (HPLC grade)	RANKEM
7	Dichloromethane (HPLC grade)	RANKEM
8	Ruthenium (III) chloride hydrate	Sigma Aldrich
9	Ethyl acetate	Merck
10	Activated charcoal	Merck
11	Choline bis(trifluoromethylsulfonyl)imide (CAS No 827027-25-8)	io-li-tec
12	50 nm Econix Silver Nanospheres (Lot# DAC 1296-MGM2091B)	nanoComposix, Inc. USA
13	550 nm Resonant Silver nanoplates (Lot# KJW2047)	nanoComposix, Inc. USA
14	Silver nanowires Ref. 200004 Av. Diameter 50 nm, length up to 50 um	EMFUTUR company Europe
15	Levulinic acid (99%)	Sigma-Aldrich
16	Sodium borohydride	Sigma-Aldrich
17	$RuCl_3.6H_2O$	Sigma-Aldrich
18	Acetic acid glacial (100%)	Merk
19	Sulfuric acid (98%)	Merk
20	Activated charcoal	Merk
21	1-Methyl imidazole (99%),	Alfa Aesar
22	Formic acid (85%),	Himedia
23	Propionic acid (99%)	LOBA Chemie
24	4-nitroaniline (>98%)	LOBA Chemie
25	Ethanol absolute (99.9%,)	AR,CYNPRAN GLUDT BV.

2.1.1 Methods used for designing of ionic liquids

Since ionic liquid is a precursor for development of ionanofluids we first synthesized the imidazolium halide based ionic liquids. Synthesis of imidazolium halide ionic liquids was carried out in two steps. 1) 1-butyl-3-methyl imidazolium chloride [C4mim][Cl], 1-butyl-3-methyl imidazolium bromide [C4mim][Br], 1-butyl-3-methyl imidazolium iodide [C4mim][I], were prepared through direct alkylation reaction. 2) For the synthesis of 1-butyl-3-methyl imidazolium tetrafluroborate [C4mim][BF_4], already synthesized [C4mim][Br] ionic liquid was reacted with sodium tetrafluroborate through anion exchange reaction. Reactions involved in the synthesis of imidazolium halide ionic liquids are presented in a Scheme 2.1. For all the four reactions, 1:1.2 mole ratios of 1-methyl imidazole and alkyl halides reacted with each other. Excess of halo butane was removed by washing with ethyl acetate, separated by decantation and traces of solvents removed with rotatory evaporator. 1-butyl-3-methyl imidazolium tetrafluroborate [C4mim][BF_4] was synthesized according to reference [1]. Obtained ILs were purified again before prior use in the development of ruthenium ionanofluids. For purification, gained IL was dissolved in 50 mL of deionised water in a round bottom flask. 1g of activated charcoal was added into this solution. The reaction mixture was stirred at 70 ^oC for 24 h under nitrogen atmosphere. This mixture was then cooled and vacuum filtered on bed of celite powder in sintering funnel. Schematic of the purification is shown in Figure 2.2. The as filtered mixture of ionic liquid and water was heated at 80 ^oC under vaccum on rotatory evaporator for 8h, to evaporate water. The remaining water was removed by drying on a vacuum line overnight to obtain dry ionic liquid. Digital photographs of the synthesized pure ILs are shown below in Figure 2.1.

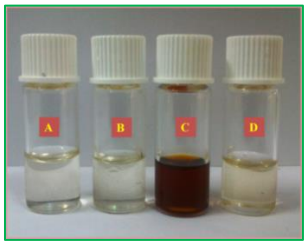

Figure 2.1 *Photographs of designed pure ionic liquids A) [C4mim][Cl], B) [C4mim][Br], C) [C4mim][I] and D) [C4mim] [BF_4]*

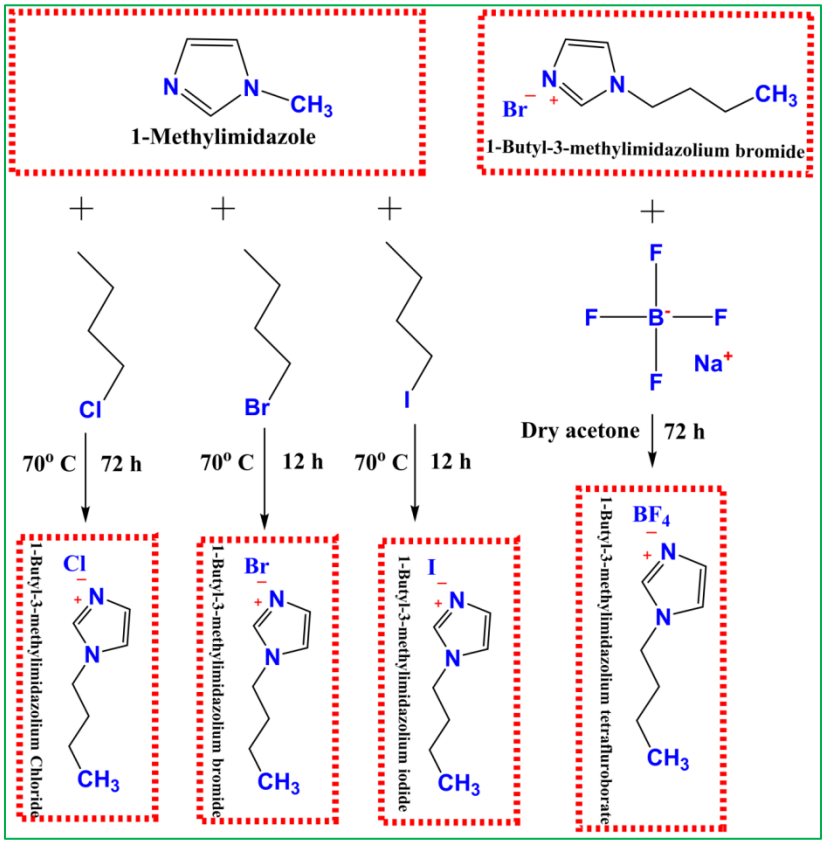

Scheme 2.1 *Reaction scheme for synthesis of 1-butyl-3-methyl imidazolium halide ionic liquids*

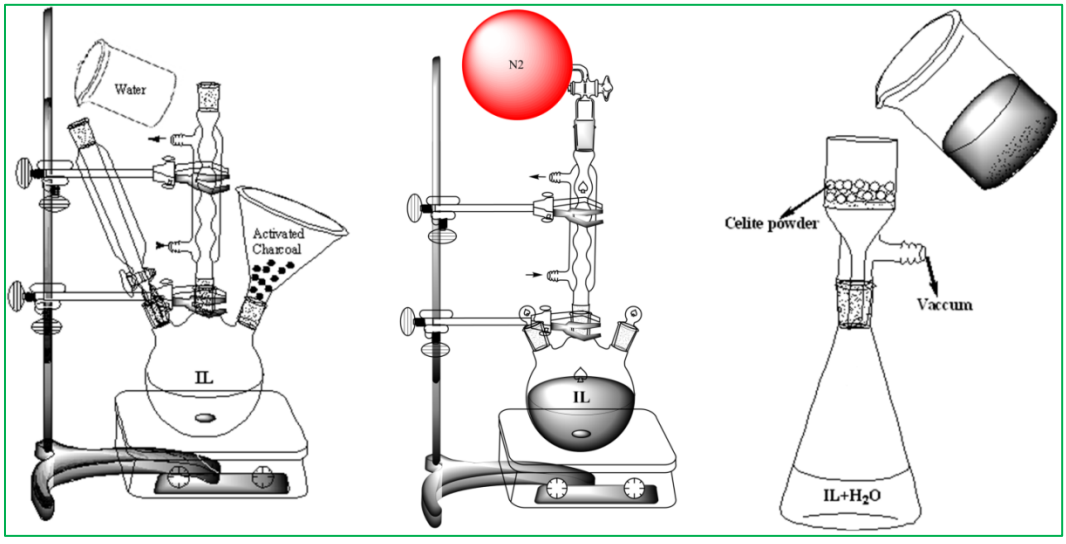

Figure 2.2 *Schematic of purification of 1-butyl-3-methyl imidazolium halide ionic liquids*

For development of catalyst for levulinic acid hydrogenation reactions we designed a series of Brønsted acidic ionic liquids. The preparation of these Brønsted acidic ionic liquids was done by neutralizing 1-Methyl imidazole base with the selected four types of acids as shown in Scheme 2.2.

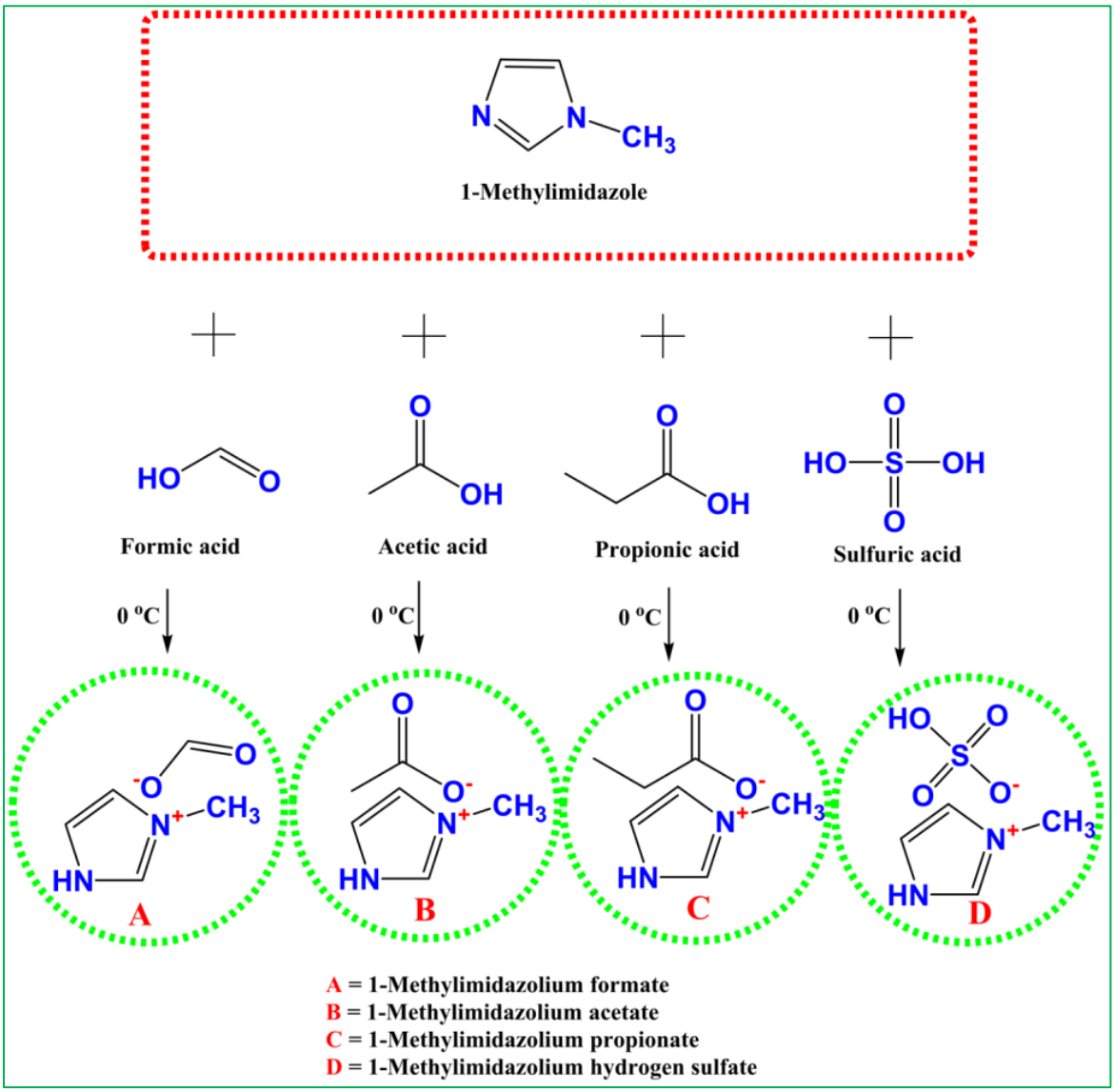

Scheme 2.2 *Reaction schemes for designing of Brønsted acidic ionic liquids*

All four imidazole based Brønsted acidic ILs *viz.* 1-methyl imidazolium formate ([Hmim][HCOO]), 1-methyl imidazolium acetate ([Hmim][CH_3COO]), 1-methyl imidazolium propionate ([Hmim][CH_3CH_2COO]), 1-methyl imidazolium hydrogen sulfate ([Hmim][HSO_4]) were prepared by mixing equimolar amounts of acid and base [2]. In a typical synthesis, dropwise addition of a base to acid was carried out for complete neutralization in an ice bath in order to control heat generation in a reaction, as shown in schematic of Figure 2.3. The reaction mixture was stirred for 6 h at room temperature. The water formed in the neutralization was removed by rotavapour at 80 ^oC for 6 h. The last traces of water and volatile impurities were removed from ILs under reduced vacuum at 70 ^oC for 10 h.

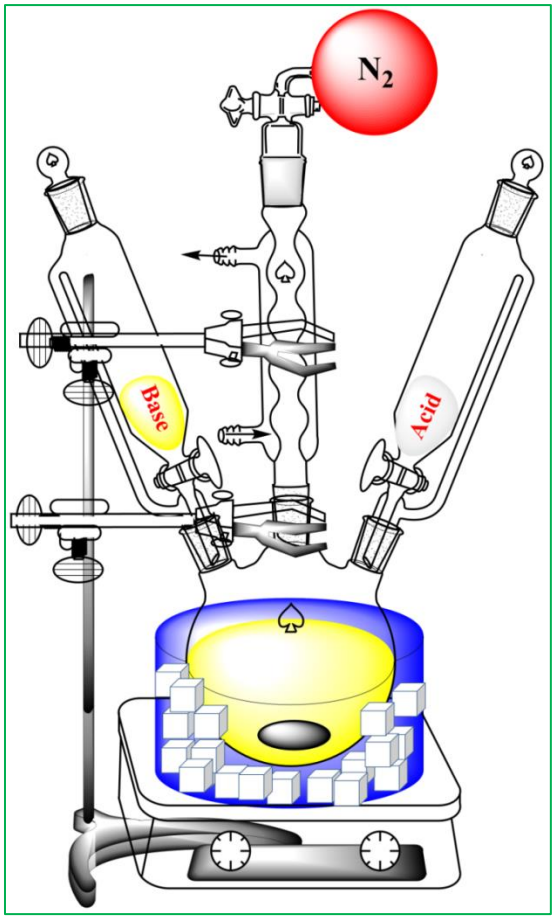

Figure 2.3 *Schematic of synthesis of Brønsted acidic ionic liquids*

2.1.2 Methods used for development of ionanofluids and catalyst

For the development of ruthenium INFs in 1-butyl-3-methyl imidazolium halide ILs, calculated amount of ruthenium metal precursor ($RuCl_3.xH_2O$) was added to the calculated amount of IL which is vacuum dried. In a typical experiment, 0.0082 gms of $RuCl_3.xH_2O$ was addead to 40 mL of dried IL. The metal precursor and IL mixture was stirred for 2 h at room temperature in N_2 environment, to make uniform solution of metal precursor in IL as a solvent. After 2 h of stirring, 1M $NaBH_4$ solution was added dropwise into the metal precursor solution in IL. For the synthesis of ruthenium nanoparticles in [C4mim][Cl] and [C4mim][I] ILs 3 mL of 1M $NaBH_4$ was utilized while for ruthenium nanoparticles in [C4mim][Br] and [C4mim][BF_4] ILs 1 mL of 1M $NaBH_4$ was utilized for complete reduction of metal precursor in base ionic liquids. After addition of 1M $NaBH_4$, [C4mim][Br] and [C4mim][BF_4] ILs based solutions were stirred for 2 h to complete the reduction of the metal precursor to metal nanoparticles. In case of [C4mim][Cl] and [C4mim][I] IL, the time required to reduce the metal precursor was 72 h. Schematic of development of ruthenium INFs is shown in Figure 2.4. The ruthenium metal nanoparticles nanofluids in ILs thus obtained are further dried under vacuum before prior use for characterization and measurement of their transport properties. Digital photographs of the prepared ruthenium INFs are shown in Figure 2.5.

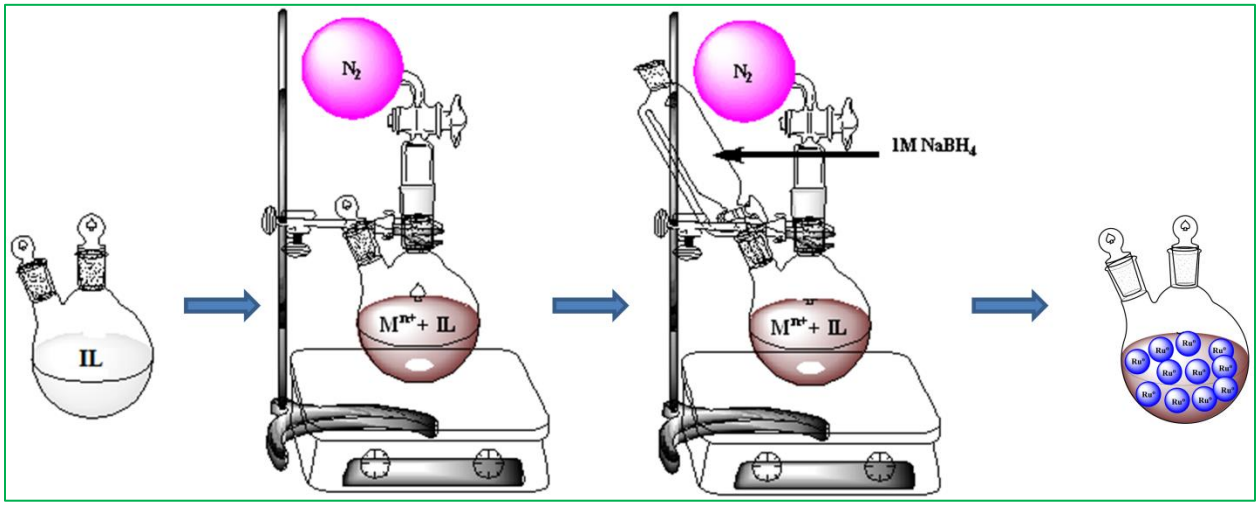

Figure 2.4 *Schematic of development of IL based ruthenium ionanofluids*

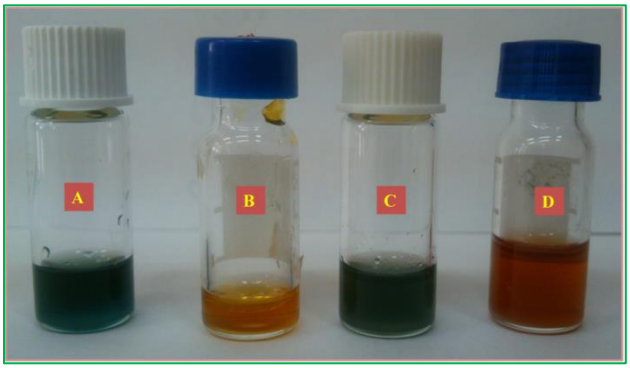

Figure 2.5 *Photographs of the prepared ionanofluids(A) Ru-[C4mim][Cl], B) Ru-[C4mim][Br], C) Ru-[C4mim][I] and D) Ru-[C4mim] [BF_4])*

To develop silver INFs with different morphologies, initially, silver nanofluids were prepared and futher used for synthesis of silver INFs. Silver nanoparticles in nanoplates form were in the form of dispersion in water. This nanofluid was used as received from the supplier. To prepare spherical silver nanofluid, 0.002 g of spherical silver nanoparticles were added to 100 mL of Millipore water. The obtained solution was sonicated for 20 minutes to obtain dispersion of silver nanospheres in water as a base fluid. After that particles were very well dispersed in water solution which became faint yellow in color. 0.002 g of silver nanowires were dispersed in 100 mL of Millipore water. For dipersion of nanowires in water, mixture was sonicate with the help of sonicator for 20 minutes. Digital photographs of all the three prepared silver nanofluids are given in Figure 2.6

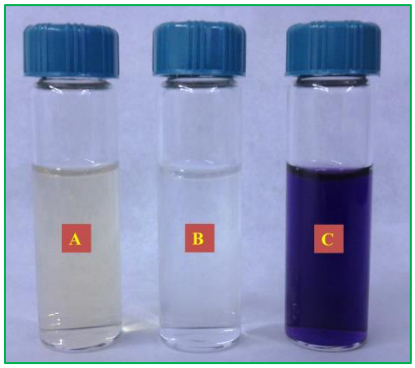

Figure 2.6 *Digital photographs of A) Ag-nanospheres nanofluid B) Ag-nanowires nanofluid C) Ag-nanoplates nanofluids*

To prepare [Choline][NTf2] IL based silver INFs with various morpholgies, equal amount of IL and Ag nanoparticles based nanofluids were mixed together in a conical flask. The mixture

forms two layes, a viscous layer of IL at bottom and another immiscible layer above it. The obtained mixture was trasfered to a round bottom flask which was then connected to rota-evaporator for mixing the Ag-nanoparticles from water phase to IL phase. This mixture was heated at 80 ^{o}C for 4 h to evaporate water from the fluid mixture. The remaining water was removed by drying on a vacuum line for two days to obtain dry silver ionanofluids as shown in Figure 2.7. For preparation of all three silver INFs namely Ag-nanospheres INF, Ag-nanowires INF, Ag-nanoplates INF, similar prepartion protocol is used in this study. Digital photograph of IL and developed silver INFs is shown in Figure 2.8.

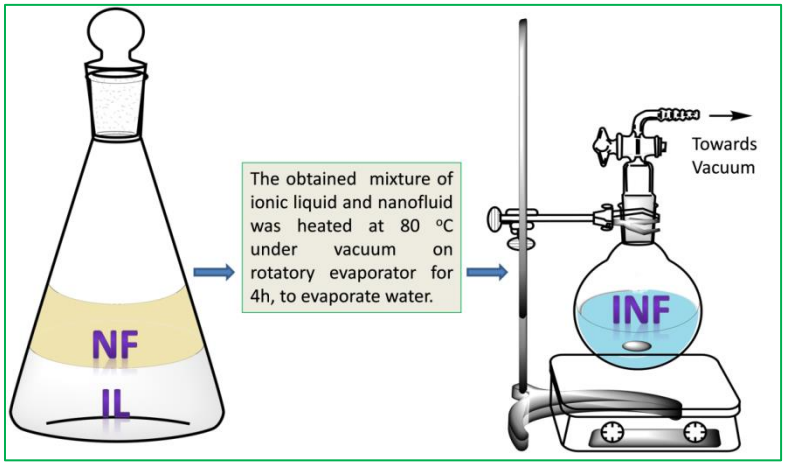

Figure 2.7 *Schematic of development of IL based silver ionanofluids*

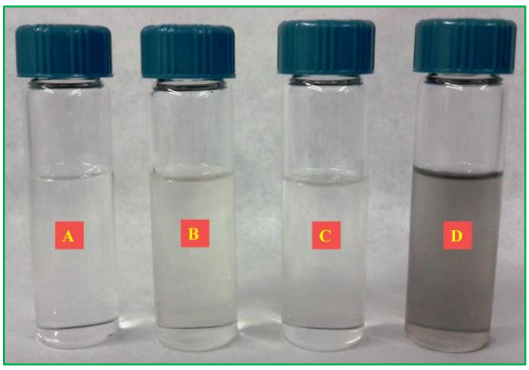

Figure 2.8 *Digital photographs of A) [Choline][NTf2]IL B) Ag-nanospheres INF C) Ag-nanowires INF D) Ag-nanoplates INF*

Ru supported on carbon support catalyst was prepared by impregnation method as shown in Figure 2.9. In a typical procedure, 2 g of the carbon support was suspended in an aqueous

medium. Calculated amount of $RuCl_3.xH_2O$ was added under stirring for 1h for obtaining 5% (w/w) loading of ruthenium metal on carbon support. It was subsequently reduced using 5 mL (1M solution in water) of $NaBH_4$. Then obtained suspension was filtered off and dried at 110 ^oC in an oven for 12 h.

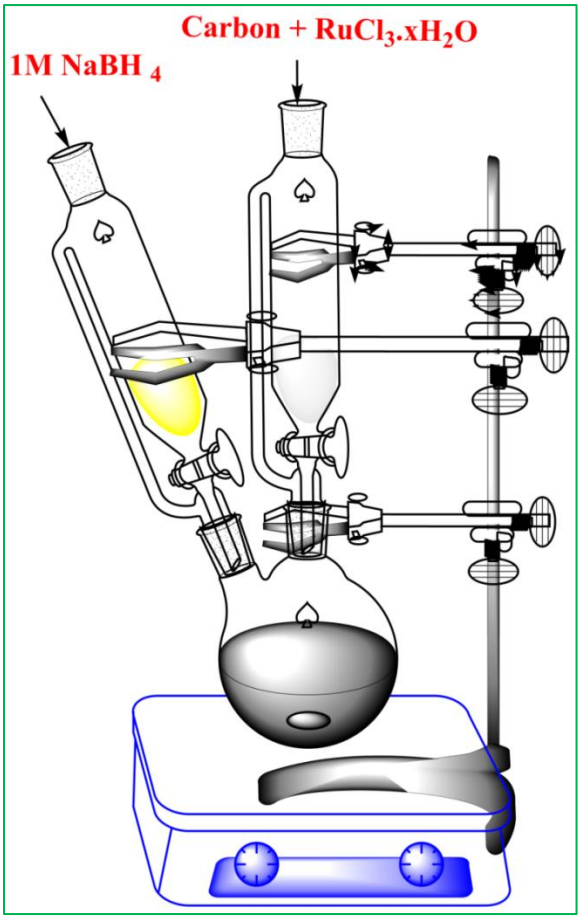

Figure 2.9 *Development of 5% Ru/C catalyst*

2.2 CHARACTERIZATION TECHNIQUES

Ultraviolet-Visible spectroscopy (UV-Visible): Optical absorptions of imidazolium halide ILs and Ru INFs, Choline (trifluromethylsulfonyl) imide IL, silver NFs and its respective silver INFs samples were measured with Shimadzu (UV-Vis) MultiSpec-1501 spectrophotometer and 8453 UV-Vis spectrophotometer respectively. For collecting optical data of imidazolium halide ILs

and Ru INFs, a quartz cell was sealed with teflon during the experiment to avoid moisture from atmosphere. The UV-Visible spectra of Brønsted acidic ionic liquids and indicator solutions were studied using (JASCO, 196 Corp., Tokyo, Japan, UV–VIS–NIR Spectrophotometer,197 Model V-670).

Infrared spectroscopy (IR) : All ATR-IR spectra of ionic liquids, nanofluids and INFs were collected in a range 600 cm^{-1} to 4000 cm^{-1} on infrared spectrometer (Fourier Transform Jasco FT/IR-600 Plus).

Nuclear magnetic Resonance spectroscopy (NMR): For all NMR analysis, approximately 10 mg of the sample was taken into 2 mm NMR tube. Samples were dissolved in a D_2O and $CDCl_3$ solvents as per solubility of sample. 0.5 ml of tetramethylsilane (TMS) solute was used as a internal reference for NMR chemical shift.

X-ray photoelectron spectroscopy (XPS) : XPS analysis was performed on a ESCA-3000 VG Scientific UK, using non-monochromatic, AlKα radiation (1486.6 eV) operating at 150 W with a spectral resolution of 0.2 eV. A thin IL film of each samples (ILs, NFs and INFs) was prepared by depositing of corresponding liquid sample onto planar stud by drop casting and introduced in UHV chamber (< $5x10^{-8}$ Pa), with exposure to air minimized. The binding energy scale was calibrated with Au 4f 7/2 peak position (84.0 eV) and the C1s peak at 285.0 eV was used as a reference. Measurements were performed at take-off angle 55^{o}. Peak deconvolution of C1s was accomplished using XPS Peak 4.1.

Scanning electron microscopy (SEM) : SEM JEOL 6400 (20 KV) machine was used to do SEM analysis of silver nanofluids and silver ionanofluids.

Energy Dispersive analysis by X-rays: (EDAX) :

Elemental composition of 5% Ru/C catalyst was studied using transmission electron microscope (HR-TEM), model JEOL 1200 EX. EDAX analysis of Ruthenium ionanofluids was done with (NOVA NANOSEM-450). Elemental mapping of silver ionanofluids was carried out on (SEM JEOL 6400 + EDX oxfort instrument)

Trasmission electron microscopy (TEM): The particle size and morphology of 5% Ru/C catalyst were studied using transmission electron microscope (HR-TEM), model JEOL 1200 EX. Samples were prepared by the procedure as follows. A small amount of the solid sample was

sonicated in 2 mL methanol for 1 min. A drop of prepared suspension was deposited on a Cu grid coated with carbon layer and grid was dried at room temperature before analysis. The morphology and particle size of as-prepared ruthenium nanoparticle colloids were characterized by HR-TEM (JEOL 2010F) at an acceleration voltage of 300 kV. TEM analysis of silver nanofluids and silver ionanofluids were carried out using TEM JEOL 1011 at an accelerating voltage of 100 kV.

X-ray diffraction study (XRD): X-ray diffraction of 5% Ru/C catalyst was recorded on a PAnalytical PXRD Model X-Pert PRO-1712, using Ni filtered Cu Kα radiation (λ = 0.154 nm) as a source (current intensity, 30 mA; voltage, 40 kV) and X-celerator detector. The samples were scanned in the 2θ range of $10–80^0$.

Thermogravimetric analysis (TGA): Thermal analysis of dried imidazolium halide ILs and their ruthenium INFs were carried out in (Perkin Elmer model TGA7 Thermo balance) equipment. Thermal stability of Brønsted acidic ILs were studied by thermal gravimetric analysis, which was carried out using TG-DTA analyser (TA instruments, SDT 2960). Thermal analysis of Choline (trifluromethylsulfonyl) imide IL, silver nanofluids and silver INFs were analyse with Mettler Toledo Model (TGA/DTA 851). Thermal analysis was carried out in a temperature range from 30 ^oC to 500 ^oC in N_2 atmosphere with heating rate of 5 ^oC/min.

2.3 MEASUREMENT OF THERMOPHYSICAL PROPERTIES

2.3.1 Measurement of Density

The density of a substance is its mass per unit volume. The symbol most often used for density is $\boldsymbol{\rho}$.

$$\rho = \frac{M}{V} \ldots\ldots\ldots\ldots\ldots\ldots (2.1)$$

Density of the material expressed in S.I unit as kg/m^3. For measurement of density of imidazolium halide ILs and ruthenium INFs "Anton Paar DMA60/512 P density cell" was used. This density cell measures the period of harmonic oscillation of the built-in U-tube, which contains the sample. Density is obtained by the comparison of the period of oscillations of

sample to that of a previous reference fluids used for calibration [3]. For measurement of density of Choline bis(trifluoromethylsulfonyl) imide IL, silver NFs and silver INFs an Anton Paar DSA 5000 density measurement cell was used. Working principle of instrument is similar as per (DMA 60/512 P) density cell, but in this case a peltier-effect controller was used to control the temperature. Before measurement of density of all ILs and INFs, they were vacuum dried. After drying of samples, their water content was measured with the help of Karl-fisher titration to ensure proper drying of ILs and INFs. Anton Paar DMA60/51 device was previously calibrated with density reference fluids (S20 and S200, Koehler Instrument Company, Inc.) [4]. A Julabo F20-ME circulating bath with a water + ethylene glycol mixture was used to control the temperature of the experiments. For "Anton Parr DSA 5000", calibration was carried out using certified density liquids provided by company. The displayed density values on the DSA 5000 density measurement cell were compared with values given on certificate for those standards. For *(*Anton Parr DSA 5000) density measuring cell density was calculated from the quotient of the period of oscillations of the U-tube and the reference oscillator.

$$\rho = KA * Q^2 * F1 - KB + F2 \text{.....(2.2)}$$

For measurement of Density with Anton Parr DMA60/512 P density cell at one single temperature and pressure following equation was used.

$$\rho = A * P2 - B \text{.....(2.3)}$$

$$A = \frac{\rho 1 - \rho 2}{P1 - P2} \text{.....(2.4)}$$

$$B = \frac{P2^2 * \rho 1 - P1^2 * \rho 2}{P1^2 - P2^2} \text{.....(2.5)}$$

$\rho =$ unknown density of sample

$\rho 1 =$ density of standard 1

$\rho 2 =$ density of standard 2

$P1 =$ period of oscillation standard 1

$P2 =$ period of oscillation standard 2

$$P = \text{period of oscillation of sample}$$

For "Anton Paar DMA 60/512 P" estimated expanded uncertainty (k=2) was 1 kg/m^3 for density and 0.1 K for temperature and and for "Anton Paar DSA 5000" 0.1 kg/m^3 for density and 0.01 K for temperature. Digital photographs of Anton Paar DSA 5000 instrument is shown in Figure 2.10.

Figure 2.10 *Photograph of (Anton Parr DSA 5000) density measurement unit*

2.3.2 Measurement of Viscosity

Viscosity is a quantity expressing the magnitude of internal friction in a fluid, as measured by the force per unit area resisting uniform flow. Viscosity (represented by the symbol η "eta") is the ratio of the shearing stress (F/A) to the velocity gradient ($\Delta vx/\Delta z$or dvx/dz) in a fluid. η = F/A / dvx/dz. The SI unit of viscosity is pascal second [Pa·s], sometimes called dynamic viscosity or absolute viscosity.

Working Principle of a (Cambridge Visco-Pro 2000):

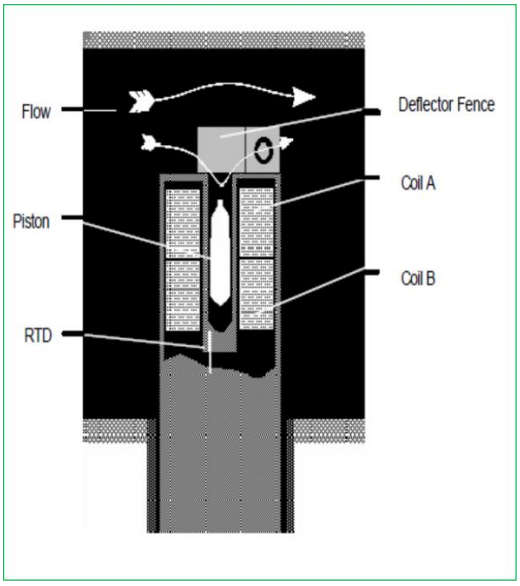

The cambridge applied systems, piston-style viscometer technology uses two magnetic coils within a 316 stainless steel sensor with the sensor inserted into the pipe line. The magnetic piston inside the chamber is surrounded by the fluid sample deflected into the measurement chamber. Two coils inside the sensor body are used to magnetically force the piston back and forth a predetermined distance (about 0.2 inches). By alternatively powering the coils with a constant force piston's round trip travel time is measured. An increase in viscosity is sensed as a slowed piston travel time. The time required for the piston to complete a two way cycle is an accurate measure of viscosity. The defelecting force acts to continuously deflect fresh sample into the measurement chamber. Since measurement of the piston motion is in two directions, variations due to gravity or flow forces are annulled. Also, because the piston has very little mass, magnetic forces greatly exceed any disturbances due to vibration. Viscosity of all samples (nanofluids, ionic liquids and ionanofluids) were measured using a piston-type viscometer (Cambridge Visco-Pro 2000). Before measurement of viscosity of all ILs and INFs they were vacuum dried. After drying of samples their water content was measured with the help of Karl-fisher titration to ensure proper drying of ILs and INFs. A (Cambridge Visco-Pro 2000) was previously calibrated with viscosity and density reference fluids (S20 and S200, Koehler Instrument Company, Inc.) [4]. Expanded uncertainty (k=2) was estimed as 0.05 mPa·s for viscosity and 0.1 K for temperature. Digital photographs of instrument used to measure density and viscosity is given as follows in Figure 2.11.

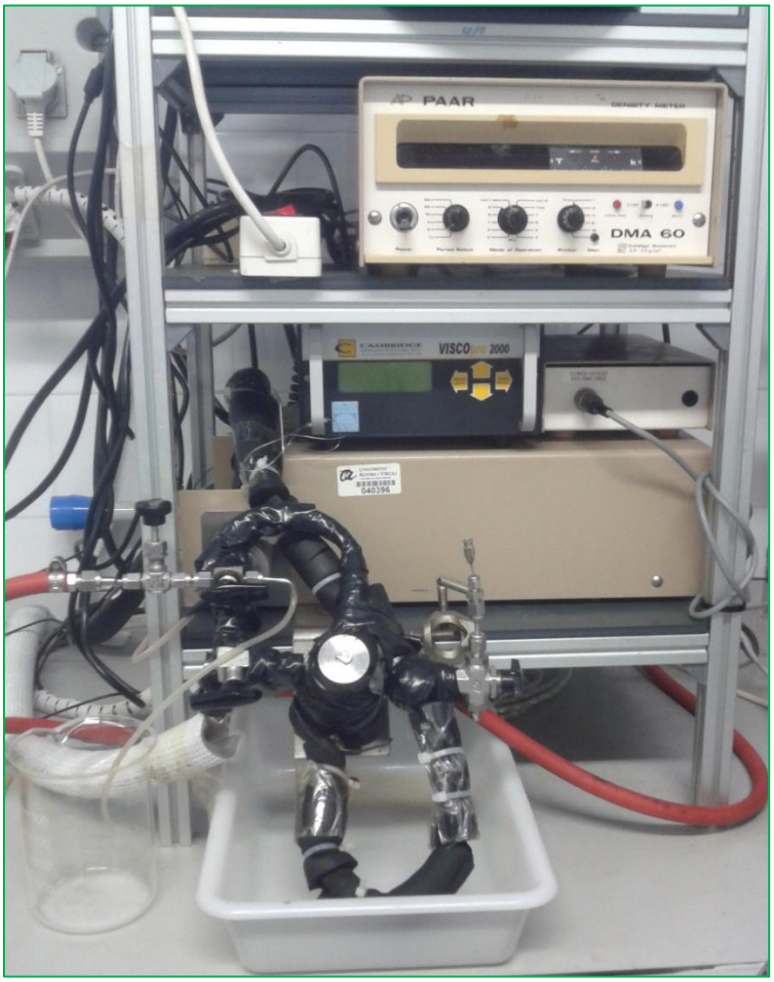

Figure 2.11 *Anton Paar DMA 60/512 P and Cambridge Visco-Pro 2000 instrument set up*

2.3.3 Mesurement of Thermal conductivity

A measure of the ability of a material to allow the flow of heat from its warmer surface to its colder surface, is determined as the heat energy transferred per unit of time and per unit of surface area divided by the temperature gradient. Mathamatically, it is shown as the temperature difference divided by the distance between the two surfaces (the thickness of the material), expressed in watts per kelvin per meter. The SI unit of thermal conductivity is watts per meter kelvin (W/(m·K)). Before measurement of thermal conductivity of all ILs and INFs they were

vacuum dried. After drying of samples, their water content was measured with the help of Karl-fisher titration to ensure proper drying of ILs and INFs. Thermal conductivity of ILs and INFs were measured from 20 ^{o}C to 30 ^{o}C using KD2 Pro™ Thermal Properties Analyzer (Decagon Devices, Inc.). The principle of the thermal conductivity measurement of KD2 Pro™ is based on the transient hot-wire technique. This device measures together the thermal conductivity and temperature. A P-Selecta Frigitherm circulating bath, with resolution 0.1 K, was used to control the temperature of the experiments. The KD2 was calibrated using distilled water and ethylene glycol before use. Expanded uncertainty (k=2) is estimated as the 5 % of the thermal conductivity value, and 0.05 K for temperature. Digital photograph of instrument used to measured thermal conductivity of all samples is given below in Figure 2.12.

Figure 2.12 *KD2 Pro Thermal Properties Analyzer*

2.3.4 Measurement of acidity of Brønsted acidic ionic liquids

A new combination of 5% Ru/C and acidic Brønsted ionic liquids were developed for the selective hydrogenation of bioderived levulinic acid to γ–valerolactone. The acidity of various Brønsted acidic ILs was determined using the Hammet method with the help of UV-Visible spectroscopy technique. Detailed description of method used for determination of Hammet acidity is described as follows. The series of indicator solutions of (4-nitroaniline) from 25 mM to 200 mM were prepared in ethanol as a solvent. The absorption of this solutions were measured with UV-Visible spectroscopy. The graph of concentration verses absorption was

plotted for present solutions [5]. The graph gives calibration curve with linearity higher than 0.99 as shown in Figure. 2.13. Solutions for studying protonated forms of ILs were prepared by adding 1:1 mixture of 4-nitroaniline and IL in 6 mL of ethanol. An amount of indicator was dissolved in IL solution with the help of utrasonicator bath for the period of 15 minutes. This freshly prepared solution was used to determine absorption of protonated forms of ILs. Brønsted acidities of ILs were determined in terms of Hammet acidity function as given below [6].

$$Ho = pK(I)aq + \log([I]s/[IH+]s\ ).....(2.6)$$

Where, pK*(I)*aq is the pKa value of the indicator (4-nitroaniline). *[I]s* is the molar concentration of unprotonated form of indicator, $[IH^+]s$ is molar concentration of protonated form of indicator. UV-Visible spectra of both unprotonated and protonated forms of indicators in ethanol showed a specific absorption at 360 nm however, the intensity increases for the protonated form. The measured values of absorbance were used to determine $[I]s/[IH^+]s$ ratio from which value of Ho was calculated for Brønsted acidic ILs.

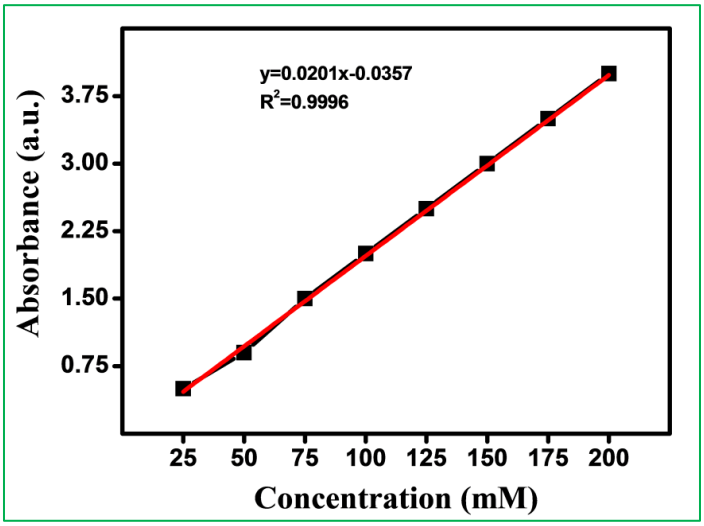

Figure 2.13 *Extinction coefficient calculation for indicator (4-nitroaniline)*

2.4 PROCEDURE FOR HYDROGENATION OF LEVULINIC ACID AND PRODUCT ANALYSIS

All the batch hydrogenation experiments were carried out in a 100 mL capacity stirred autoclave supplied by Parr Instruments Co. USA. It was equipped with heating arrangement, overhead stirrer, thermo well, internal cooling coil, gas inlet and outlet, liquid sampling valve, safety rupture disc, pressure gauge as well as transducer for digital pressure display, separate automatic controller to control the temperature, agitation speed, solenoid valve and high temperature cutoff module. Water circulation through the internal cooling loop equipped with automatic cut-off arrangement controlled the temperature inside the reactor with an accuracy of ±1° C.

A schematic of the batch reactor set-up is shown in Figure 2.14.

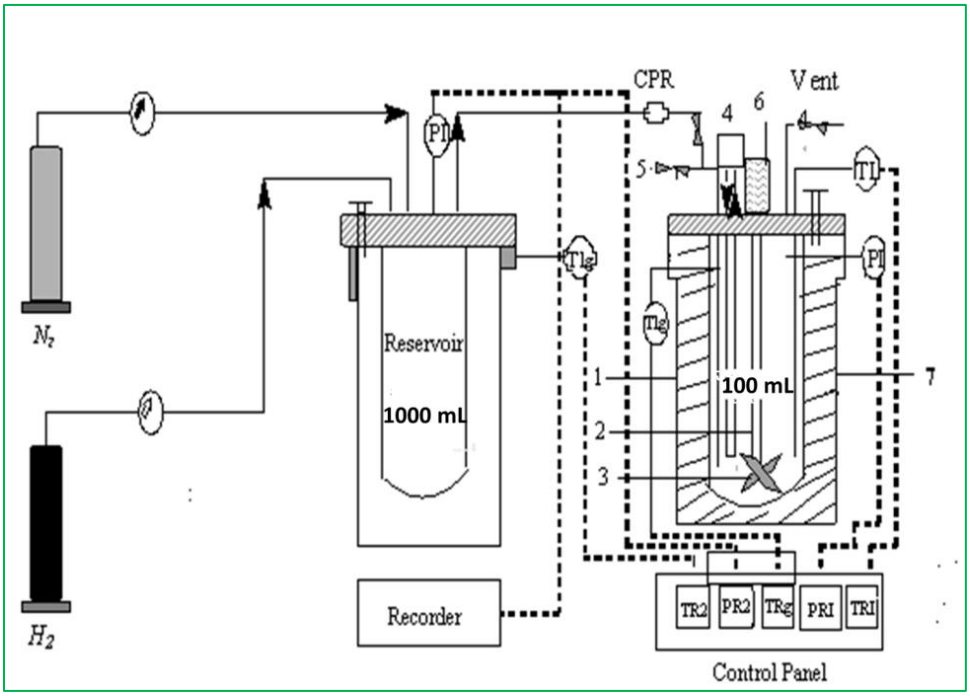

Figure 2.14 *Parr reactor setup; (1) Reactor (2) stirrer shaft (3) impeller (4) cooling water (5) sampling valve (6) magnetic stirrer (7) electric furnace; TI: Thermocouple PI: Pressure transducer TIg: Thermocouple for gas N: Nitrogen cylinder H2: Hydrogen gas cylinder PR: Pressure regulator CPR: Content pressure regulator TR1: Reactor temperature indicator PR1: Reactor pressure indicator TR2: Reservoir temperature indicator TRg: Gas temperature indicator PR2: Reservoir pressure indicator*

In a typical hydrogenation reaction, The reaction contents were first flushed 2-3 times with N_2 gas for the removal of trapped air and then flushed with H_2 gas. Afterwards the temperature was ramped for attaining the desired temperature, the system was then pressurized with H_2 gas to the desired pressure. The reaction were maintained under stirring at 1000 rpm by switching the stirrer on for required time. Initial liquid sample was withdrawn before starting the reaction and the progress of the reaction was monitored by observing the pressure drop in the reservoir as a function of time. When the reaction was over, as indicated by a constant H_2 pressure on the pressure display, the reactor was cooled to room temperature and excess H_2 gas was vented out safely and the reactor contents were discharged. Digital photograph of a Parr reactor is shown in Figure 2.15.

Figure 2.15 *Digital photograph of Parr reactor setup*

Reaction samples were withdrawn at regular time intervals for the analysis using gas chromatography technique and analyzed by GC (Shimadzu GC 2025) having an AB-FFAP (30m, 0.53 mm Id, 1um) column coupled with a FID detector.

The term % conversion and % selectivity used herein are defined as follows:

$$\%, \text{Conversion} = \frac{\text{Intial moles of substrate} - \text{Final moles of substrate}}{\text{Initial moles of substrate}} \text{ x } 100 \qquad (2.7)$$

$$\%, \text{Selectivity} = \frac{\text{moles of product formed}}{\text{moles of substrate consumed}} \text{ x } 100 \qquad (2.8)$$

2.5 CONCLUSIONS

In conclusion, present chapter focuses on to provide details of instruments and methods involved in preparing the ionic liquids studied in this work. Details of how ruthenium and silver ionanofluids were developed along with development details of 5% Ru/C catalyst were also described in this chapter. The experimental details of measurement of density, viscosity, thermal conductivity and acidity measurement of Brønsted acidic ionic liquids is described in this chapter. Experimental details of hydrogenation reaction set up and product analysis are also provided at last. Finally, this chapter gives a general idea about experimental materials, methods and procedures involved in designing of ionic liquids and development of transition metal nanoparticle based ionanofluids.

2.6 REFERENCES

[1] Dewan M.; Kumar A.;Saxena A.; De A.; Mozumdar S. Using Hydrophilic Ionic Liquid, [bmim] BF4 – Ethylene Glycol System as a Novel Media for the Rapid Synthesis of Copper Nanoparticles PLOS ONE 7(2012) 1 e29131

[2] Fukumoto K.; Yoshizawa M.; Ohno H. Room temperature ionic liquids from 20 natural amino acids J Am Chem Soc 127 (2004) 2398-2399

[3] Daniel Salavera. Propiedades Termofísicas de Nuevos Fluidos de Trabajo (H_2O + LiBr + $LiNO_3$ + LiCl + LiI , NH_3 + H_2O + NaOH y NH_3 + H_2O + KOH) para sistemas de Refrigeraciónpor Absorción PhD Thesis (2005) URV, Tarragona, Spain.

[4] Chaudhari S. K.; Salavera D.; Coronas A. Densities, viscosities, heat capacities, and vapor-liquid equilibria of ammonia + sodium thiocyanate solutions at several temperatures J Chem Eng Data 56 (6) (2011) 2861-2869

[5] Elavarasan P.; Kishore K. K. V.; Upadhyayula S. Relative acidity measurement of Bronsted acid functional ionic liquids by UV-spectroscopy Bulletin of the Catalysis Society of India 8 (2009) 107-113

[6] Duan Z.; Gu Y.; Zhang J.; Zhu L.; Deng Y. Proticpyridinium ionic liquids: Synthesis, acidity determination and their performances for acid catalysis J Mol Catal A Chem 250 (2006) 163-168.

Chapter 3

Structural, morphological and thermal properties of imidazolium ionic liquids and ruthenium ionanofluids

Chapter 3 includes designing of ionic liquids with common cation and variable anions. Study of effects of variation of anion counterparts of the ionic liquid on density, viscosity and thermal conductivity of ILs and INFs are presented. In this chapter, ruthenium nanoparticle INFs are developed at room temperature and the effect of ruthenium nanoparticles on improvement of thermal properties is investigated.

3.1 INTRODUCTION

Considering the importance of ruthenium nanoparticles for various potential applications, recently, solute effect on synthesis and stability of ruthenium nanoparticles was studied in IL media [1]. Details on the preparation and associated problems of nanofluids have been presented recently [2]. Today INFs are mostly prepared with nano additives by two-step method: 1) initial preparation of nanomaterial's and 2) their subsequent addition into base ILs. However, in the one-step method, the nanoparticles are formed inside the nanofluid, and their morphology (size, aggregation) is highly dependent on the reaction media, namely on the structural organization of ILs, which play an important role in stabilization of metal nanoparticles. The formation and stabilization of NPs occur with the re-organization of the hydrogen bond network, along with the role played by polar and non-polar regions in ILs [3]. Protection against aggregation and /or agglomeration of NPs is achieved by the formation of IL protective layer composed of imidazolium aggregates at the nanoparticle surface – the IL/NP interface. Such protective layer is active both sterically and electronically in the ultimate control of NPs size. This effect has been discussed in reference [4] for the thermal conductivity of ionanofluids. There are several evidences indicating that non functionalized ILs also interact relatively strongly with the surface of the metal NPs dispersed in ILs [5]. In general metal precursors in the form of metal complexes or metal salts dispersed and/or dissolved in the desired IL is reduced to metal NPs by any of the suitable reducing agents such as ethylene glycol, ascorbic acid, hydrazine [5], hydrogen gas [6], electro reduction [7], and photochemical reduction [8].

Structure of IL is such that the thermophysical properties change with variation of anions of ILs [9]. Particularly Ruthenium nanoparticle colloids in ILs are synthesized by decomposition of organometallic precursor [Ru(COD)(COT)] by molecular hydrogen while additional ligands (1-octylamine, 1-hexadecylamine) is also used during synthesis [10]. Patharkar et al. synthesised ruthenium nanoparticles in ILs by chemical reduction of metal precursor with $NaBH_4$ while sodium dodeycyl sulphate (SDS) was used as a stabilizing agent [11]. Recently ruthenium nanoparticles were prepared at temperature up to 90 ^{o}C in dihydroxyl ILs which acts as solvent, ligand, stabilizer and reducing agent. NPs thus formed in ILs were reported to be successfully used for hydrogenation of unsaturated hydrocarbons [12]**.**

In the present work, we prepared ionanofluids (INFs) with ruthenium in 1-butyl-3-methyl imidazolium cation, by reduction of ruthenium metal precursor with $NaBH_4$ as a reducing agent in one step. To the best of our knowledge, this is the first report of single step, room temperature synthesis of ruthenium INFs without the use of stabilizing agent. IL plays a dual role; as a stabilizing agent and as a solvent. INFs have an emerging future as a new generation heat transfer fluid. Considering the application of INFs as heat transfer fluid in mind, the present work was taken up. Study of the anion effect on structure, stability and thermo physical properties of INFs becomes an essential part of the research for designing new generation heat transfer fluids. In the present work, we studied the effect of halide anions, namely, Cl^-, Br^-, I^- and BF_4^- anion on thermophysical properties like density, viscosity and thermal conductivity of Ru-INFs**.** For comparison anion effects on thermophysical properties of base ILs are also studied. In turn, the anion and cation counterparts' role in stabilization of Ru-INFs and its effect on thermo physical properties are investigated. A possible mechanism of formation (Ru-INFs) has been proposed.

3.2 EXPERIMENTAL

Four halide based ionic liquids with 1-butyl-3-methyl imidazolium as a cation choosed to study effect of anion on structural, morphological and thermal properties of ILs and INFs. With the aim to sythesisize more pure ILs we design four ionic liquids namely 1-Butyl-3-methyl imidazolium Chloride ([C4mim][Cl]), 1-Butyl-3-methyl imidazolium Bromide ([C4mim][Br]), 1-Butyl-3-methyl imidazolium Iodide ([C4mim][I]), 1-Butyl-3-methyl imidazolium Tetrafluroborate ([C4mim][BF_4]) in lab. The ionic liquids designed in lab were further purified to achieve more pure ionic liquids. First three halide anion based ionic liquids were synthesized by direct alkylation reaction while [C4mim][BF_4] ionic liquid was sythesied from anion exchange reaction of 1-butyl-3-methyl imidazolium bromide with sodium tetrafluroborate salt. Designed ionic liquids were further used for the development of ruthenium ionanofluids. With aim to study the effect of anion on thermal properties of ionic liquids and ruthenium INFs we developed ruthenium ionanofluids at room temperature without use of additional stabilizing agents. Reactions and schematic of designing of ILs, purification of ILs and development of ruthenium INFs are given in detail in subsection 2.1.1 and 2.1.2 of chapter 2.

Influence of anions on structures of ILs and INFs were studied with NMR and IR technique. Optical absorptions and stabilities of ILs and INFs was investigated with UV-Visible absorption spectroscopy. Thermal stabilities of ILs and INFs were studied with thermal gravimetry analysis to study the effect of anion. Effect of anion variation on structure and particle size of Ru nanoparticles was studied by high resolution transmission electron microscopy (HR-TEM). X-ray photoelectron spectroscopy (XPS) analysis is performed to know the electronic environment of Ru-INFsfor different anions. Techniques used to characterize ILs and INFs are described in details in section 2.2 of chapter 2. To study the effect of anion variation of ionic liquids and ruthenium INFs density, viscosity and thermal conductivity of ILs and Ru-INFs studied at various temperatures. Details of the equipment used to measure the properties of ILs and INFs are mention in 2.3 of Chapter 2.

3.3 SPECTRAL AND MORPHOLOGICAL CHARACTERISATION AND STABILITY OF ILs AND INFs

Effect of anions on optical absorptions were studied using UV-Visible spectroscopy technique. .

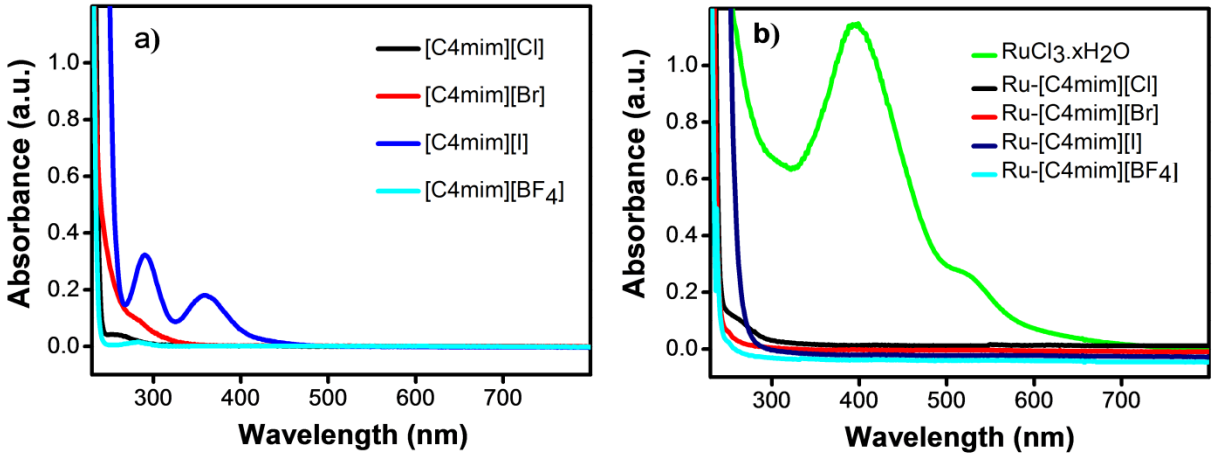

Figure 3.1 *UV–Visible absorption spectra of the base ILs and Ru-INFs along with precursor* $RuCl_3.xH_2O$

Figure 3.1 shows UV-Visible absorption spectra of different ILs and Ru-INFs used in this study Nanosized metal particles exhibit unique optical characteristics with an exponential decay of the

absorption profile with increasing wavelength. The absorption spectra of most commonly used imidazolium ILs show absorbance maxima below 350 nm due to the imidazolium moiety [13]. It is also reported that the long absorption tail is observed beyond 400 nm. It can be seen that, in the cases of ILs, the profiles of the absorption curves beyond 400 nm, are very consistent with the Mie characteristics. Among 4 ILs, [C4mim][I] neat IL shows absorption peaks at 278 and 360 nm while its Ru-INF counterpart i.e. Ru-[C4mim][I], the absorption peaks disappear while the Mie characteristics continue to show its presence. Various Ru-INFs show colors that depend on the formation of Ru nanoparticles after reduction of $RuCl_3.xH_2O$ and its subsequent interaction with ILs. The first significant observation is that the two broad peaks at about 396 and 525 nm shown by Ru precursor in ILs are not observed in any INFs [14]. Thus, metal-ligand transition interaction signatures of Ru precursors are no more continued after INFs formation. These measurements confirm that in each case**,** the Ru^{+3} ions are completely reduced to Ru metal nanoparticles.

Stability of ruthenium ionanofluids further studied using UV-Visible spectroscopy technique. Variation in color appearance and optical absorption of INFs are displayed in Figure 3.2 below.

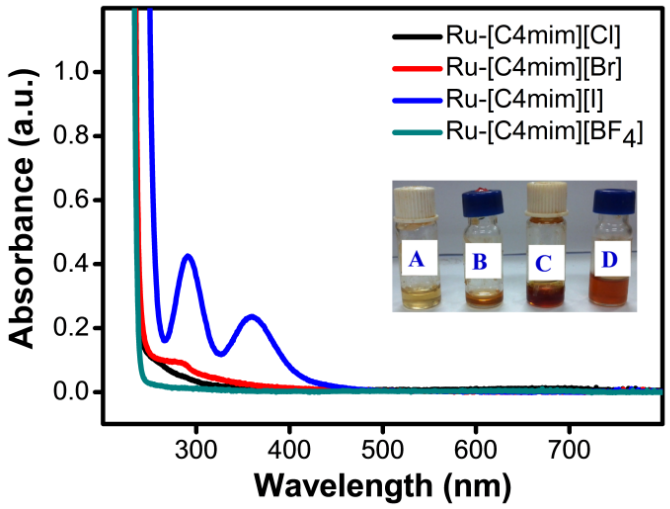

Figure 3.2 *UV–Visible absorption spectra and inset photograph of Ru-[C4mim][Cl], Ru-[C4mim][Br], Ru-[C4mim] [I] and Ru-[C4mim][BF_4] after period of aging of ca.one year*

The colloidal dispersion of ruthenium nanoparticles in ILs was stored in vacuum for the period of one year. If color of INF is any indication of stability, Ru-[C4mim][Cl] and Ru-[C4mim][I], both are incapable to stabilize ruthenium nanoparticles for a period of one year as they change their

color from blue to pale yellow and brown respectively as shown in inset photograph of Figure 3.2. Ru-[C4mim][Cl] and Ru-[C4mim][I] colloidal solutions are stable up to 1.5 and 2 months respectively. Ru-[C4mim][BF_4] INF has same color as a color of freshly prepared INF; however, salt sedimentation is observed at the bottom of the fluid. The colloidal dispersion of Ru-[C4mim][Br] is found to be extremely stable despite the fact that no external surfactant is used for stabilization of INF. UV-Visible of Ru-[C4mim][Br] also reflects same absorption as that for fresh INF.

Figure 3.3 displays, thermal degradation temperatures of base ILs and their corresponding Ru-INFs, indicating the effect of anion variation.

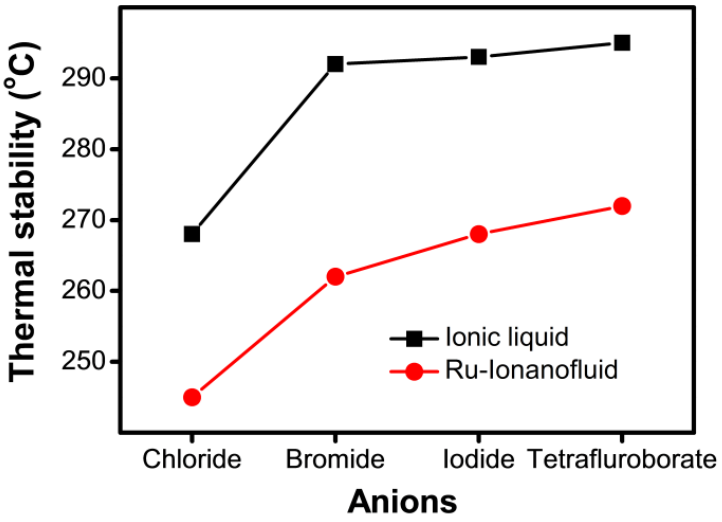

Figure 3.3 *Thermal stabilities of ILs and Ru-INFs as a function of anions*

The thermo gravimetric behaviour of base ILs and Ru-INFs over the temperature range 30 °C – 500 °C at the heating rate of 5 °C/min in nitrogen atmosphere is shown in Figure 3.4 and Figure 3.8. Generally, imidazolium salts have high thermal stability; however, they begin to decompose at around 400 °C [15]. Recent report [15] has shown that the presence of a halide anion reduces the thermal stability of imidazolium ionic liquids. This occurs due to increased nucleophilic and basic character of anions [15] leading to decomposition onset occurring at least a 100 °C below the temperature of decomposition of imidazolium salts as observed in the present work. Thus, the thermal stability of Ru-INFs follows the trend [BF_4] > [I] > [Br] > [Cl] to show the effect of anions

[16]. For ILs and corresponding Ru-INFs, initially, 1 to 4% weight loss occurs up to 100 ^{o}C due to removal of water molecules. Weight loss assigned to evaporation of water, observed in thermogram (Figure 3.5 d)), is understandable as ILs are hygroscopic and water absorption might occur during the handling of sample at the time of sample mounting before measurement. Further, it can be observed in Figure 3.5., that in case of Ru-INFs further weight loss in TGA occurs at temperature 30 ^{o}C lower than that of corresponding IL; which shows decreased thermal stability in Ru-INFs [17]. Imidazolium based ILs that are substituted with methyl group at C2-position were found to be more thermally stable due to removal of the acidic hydrogen [18]. However, this generalization is not consistent in case of [C4mim][BF_4] which does not seem to decompose at the C2-position, suggesting the formation of imidazolium cation [C4mim]$^{+}$, methyl fluoride and BF_3 [19].

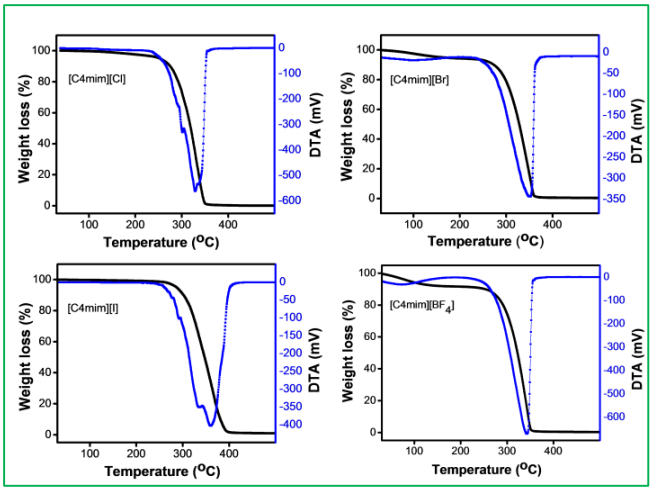

Figure 3.4 *TGA-DTA graph of [C4mim][Cl], [C4mim][Br], [C4mim][I] and [C4mim][BF_4]*

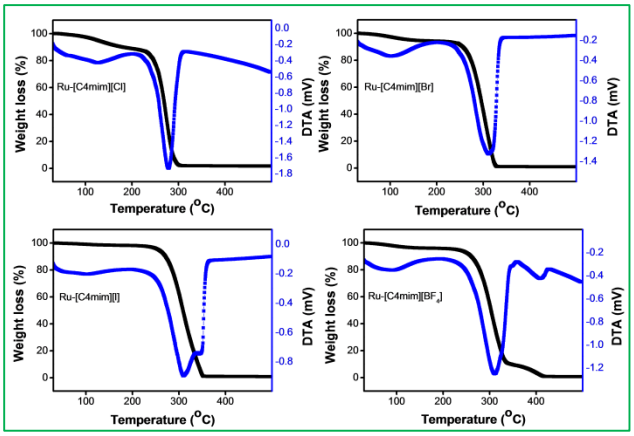

Figure 3.5 *TGA-DTA graph of Ru-[C4mim][Cl], Ru-[C4mim][Br], Ru-[C4mim][I] and Ru-[C4mim][BF_4]*

3.3.1 Influence of anions on bonding of ILs and INFs

Anion variation from ionic liquid counterparts influences the bondings of ILs and INFs the bonding effect of ILs and INFs studied with the help of ATR-IR analysis. Obtained results are shown in Figure 3.6.

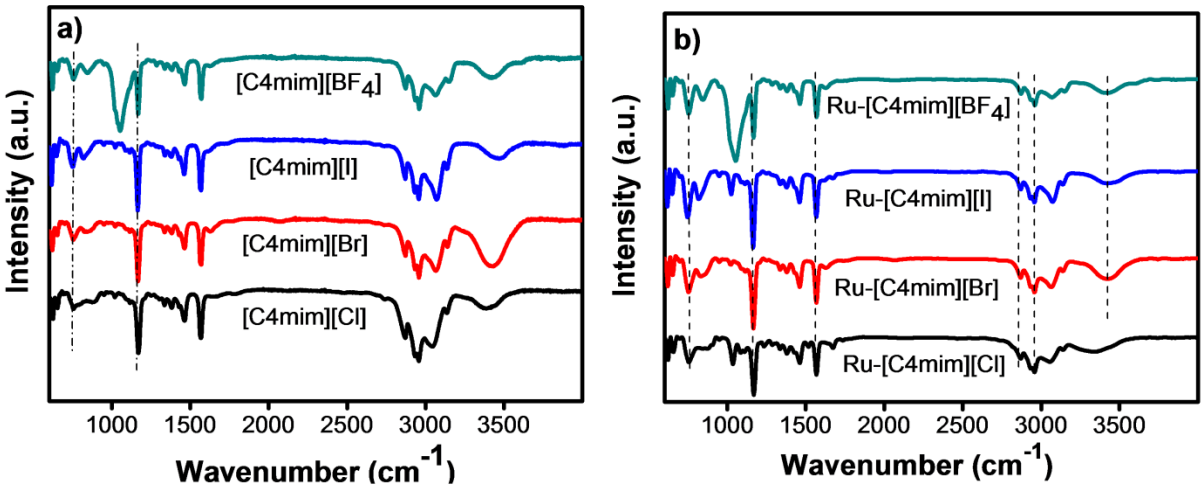

Figure 3.6 *ATR-IR spectrum of a) [C4mim][Cl], [C4mim][C4mim][Br], [C4mim][I], [C4mim][BF_4] b) Ru-[C4mim][Cl], Ru-[C4mim][Br], Ru-[C4mim][I] and Ru-[C4mim][BF_4]*

ATR-IR spectra are useful to find out bonding changes in the ILs and ILs composite materials. IR absorption spectra were recorded in the range of 600–400 cm^{-1} for parent/base ILs and neat Ru-

INFs. From the Figure 3.6 a) , all ILs show characteristic peaks in the range 3550–3300 cm^{-1} assigned to the (quaternary amine salt formation with anion) [20], 3200–2800 cm^{-1} (C-H stretching in the imidazole ring) [21], 1164 cm^{-1} (imidazole H-C-C and H-C-N bending carbine species [22], near 840 cm^{-1} (C-N stretching vibration) [18], 752 cm^{-1} (out of plane C-H bending of imidazole ring) and 648 cm^{-1} (imidazole C-N-C bending) [23]. The $[C4mim]^+$ can further be identified by spectral features in the range of 700-550 cm^{-1}, 1800-1130 cm^{-1} and 3200–2800 cm^{-1} [24]. The peak at 1056 cm^{-1} is due to B-F stretching vibration of $[BF_4]^-$ anion [25,26]. Figure 3.6 b) shows ATR-IR spectra of all neat Ru-INFs recorded at the same conditions of the base ILs. The peak values are given in Table 1 below. It may be noted from Figure 3.6 that the peak intensities of imidazolium ring C-H (3200-2800 cm^{-1} and imidazolium ring (C-H stretch (1600–1500 cm^{-1}) are lowered and shifted in comparison to corresponding neat and base ILs respectively. This is attributed to the strong interaction between $[C4mim]^+$ cation and Ru metal in the composite materials. The characteristic bands and their corresponding vibration mode are tabulated in Table 3.1.

Table 3.1 *ATR-IR spectral assignements of ILs and Ru-INFs*

Entry	Wavenumber (cm^{-1})	Assignment	Reference
1	3550-3300	Quaternary amine salt	[39]
2	3200-2800	C-H stretching in imidazole ring	[40]
3	1164	Imidazole H-C-C & H-C-N bending carbine species	[41]
4	Near 840	C-N stretching vibrations	[39]
5	700-550, 1800-1130, 3200-2800	$[C4mim]^+$	[43]
6	1056	B-F stretching vibrations	[38],[39]
7	1600-1500	C-H stretching	[43]

The inference from IR studies is Ru-INFs with various anions are formed as intended and also there are specific signatures of Ru interaction with IL reflected in the spectra. This inference is consistent with the conclusion drawn from UV-Visible absorption studies.

3.3.2 X-ray photoelectron spectroscopy study of ILs and INFs

To validate the chemical nature of Ru species in INFs and its interactions within imidazolium based ILs, chemical analysis of the Ru-INFs was performed using XPS. The surface sensitive technique of XPS can provide important information about the interactions of chemical species present near surface of samples [29]. Since this study focuses on the influence of the anion on the electronic structure of the imidazolium cation, only the C1s and N1s spectra will be discussed. To identify the interaction between imidazolium cation and Ru, a curve-fitting procedure was employed to analyze C1s and Ru3d, high resolution XPS results. The samples of Ru-INFs give a multi component C1s spectrum with five binding energy components. Observed binding energies (B.E.s) are at 280.0, 284.1, 285, 286.4 and 288.5 eV.

Figure 3.7. shows the XPS spectra within the binding energy range 275-292 eV for all four Ru-INFs.

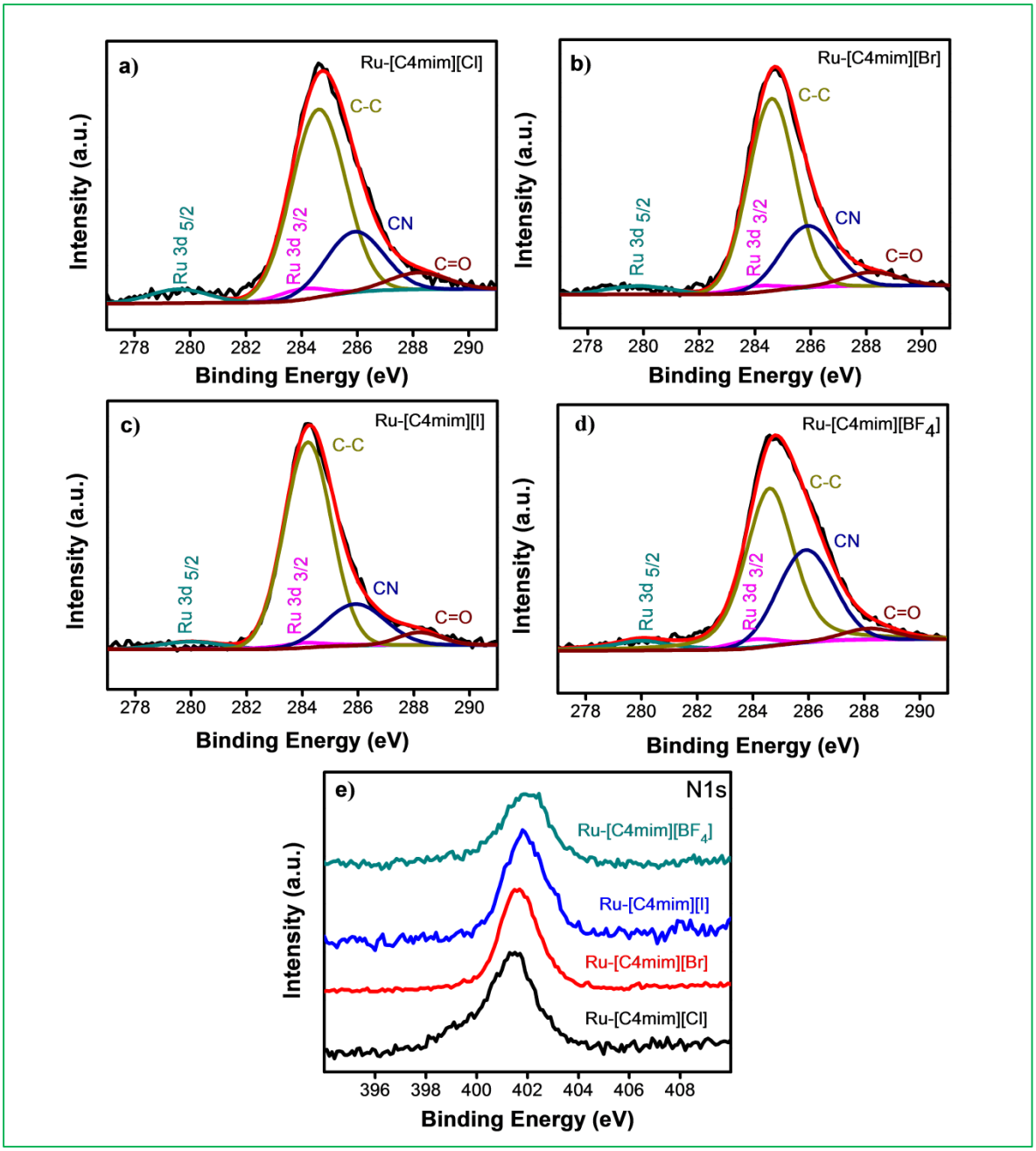

Figure 3.7 *XPS spectra of a), b), c), d) the C1S, Ru 3d 5/2 and Ru 3d 3/2 for four Ru-INFs which are deconvoluted to resolve individual components. The dotted lines correspond to nonlinear least-square fits to the experimental data and e) the N1s spectra of four Ru-INFs*

The peak at 280.0 and 284.1 eV corresponds to Ru $3d_{5/2}$ and Ru $3d_{3/2}$ respectively in metallic Ru with the energy separation of 4.1 eV [28]. The peak at 285.0 eV is assigned to C atoms in an alkyl chain [27] and is denoted as C_{alkyl}. The second feature in the C1s region is the peak /shoulder at higher B.E. than that of C_{alkyl}. Such a peak at higher B.E. than that of C_{alkyl} is due to C-N bonds formed with more electronegative nitrogen atoms of the imidazolium ring [48]. Such a bond has been reported in the literature and called as C_{hetero} [29]. Further, the peak separation in B.E. of C_{hetero} and C_{alkyl} is larger in anion (Cl^-) having the high coordinating ability of anion (Cl^-) than that of (BF_4^-) anion, consistent with the earlier results [27]. Still, it cannot rule out the possibility of the presence of chemisorbed oxygen, in the form of hydroxyl, carbonyl/carboxyl species on Ru surface, as indicated by C1s spectrum showing peaks at 286.3 eV (carbonyl carbon) and 288.0 eV (carboxyl carbon) [30]. This suggests the presence of the oxygen-containing contaminants at NP surface. The low intensity signal of Ru3d XPS spectrum is attributed to low content of Ru and alternatively can be attributed to the masking of Ru NPs with ILs. The corresponding N1s spectra are displayed in Figure 3.7 e). For all ILs a symmetric peak is observed at around 402 eV. It is known that such a peak is due to the presence of two nitrogen atoms of imidazolium ring; however, these nitrogen atoms are indistinguishable by XPS [31,32]. Although, the signal for Ru NPs in XPS is weak, its presence is ascertained by EDAX (Figure 3.8) studies which show a clear signal for Ru.

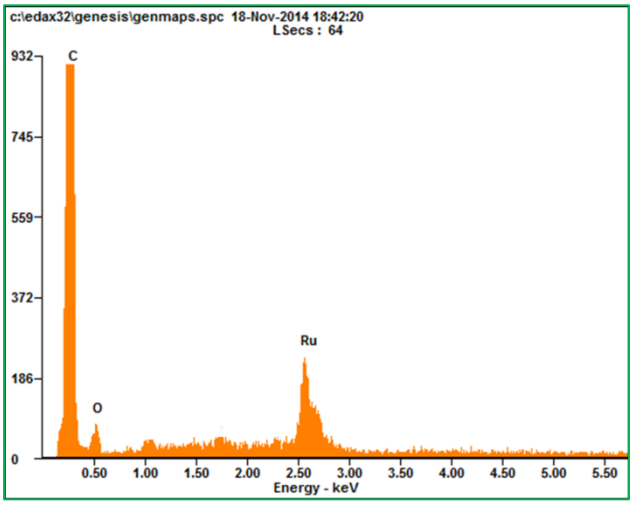

Figure 3.8 *EDAX spectrum of Ru-[C4mim] [Br]*

To summarize XPS results it can be inferred that for small size and high coordinating ability of anions, show the B.E. with lower values. As against this the highest B.E. values are recorded for large size and least coordinating anions like $[BF_4]^-$. The details of qualitative analysis of all spectra are given in the Table 3.2 below.

Table 3.2 *Binding energies assignments for ruthenium ionanofluids*

Entry	Compound	Assignments of XPS binding energies (eV)				
		C-C	C=N	C-O	Ru 3d $_{5/2}$	Ru 3d $_{3/2}$
1	Ru-[C4mim][Cl]	284.6	285.9	288.2	280	284.1
2	Ru-[C4mim][Br]	284.6	285.9	288.2	279.8	283.9
3	Ru-[C4mim][I]	284.6	286.3	288.6	280.4	284.4
4	Ru-[C4mim][BF_4]	284.6	285.9	288.2	279.9	284

3.3.3 Morphology of Ru nanoparticles

The general observations to be noted from TEM are 1) 'Cl' anions in INF form particles smaller (< 3 nm) and most probably spherical. 2) 'Br', I and 'BF_4' anions in INF form spherical particles with increasing size in that order. The respective histograms of Ru NPs in Ru-INFs samples are also shown in corresponding insets.

From HR-TEM image, the planes of crystal growth of the Ru-INFs nanoparticles is ascertained from the fringes observed (shown in the corresponding insets). In the insets of Figure 3.9., very clear lattice fringes with the fringe spacing of 0.23 nm is observed, which is in good agreement with the space between the Ru (100) lattice planes (JCPDS File No. 01-1253). The conventional double layer formation mechanism of stabilization of NPs in ILs (DLVO theory) does not explain many experimental results. Also, we have mentioned above that a metal particle in IL is a complex system as IL itself behaves as a 'supramolecular' entity.

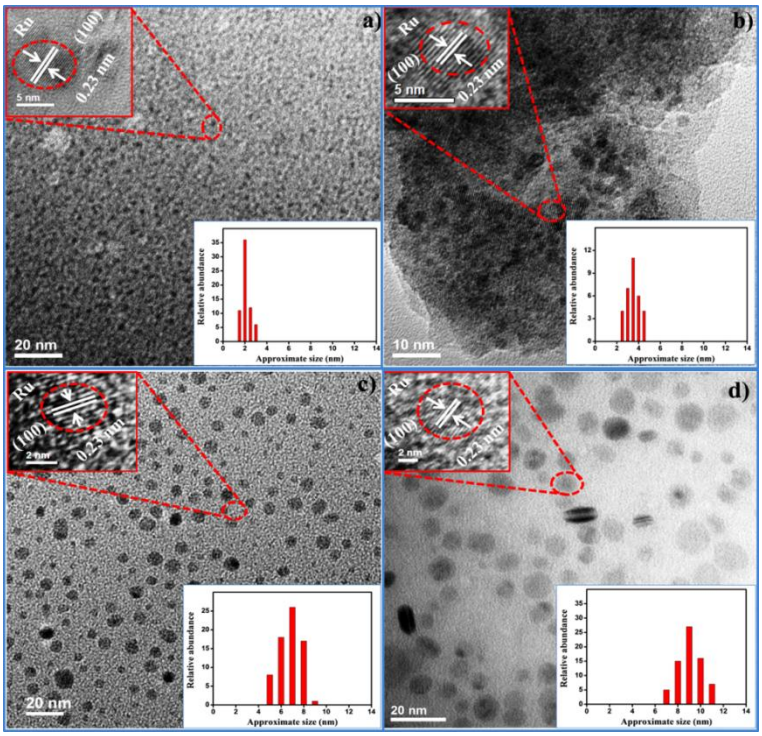

Figure 3.9 *TEM, HR-TEM micrographs and particle size histogram of a) Ru-[C4mim][Cl], b) Ru-[C4mim][Br], c) Ru-[C4mim][I], d) Ru-[C4mim][BF_4]*

The recent theoretical studies suggest that Ru(0) nanoparticles in imidazolium-based ILs preferentially get solvated by the charged moieties of the ions, forming one layer thick interface [33]. This has been observed for MWCNT's also in [C4mim][BF_4] [4]. Consequently, it implies that both cations and anions are in actual contact with the particle surface, forming a 'capping' and thus protecting it from further growth. Such observation is reported in case of Pd(0) nanoparticles surface in close contact with IL [34]. In our XPS study, a possibility of the formation of N-heterocyclic carbenes is suggested. This is consistent with the suggestion where alkyl-imidazolium salt interacts with metal NP surface [35]. Moreover, the possibility of an oxide layer on metal NP was suggested in XPS studies which also can be a cause of the stabilization of metal nanoparticles [36]. The oxide formation can also be reasoned out as a consequence of the hygroscopic nature of IL and its subsequent effects as shown in TGA-DTA studies.

3.3.4 Effect of hydrogen bonding on particle size of ruthenium nanoparticles

The data from the characterization of Ru-INFs and imidazolium salt are expected to be compatible with the structures of IL salt and Ru-INF. We have used non functionalized ILs to develope Ru-

INF and studied the effect of anion on base ILs and Ru-INFs. The characteristics of base IL salts are well reported by Du pont and Scholten [6]. We make use of this model to explain the data collected in the present study. The model proposes IL to be supramolecular structure formed by the effective contribution of hydrogen bonds, polar and nonpolar entities of ILs along with a contribution of Van der Waal forces.

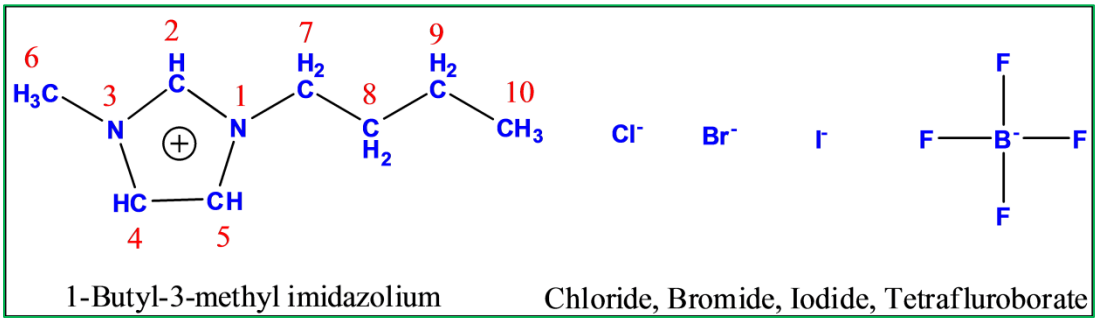

Figure 3.10 *Chemical structure of typical imidazolium cation and anions associated with it*

In order to evaluate the nature of different interactions such as hydrogen bonding between cation and anion in any given IL, ^{1}H and ^{13}C NMR spectra of the base and neat ILs were recorded [29]. The H/D and D/H labeling measurements were also useful to assess the interaction between imidazolium ILs and metal NPs.

For all ILs, the spectra arising from the H^2, H^4 and H^5 protons and the corresponding C^2, C^4 and C^5 carbon atoms of the cation (labeled in Figure 3.10) are shown Figure 3.12 and Figure 3.13. Both the ^{1}H and ^{13}C NMR spectra show anion dependant shifts. The C(2)-H proton showed the chemical shift of 9.48, 9.28, 8.78 and 8.71 ppm, respectively for [C4mim] X (X=Cl, Br, I and BF_4). All peaks shift towards lower ppm values when going from small size to larger size anions. Other important criteria for possible hydrogen bonding are basicity and strongly coordinating capability of anions.

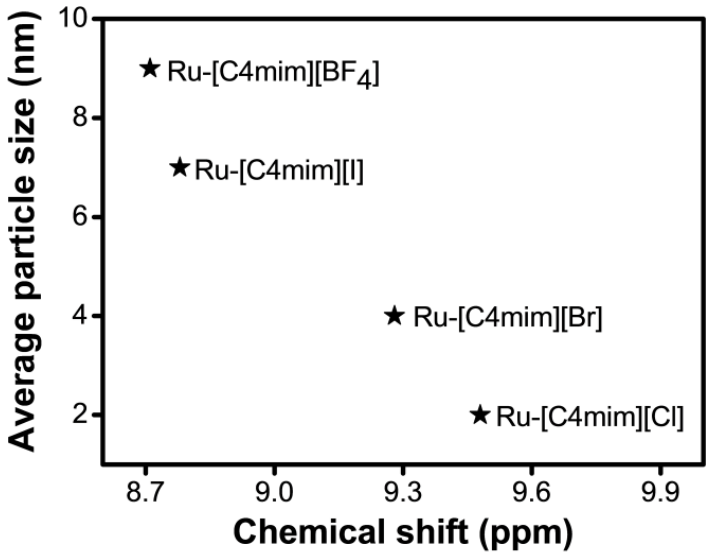

Figure 3.11 *Plot of ^{1}H NMR chemical shift of C(2)-H proton from Ru-INFs versus their average particle size obtained for their respective ruthenium ionanofluids*

Lower basicity and weaker coordinating anions also show NMR shift of low ppm. This is an indication of lowering of hydrogen bonding in the formation of supramolecular structure of the IL around Ru NPs. Such a trend is in good agreement with previous work [29]. As per the differential functional theory (DFT) ion-pair model calculations, halide anions are expected to be in plane of imidazolium ring while BF_4^- is believed to be located above the imidazolium ring and thus farther away from C(2)-H hydrogen, resulting into weak hydrogen bonding [37]. This is in support of our inference stated above.

Obtained results suggets that particle size of Ru nanoparticles can be monitored by the use of specific anion. Figure 3.11 shows the observed relation between chemical shift of C(2)-H proton and particle size. Thus, the average particle size increases in the order (2 nm) Cl < (4nm) Br < (7nm) I < (9 nm) BF_4. However, we are aware of the fact that particle size of ruthenium NPs is also dependent on the stabilizing factors (electrostatic or steric stabilization) as proposed in reference [38].

^{1}H NMR and ^{13}C NMR analysis of ionic liquids

Figure 3.12 (a), b), c), d)) shows ^{1}H NMR spectra of 1-Butyl-3-methyl imidazolium halide ionic liquids used in present research study. The NMR peak assignments were made on the basis of chemical shifts and peak integrals of ^{1}H NMR spectrum and verified with ^{13}C NMR spectra as shown in Figure 3.13 (a), b), c), d)).

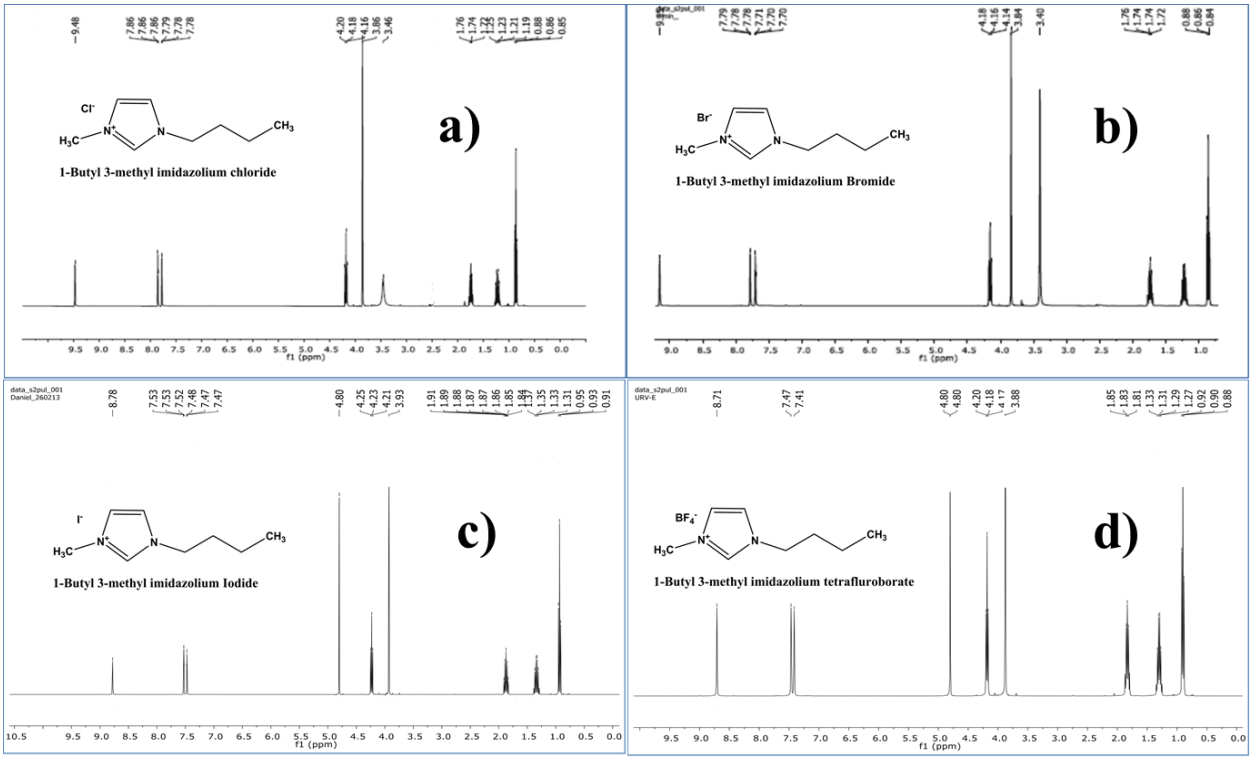

Figure 3.12 *^{1}H NMR spectra of a) 1-Butyl-3-methyl imidazolium Chloride ([C4mim][Cl]), b) 1-Butyl-3-methyl imidazolium Bromide ([C4mim][Br]), c) 1-Butyl-3-methyl imidazolium Iodide ([C4mim][I]), d) 1-Butyl-3-methyl imidazolium Tetrafluroborate ([C4mim][BF$_4$])*

a) ^{1}H NMR of 1-Butyl-3-methyl imidazolium Chloride ([C4mim][Cl]), ^{1}H NMR(400MHz: D2O; δ/ppm relative to TMS): 0.86 (3H, t, but-CH3), 1.23 (2H, m, CH2), 1.74 (2H, m, CH2), 3.46 (2H, t, NCH2), 4.16 (3H, s, NCH3), 7.78 (1H, s, NCH), 7.86 (1H, s, NCH), 9.48 (1H, s, NCHN)

b) ^{1}H NMR spectra of 1-Butyl-3-methyl imidazolium Bromide ([C4mim][Br]), ^{1}H NMR (400MHz: D2O; δ/ppm relative to TMS): 0.84 (3H, t, but-CH3), 1.42 (2H, m, CH2), 1.74 (2H, m,

CH2), 3.40 (2H, t, NCH2), 3.84 (3H, s, NCH3), 7.70 (1H, s, NCH), 7.78 (1H, s, NCH), 9.28 (1H, s, NCHN)

c) H^1 NMR spectra of 1-Butyl-3-methyl imidazolium Iodide ([C4mim][I]), ^{1}H NMR (400MHz: D2O; δ/ppm relative to TMS): 0.93 (3H, t, but-CH3), 1.35 (2H, m, CH2), 1.86 (2H, m, CH2), 3.93 (2H, t, NCH2), 4.23 (3H, s, NCH3), 7.47 (1H, s, NCH), 7.53 (1H, s, NCH), 8.78 (1H, s, NCHN)

d) H^1 NMR spectra of 1-Butyl-3-methyl imidazolium Tetrafluroborate ([C4mim][BF_4]), ^{1}H NMR (400MHz: D2O; δ/ppm relative to TMS): 0.90 (3H, t, but-CH3), 1.31 (2H, m, CH2), 1.83 (2H, m, CH2), 3.88 (2H, t, NCH2), 4.18 (3H, s, NCH3), 7.41 (1H, s, NCH), 7.47 (1H, s, NCH), 8.71 (1H, s, NCHN)

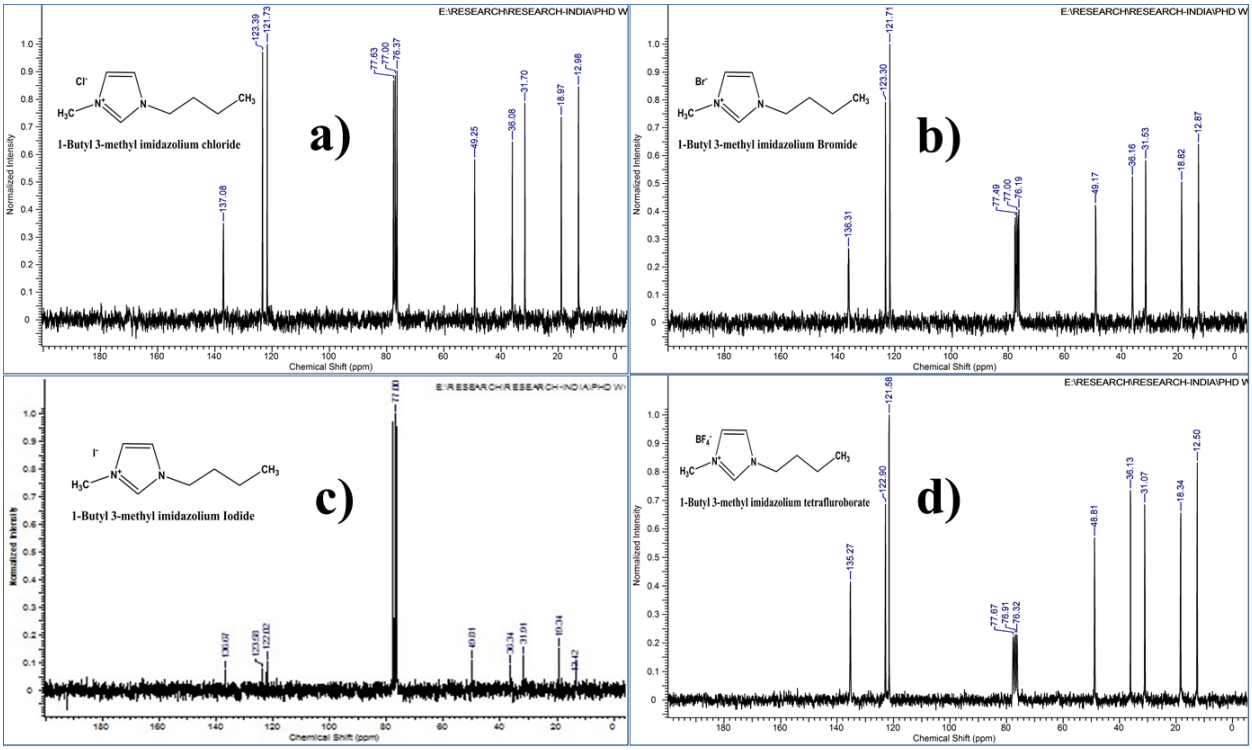

Figure 3.13 *^{13}C NMR spectra of of a) 1-Butyl-3-methyl imidazolium Chloride ([C4mim][Cl]) b) 1-Butyl-3-methyl imidazolium Bromide ([C4mim][Br]) c) 1-Butyl-3-methyl imidazolium Iodide ([C4mim][I]) d) 1-Butyl-3-methyl imidazolium Tetrafluroborate ([C4mim][BF_4])*

a) ^{13}C NMR spectra of 1-Butyl-3-methyl imidazolium Chloride ([C4mim][Cl]) ^{13}C NMR (200 MHz: $CDCl_3$; δ/ppm relative to TMS): 12.98 (3H, but-CH3), 18.97 (2H, CH2), 31.70 (2H, CH2), 36.08 (3H, NCH3), 49.25 (2H, NCH2), 121.73 (1H, NCH), 123.39 (1H, NCH), 137.08 (1H, NCHN)

b) ^{13}C NMR spectra of 1-Butyl-3-methyl imidazolium Bromide ([C4mim][Br]) ^{13}C NMR (200 MHz: $CDCl_3$; δ/ppm relative to TMS): 12.87 (3H, but-CH3), 18.82 (2H, CH2), 31.53 (2H, CH2), 36.16 (3H, NCH3), 49.17 (2H, NCH2), 121.71 (1H, NCH), 123.30 (1H, NCH), 136.31 (1H, NCHN)

c) ^{13}C NMR spectra of 1-Butyl-3-methyl imidazolium Iodide ([C4mim][I]) ^{13}C NMR (200 MHz: $CDCl_3$; δ/ppm relative to TMS): 12.12 (3H, but-CH3), 19.34 (2H, CH2), 31.91 (2H, CH2), 36.31 (3H, NCH3), 49.81 (2H, NCH2), 122.02 (1H, NCH), 123.33 (1H, NCH), 136.07 (1H, NCHN)

d) ^{13}C NMR spectra of 1-Butyl-3-methyl imidazolium Tetrafluroborate ([C4mim][BF_4]) ^{13}C NMR (200 MHz: $CDCl_3$; δ/ppm relative to TMS): 12.50 (3H, but-CH3), 18.34 (2H, CH2), 31.07 (2H, CH2), 36.13 (3H, NCH3), 48.81 (2H, NCH2), 121.58 (1H, NCH), 122.90 (1H, NCH), 135.27 (1H, NCHN)

3.4 INFLUENCE OF ANION ON THERMAL PROPERTIES

In this study we vary the anions of ILs and INFs and studied their properties density, viscosity and thermal conductivity for investigation of anion influence on heat transport properties. This section describes in detail the effect of anions on heat transport properties of designed ionic liquids and developed ruthenium ionanofluids.

Effect on density of ILs and INFs

Knowledge of density of ILs and INFs is important from the viewpoint of applications, especially for future process and equipment design. Figure 3.14 shows the experimental densities of [C4mim] halides and tetrafluroborate ionic liquids along with their corresponding Ru-INFs at temperatures from 20 ºC to 70 ºC. Experimantal values are collected in Table 3.3.

Table 3.3 *Density variation with temperature for pure ionic liquids and for IoNanofluids (IL+Ru), at atmospheric pressure*

T/K	293.15	303.16	313.14	323.14	333.14	343.14
Fluid			ρ/g·cm^{-3}			
[C4mim][Cl]	1.0869	1.0824	1.0777	1.0732	1.0684	1.0637
Ru-[C4mim][Cl]	1.0931	1.0872	1.0811	1.0752	1.0695	1.0637
[C4mim][Br]	1.2977	1.2898	1.2822	1.2745	1.2670	1.2591
Ru-[C4mim][Br]	1.2760	1.2670	1.2626	1.2569	1.2516	1.2447
[C4mim][I]	1.4890	1.4836	1.4762	1.4693	1.4637	1.4563
Ru-[C4mim][I]	1.4372	1.4250	1.4133	1.4011	1.3894	1.3771
[C4mim][BF4]	1.2712	1.2688	1.2623	1.2541	1.2486	1.2398
Ru-[C4mim][BF4]	1.2546	1.2476	1.2406	1.2336	1.2227	1.2198

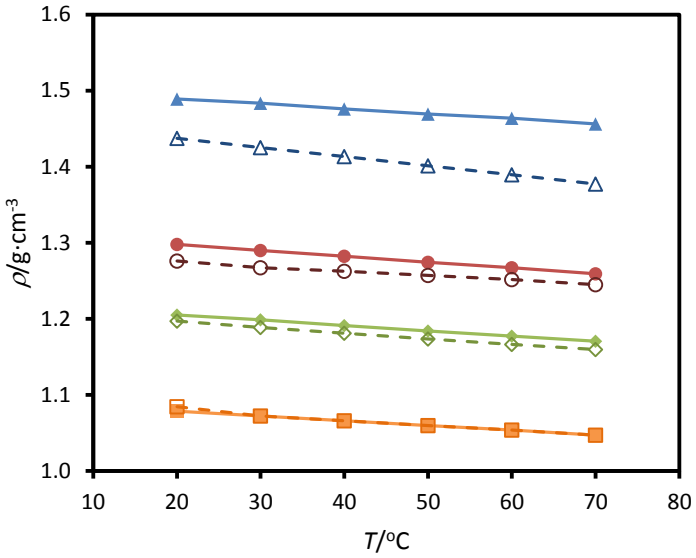

Figure 3.14. Experimental densities of the dried ionic liquids and their respective Ru-INFs as a function of temperature: (■), [C4mim][Cl] ; (-□-), Ru-[C4mim][Cl] ; (●), [C4mim][Br]; (-○-), Ru-[C4mim][Br]; (▲), [C4mim][I]; (-△-), Ru-[C4mim][I]; (◆), [C4mim][BF_4]; (-◇-), Ru-[C4mim][BF_4]

Obtained densities are decreasing linearly with rise in temperatures. As the molar mass of an anion increase, densities also increase [39]. As the molar mass of the anion grows with similar cation it significantly enhances the density of ILs [40]. From Figure 3.14., it can be seen that densities of

halides based ILs significantly rises from Cl^- to I^- anions due to increase in molar mass of ILs. Consistent with this trend, it was expected that the density of [C4mim][BF_4] should be more than [C4mim][Br], as against that it is clearly observed that densities of [C4mim][Br] are higher that [C4mim][BF_4]. The higher density of [C4mim][Br] than [C4mim][BF_4] is assigned to compactness between cation and anion [41]. For all ILs and INFs shown in Figure 3.14, it is observed that densities linearly decrease with increasing temperature which is consistent with the literature [42,43]. The smallest chloride anion in [C_4mim][Cl] INF shows the same density as that of base IL. However, as size of halide anion increases in the order $Cl^- < Br^- < I^-$, the densities of Ru-INF turn out to be lower than that of base IL.

Effect on viscosity of ILs and INFs

The viscosity is related to the internal resistance of a fluid to a shear stress and the rheological measurements can provide useful information about the microstructure of fluids. Viscosities of pure imidazolium based ILs and their respective Ru-INFs measured at different temperatures from 30 ºC to 100 ºC are presented in Table 4 and Figure 3.15.

Table 3.4 *Viscosity variation with temperature for pure ionic liquids and for IoNanofluids (IL+Ru), at atmospheric pressure*

T/K	303.15	313.15	323.15	333.15	343.15	353.15	363.15	373.15
Fluid				η/mPa·s				
[C4mim][Cl]				545	272	147	88.2	56.2
Ru-[C4mim][Cl]	566	290	155	82.2	52.3	37.6	26.5	17.4
[C4mim][Br]	215	118	73.8	47.6	31.9	22.1	16.1	12.3
Ru-[C4mim][Br]	58.9	35.3	24.6	17.5	12.2	9.9	7.3	5.9
[C4mim][I]	379	202	119	73.7	47.3	32.4	23.1	17.3
Ru-[C4mim][I]	54.5	34.2	23.8	14.4	10.5	8.1	6.2	4.8
[C4mim][BF4]	76.9	50.0	34.3	24.5	18.0	13.7	11.0	8.9
Ru-[C4mim][BF4]	40.0	25.1	14.8	10.1	7.0	4.9	3.4	2.6

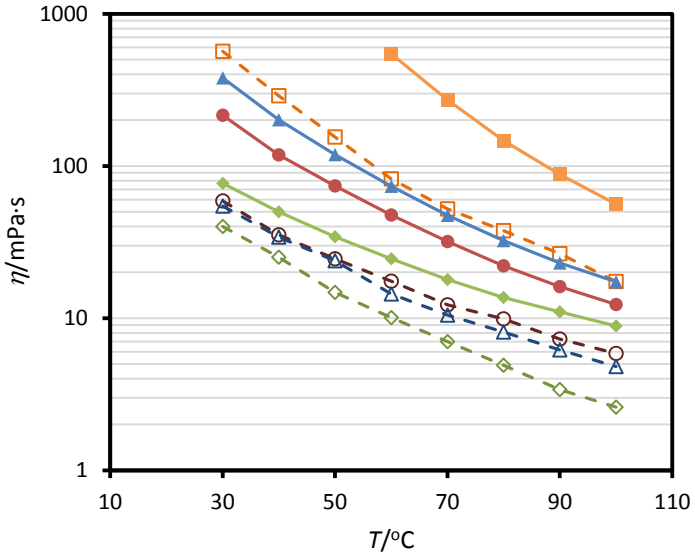

Figure 3.15. Experimental viscosities of the ionic liquids and their Ru-INFs as a function of temperature: (■), [C4mim][Cl] ; (-□-), Ru-[C4mim][Cl] ; (●), [C4mim][Br]; (-○-), Ru-[C4mim][Br]; (▲), [C4mim][I]; (-△-), Ru-[C4mim][I]; (◆), [C4mim][BF_4]; (-◇-), Ru-[C4mim][BF_4]

Viscosities of ILs and INFs decreased with increase in temperature, as expected. Also, the present experimental data show that the viscosities of ILs get lowered following the trend [C4mim][Cl] > [C4mim][I] > [C4mim][Br] > [C4mim][BF_4]. The important parameters that decide the viscosity of IL are hydrogen bonding, symmetry of the ions, interaction of cation and anion and van der Waals forces. Considering the structures of ILs with anions under consideration, i.e. Cl^-, Br^-, and I^-, hydrogen bonding, symmetry of the ions and interaction of cation and anion, would be qualitatively same. However, the particle size of anions would change the quantitative contribution of each parameter. As plotted in Figure 3.15., the viscosity of INFs (0.003 M Ru) dramatically decreases with increasing temperature [44,45]. Since, increase of temperature has weakened the effect of the parameters mentioned above, leads to lowering of viscosity [46]. The extent of

lowering of viscosity of Ru-INFs shows the trend in the order, Ru-[C4mim][Cl] > Ru-[C_4mim][BF_4] > Ru-[C_4mim][Br] > Ru-[C4mim][I]. In fact, the viscosity of the resulting Ru-INFs was found to be lower than that of base ILs, because of the lower density and the lubricating properties of NPs [47]. Normally, it is desired to have low viscosity, heat transfer fluid in industrial applications as it lowers the pumping cost. Low viscosity of ruthenium INFs as compared to base ILs is favorable for their potential application as heat transfer fluids.

Effect on thermal conductivity of ILs and INFs

Thermal conductivity data from 20 ºC to 60 ºC at atmospheric pressure for ILs and Ru-INFs (0.003 M Ru) are shown in Table 3.5 and Figure 3.16.

Table 3.5 *Thermal conductivity variation with temperature for pure ionic liquids and for IoNanofluids (IL+Ru), at atmospheric pressure*

T/K	293.15	303.16	313.14	323.14	333.14
Fluid			$\lambda(W\cdot m^{-1}\cdot K^{-1})$		
[C4mim][Cl]	0.176	0.176	0.174	0.173	0.173
Ru-[C4mim][Cl]	0.177	0.176	0.175	0.175	0.174
[C4mim][Br]	0.160	0.160	0.159	0.158	0.155
Ru-[C4mim][Br]	0.161	0.160	0.160	0.159	0.158
[C4mim][I]	0.131	0.130	0.130	0.130	0.129
Ru-[C4mim][I]	0.135	0.134	0.134	0.133	0.133
[C4mim][BF4]	0.162	0.162	0.161	0.161	0.160
Ru-[C4mim][BF4]	0.168	0.166	0.165	0.164	0.163

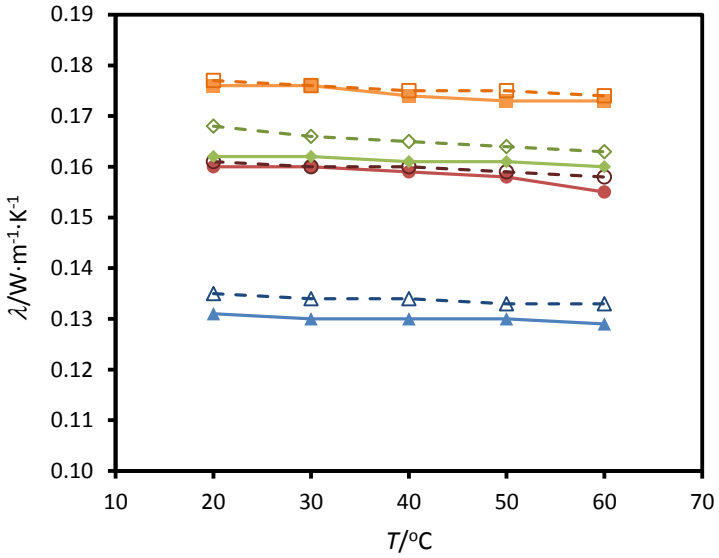

Figure 3.16. Experimental thermal conductivities of the dried ionic liquids and their respective Ru-INFs as a function of temperature: (■), [C4mim][Cl] ; (●), Ru-[C4mim][Cl] ; (▲), [C4mim][Br]; (▼), Ru-[C4mim][Br]; (◄), [C4mim][I] ; (►), Ru-[C4mim][I]; (♦), [C4mim][BF_4] ; (*), Ru-[C4mim][BF_4].

The low thermal conductivity values in base ILs indicate that these ILs are relatively poor thermal conductors. However, the thermal conductivity for Ru-INFs shows an enhancement of thermal conductivity of about 4% with addition of just 0.003 M Ru precursor. It may be pointed out from Figure 3.16, that smaller the anionic size, higher the thermal conductivity values. The experimental values show the thermal conductivity decreases, following the order [C_4mim][Cl] > [C_4mim][Br] > [C_4mim][BF_4] > [C_4mim][I]. The thermal conductivity enhancement in traditional nanofluids and ionanofluids has been discussed in numerous papers [5, 4, 48-52]. The thermal conductivity of the Ru-INFs composite depends on thermal conductivity of base ILs and thermal conductivity of solid Ru NP and its volume fraction in composite [53]. Various mechanisms have been proposed to account for the enhancement in thermal conductivity of the suspensions. The most important points which need consideration are (i) Brownian motion of the nanoparticles suspended in fluid,

(ii) liquid stacking at the particle / liquid interface, and its extension in space (iii) heat transport within the nanoparticles, nanoparticle clustering [54] and particle surface chemistry [53-55].

Deviation of imidazolium halide ionic liquids data with literature data:

Experimental data of density ρ, viscosity η and thermal conductivity λ of the ionic liquids studied were fitted with temperature T using polynomial equations (Eq 3.1-3.3).

$$\rho/\mathrm{kg\cdot m^{-3}} = a_1 + a_2\cdot(T/\mathrm{K}) \quad (3.1)$$

$$\mathrm{Ln}(\eta/\mathrm{mPa\cdot s}) = b_1 + b_2\cdot(T/\mathrm{K}) + b_3\cdot(T/\mathrm{K})^2 \quad (3.2)$$

$$\lambda/\mathrm{W\cdot m^{-1}\cdot K^{-1}} = c_1 + c_2\cdot(T/\mathrm{K}) \quad (3)$$

where a_1, a_2, b_1, b_2, b_3, c_1 and c_2 are the fitting coefficients.

Density values from this study and literature were compared using Eq.(3.1), and the deviations are shown in Figure 3.17. for the pure ionic liquids. In the case of the [C4mim][BF_4] ionic liquid, only some references were selected, because the number of them in literature is large, and the deviations were lower than 0.4 %. For the other ionic liquids the literature data are scarce and scattered. For [C4mim][Cl], our data agree with refs.[65,67] but less with refs.[64,66]. All of them used the vibrating-tube technique. For [C4mim][I] our data agree with ref.[68] how used the vibrating-tube technique, but do not agree with refs.[56,67,69] who used a pycnometer to determine the density. Finally, for [C4mim][Br] only two references were found [15,69], using the vibrating-tube and pycnometer techniques, respectively. Deviations were lower than 1 %.

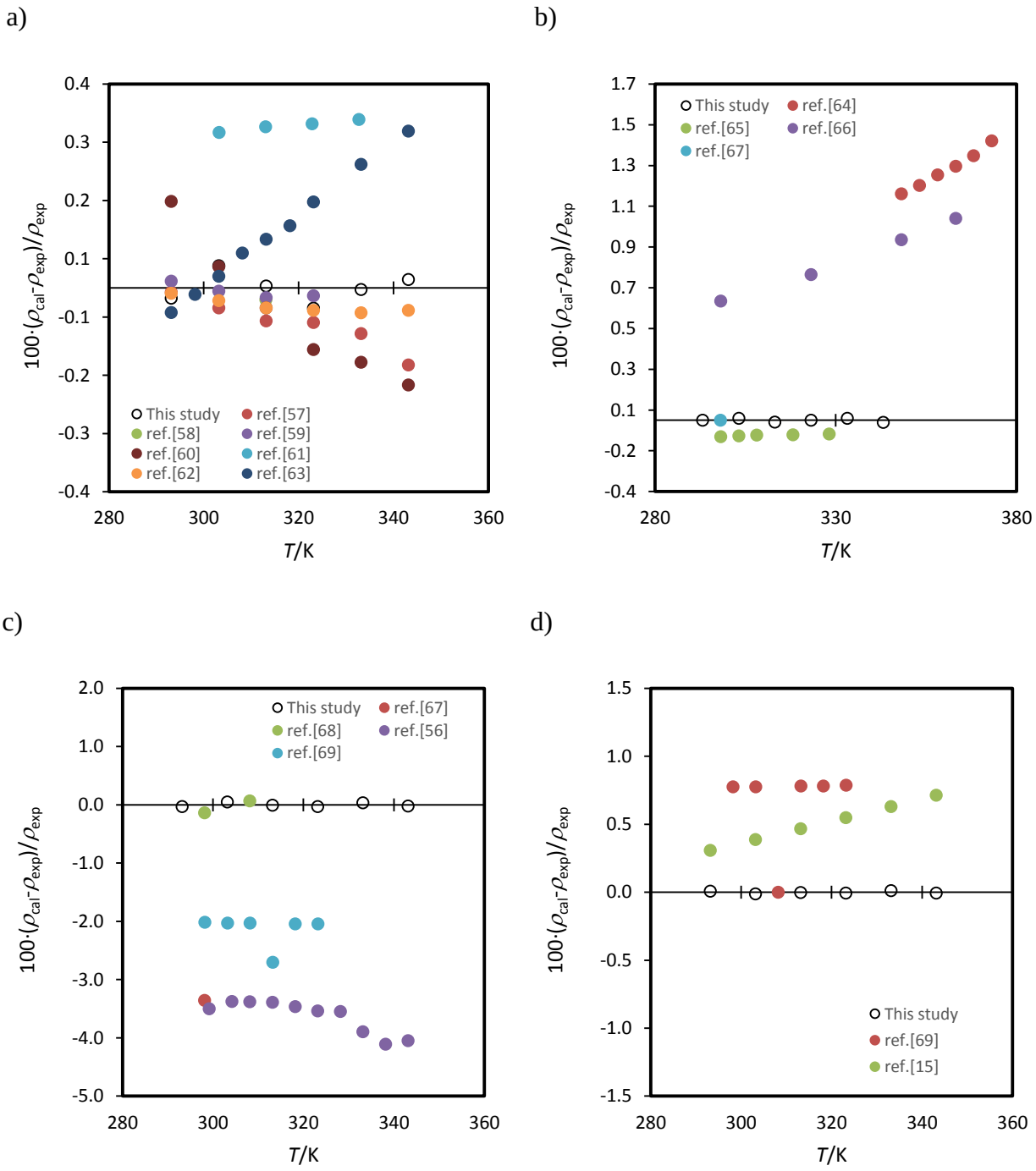

Figure 3.17. Deviations in density data between this study and literature as a function of temperature: a) [C4mim][BF_4]; b) [C4mim][Cl] ; c) [C4mim][I]; d) [C4mim][Br]

For viscosity comparison, literature data are scarce and scatterered (Figure 3.18). For [C4mim][BF_4], most of the data compared agree with deviations lower than 10 %, except refs. [67,70] which show high deviations at low temperature. Probably this is due to the different water content in the samples. For the other ionic liquids, the comparison is not so decisive. For [C4mim][Cl] only two references were found [74,75] showing deviations lower than 20 %. In the case of the [C4mim][I] three references were found [56,61,69] and the results are very different. Our data were around 40 % lower than those reported in ref. [69], but 10 % higher than those reported in ref. [56]. Deviations with ref. [61] were higher than 50 %. Finally, the only reference found for [C4mim][Br] were a plot reported in ref. [15] who did not show data or equations. Data were obtained directly from the plot. Deviations at low temperature are small but increase with temperature.

Finally, for thermal conductivity of [C4mim][Cl], [C4mim][Br] and [C4mim][I] IL no data available in literature were found. Only in ref. [76] thermal conductivity data for [C4mim][BF_4] are presented. Deviations are shown in Figure 3.18, and it can be seen that our experimental data agree with reported data in ref.[76].

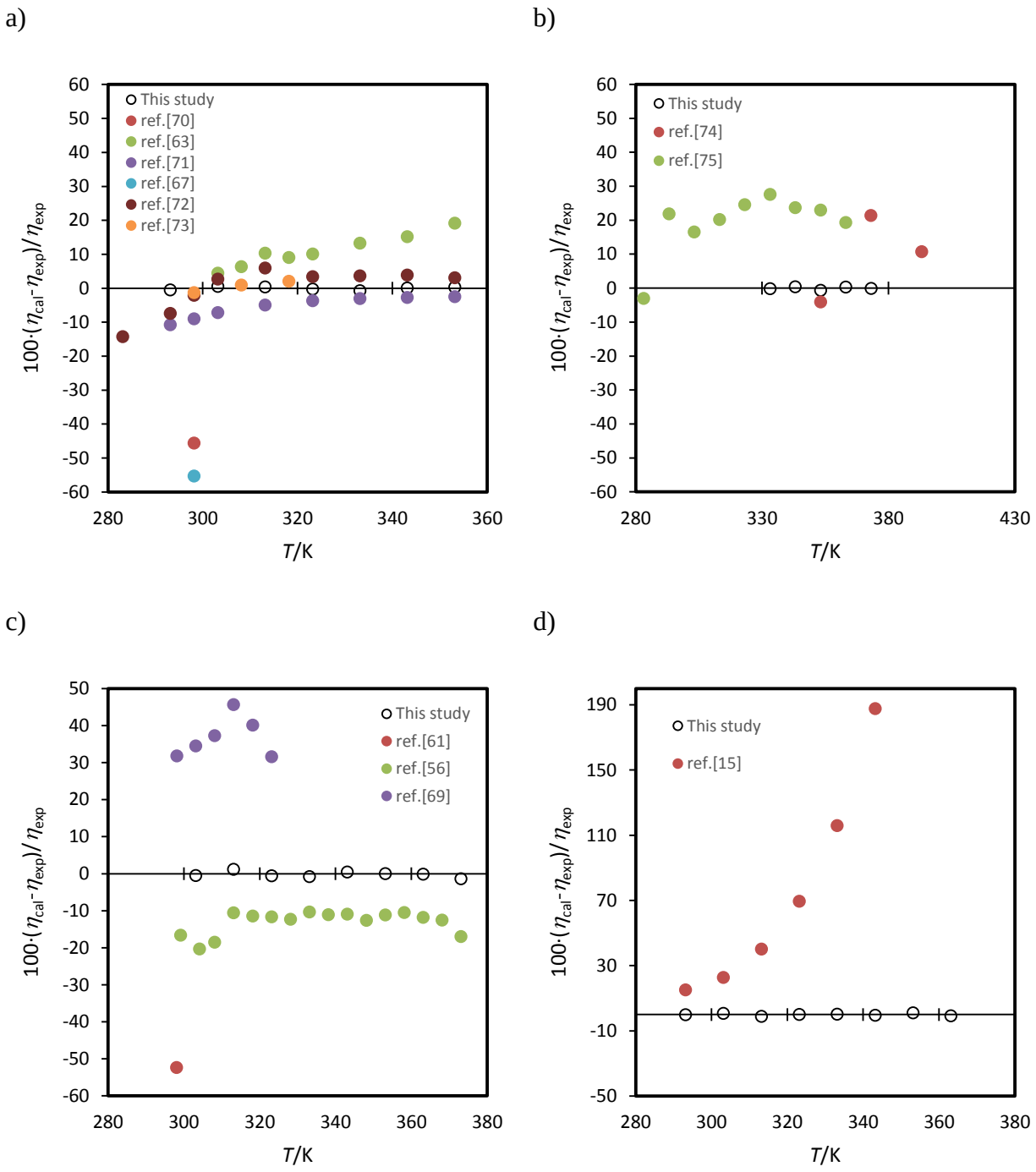

Figure 3.18. Deviations in viscosity data between this study and literature as a function of temperature: a) [C4mim][BF_4]; b) [C4mim][Cl] ; c) [C4mim][I]; d) [C4mim][Br]

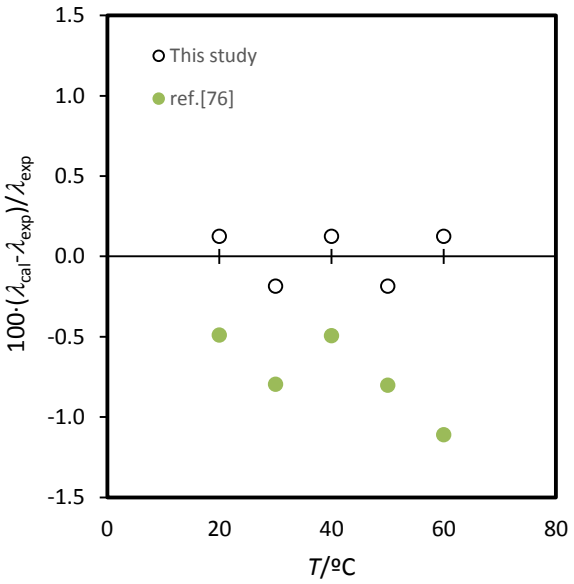

Figure 3.19. Deviations between our thermal conductivity data and ref.[76].

3.5 MECHANISM OF Ru NANOPARTICLES STABILIZATION IN ILs

Pure imidazolium-based ILs should be considered as a 3 dimensional network of cation and anion (hydrophobic and hydrophilic) link by weak interactions (such as hydrogen bonds and van der walls and coulomb forces) regarded as supramolecular polymeric structures with a high degree of self-organization. Thus, IL can be used as a fine-tuning tool in nano synthesis of NPs [77]. The Ru NP size obtained with IL depends on the volume of the IL anion. NPs are considered stabilized from growth-agglomeration in the ILs by the formation of protective anionic and cationic layer around them in a core-shell system [78,79]. We believe that the thickness of the stabilizing shell around RuNP depends on the IL molecular ion volumes. According to DLVO theory [80] the first inner shell must be anionic, and then the IL anion will have the highest influence of the size and the electrostatic stabilization of the Ru NP. The anion molecular volume determines the region of the nanoparticle size. At a constant concentration of Ru precursor, the nanoparticle growth is

probably controlled by the size of polar domain. The Ru NPs are obtained by $NaBH_4$ reduction of Ru salts dissolved in ILs. The presence of n-butylimidazole Ru particles has a narrow size distribution in the diameter range of 2-10 nm, which increased with molecular volume of the IL anion [81]. Thus, the size of Ru(0) NPs prepared by reduction of $RuCl_3$ in C4mimX (X= Cl, Br, I and BF_4) ILs increases with the anion volume. In this case the NPs size increases with the decrease of the anion coordination ability. Thus, ~ 2-10 nms Ru particle in ILs reveal that the nanoparticles are solvated preferentially by the charged species of the IL ions and both the cation and anion are in contact with the nanoparticles [33]. The molecular hydride ($NaBH_4$) is most frequently used as reducing agents for the generations of metal NPs (Scheme 1). However, hydride sources are not likely to be used in ILs, due to their basic character, leading to deprotonate the imidazolium cation and generate carbenes that may bind to metal surface. The reducing agent produces various by-products, such as Na and B compounds, that are difficult to remove from the ILs.

$$RuCl_3 + 3NaBH_4 + 9H_2O \longrightarrow [Ru(0)]n + 3NaCl + 3H_3BO_3 + 3HCl + 9H_2 \quad \text{.....(3.1)}$$

Scheme 3.1 *Ru NP synthesis in ILs using sodium borohydride as reducing agent in the presence of nitrogen*

3.6 CONCLUSIONS

Ionic liquids offer possibilities for the preparation, stabilization and investigations of the structural and surface properties of ruthenium metal without the use of the external stabilizing agent which makes this synthesis protocol as simple and energy intensive. A stable dispersion of Ru NPs with small size and narrow distributions, can be prepared from ruthenium metal precursor in the presence of ILs in one step method. ILs provide a protective layer, with the Ru nanoparticle surface through cation and anionic species and by the formation of carbene fragment together with an oxide layer on the metal surface. The density and viscosity of Ru-INFs decreases with increase mass of anion which reflects that small anion more compactly situated with Ru nanoparticle than large size anions. Viscosity of Ru-INFs is smaller compare to base ILs at low concentration of Ru precursor. The nanoparticle/ILs/stabilizer combination usually exhibits an excellent synergistic

effect that enhances the thermal conductivity of the material and reduced viscosity for new generation heat transfer applications.

3.7 REFERENCES

[1] Salas G.; Podgorsek A.; Campbell P. S.; Santini C. C.; H. Pa´dua A. A.; Costa Gomes M. F.; Philippot K.; Chaudretd B.; Turminee M. Ruthenium nanoparticles in ionic liquids: structural and stability effect of polar solutes Phys Chem Chem Phys 13 (2011) 13527-13536

[2] Murshed S. M. S.; Nieto de Castro C. A. Nanofluids: Synthesis, Properties and Applications:, Eds., NOVA Science Publishers, Inc., New York, (2014), ISBN (978-1-63321-677-8)

[3] Dupont J. From Molten Salts to Ionic Liquids: A "Nano" Journey Accounts Chem Res 44 (2011) 1223-1231

[4] A. P. C. Ribeiro, S. I. C. Vieira, P. Goodrich, C. Hardacre, M. J. V. Lourenço, C. A. Nieto de Castro, Thermal Conductivity of $[C_n mim][(CF_3SO_2)_2N]$ and $[C_4mim][BF_4]$ IoNanofluids with Carbon Nanotubes-Measurement, Theory and Structural Characterization J Nanofluids 2 (2013) 55-62

[5] Dupont J.; Scholten J. D. On the structural and surface properties of transition metal nanoparticles in ionic liquids Chem Soc Rev 39 (2010) 1780-1804

[6] Gutel T.; Garcia-Anton J.; Pelzer K.; Santini C. C.; Chauvin Y.; Chaudret B.; Besset J.-M. Influence of the self-organization of ionic liquids on the size of Ruthenium nanoparticles: effect of the temperature and stirring J Mater Chem 17 (2007) 3290-3292

[7] Safavi A.; Maleki N.; Tajabadi F.; Farjami E. High electrocatalytic effect of palladium nanoparticle arrays electrodeposited on carbon ionic liquid electrode Electrochem Commun 9 (8) (2007) 1963-1968

[8] Batra D.; Seifert S.; Varela L. M.; Liu A. C. Y.; Firestone M. A. Solvent-Mediated Plasmon Tuning in a Gold-Nanoparticle-Poly(Ionic Liquid) Composite Adv Funct Mater 17 (8) (2007) 1279-1287

[9] Govinda V.; Reddy P. M.; Bahadur I.; Attri P.; Venkatesu P.; Venkateswarlu P. Effect of anion variation on the thermophysical properties of triethylammonium based protic ionic liquids with polar solvent thermochim. Acta, 556 (2013) 75-88

[10] Salas G.; Santini C. C.; Philippot K.; Collie`re V.; Chaudret B.; Fenet B.; Fazzini P. F.; Dalton Trans 40 (2011) 4660-4668

[11] Patharkar R. G.; Nandanwar S. U.; Chakraborty M. Synthesis of Colloidal Ruthenium Nanocatalyst by Chemical Reduction Method Journal of Chemistry Article ID 831694 5 (2013) 1-7

[12] Darwich W.; Gedig C.; Srour H.; Santini C. C.; Martin H. G. P. Single step synthesis of metallic nanoparticles using Dihydroxyl functionalized ionic liquids as reductive agent RSC Adv 3 (2013) 20324-20331

[13] Paul A.; Mandal P. K.; Samanta A. On the optical properties of the imidazolium ionic liquids J Phys Chem B 109 (18) (2005) 9148-9153

[14] Chen W.; Davies J. R.; Ghosh D.; Tong M. C.; Konopelski J. P.; Chen S. Carbene-functionalized ruthenium nanoparticles Chem Mater 18 (22) (2006) 5253-5259

[15] Tshibangu P. N.; Ndwandwe S. N.; Dikio E. D. Density, Viscosity and Conductivity Study of 1-Butyl-3-Methylimidazolium Bromide Int J Electrochem Sci 6 (2011) 2201-2213

[16] Maton C.; De Vos N.; Stevens C. V. Ionic liquid thermal stabilities: decomposition mechanisms and analysis tools Chem Soc Rev 42 (2013) 5963-5977

[17] Ferreira A. G. M.; Simoes P. N.; Ferreira A. F.; Fonseca M. A.; Oliveria M. S. A.; Trino A. S. M. J Chem Thermodynamics 64 (2013) 80-92

[18] Esumi K.; Ishigami M.; Nakajima A.; Sawada K.; Honda H. Chemical treatment of carbon nanotubes Carbon 34 (1996) 279-281

[19] Kroon M. C.; Buijs W.; Peters C. J.; Witkamp G. J. Quantum chemical aided prediction of the thermal decomposition mechanisms and temperatures of ionic liquids Thermochim Acta 465 (1-2) (2007) 40-47

[20] Dharaskar S. A.; Varma M. N.; Shende D. Z.; Yoo C. K.; Wasewar K. L. Synthesis, Characterization and Application of 1-Butyl-3-methylimidazolium Chloride as Green Material for Extractive Desulfurization of Liquid Fuel The Scientific World Journal Article ID 395274 (2013) 9.

[21] Dupont J.; Meneghetti M. R. On the stabilization and surface properties of soluble transition-metal nanoparticles in non-functionalised imidazolium-based ionic liquids Curr Opin Colloid & Interface Sci 18 (1) (2013) 54-60

[22] Coates J. Interpretation of infrared spectra, A practical approach, Encyclopedia of analytical chemistry, John Wiley & Sons Ltd, Chichester (2006), pp. 10815-10837.

[23] Amman M.; Fransaer J. Synthesis and characterization of hybridmaterials based on 1-butyl-3-methylimidazolium tetrafluoroborate ionicliquid and Dawson-type tungstophosphate K7[H4PW18O62] _ 18H2O andK6[P2W18O62] _ 13H2O J Solid State Chem 184 (2011) 818-824

[24] Wu W.; Li W.; Han B.; Zhang Z.; Jiang T.; Liu Z. A green and effective method to synthesize ionic liquids: supercritical CO2 route Green Chem 7 (2005) 701-704

[25] Katsyuba S. A.; Dyson P. J.; Vandyukova E. E.; Chernova A. V.; Vidiš A. Molecular Structure, Vibrational Spectra, and Hydrogen Bonding of the Ionic Liquid 1-Ethyl-3-methyl-1H-imidazolium Tetrafluoroborate Helvetica Chimica Acta 87 (10) (2004) 2556-2565

[26] Katsyuba S. A., Zvereva E. E., Vidis A., Dyson P. J. Application of Density Functional Theory and Vibrational Spectroscopy Toward the Rational Design of Ionic Liquids J Phys Chem A 111 (2) (2007) 352-370

[27] Kolbeck C.; Cremer T.; Lovelock K. R. J.; Paape N.; Schulz P. S.; Wasserscheid P.; Maier F.; Steinruck H. P. Influence of different anions on the surface composition of ionic liquids studied using ARXPS J Phys Chem B 113 (25) (2009) 8682-8688

[28] Cai Q.; Paulose M.; Varghese O. K.; Grimes C. A. The effect of electrolyte composition in the fabrication of self-organized titanium oxide nanotube arrays by anodic oxidation Journal of Materials Research 20 (01) (2005) 230-236

[29] Cremer T.; Kolbeck C.; Lovelock K. R. J.; Paape N.; Wolfel R.; Schulz P. S.; Wasserscheid P.; Weber H.; Thar J.; Kirchner B.; Maier F.; Steinruck H.-P. Towards a molecular understanding of cation-anion interactions probing the electronic structure of imidazolium ionic liquids by NMR spectroscopy, X-ray photoelectron spectroscopy and theoretical calculations Chem Eur J 16 (30) (2010) 9018-9033

[30] Banerjee S., Wong S. S. Rational sidewall functionalization and purification of single-walled carbon nanotubes by solution-phase ozonolysis J Phys Chem B 106 (47) (2002) 12144-12151

[31] Smith E. F.; Garcia I. J. V.; Briggs D.; Licence P. Ionic liquids in vacuo; solution-phase X-ray photoelectron spectroscopy Chem Commun (2005) 5633- 5635

[32] Lovelock K. R. J.; Kolbeck C.; Cremer T.; Paape N.; Schulz P. S.; Wasserscheid P.; Maier F.; Steinruck H. P. Influence of different substituents on the surface composition of ionic liquids using ARXPS J Phys Chem B 113 (9) (2009) 2854- 2864

[33] Pensado A. S.; Padua A. A. H. Solvation and stabilization of metallic nanoparticle in ionic liquids Angew Chem Int Ed 123 (37) (2011) 8842-8846

[34] Souza B. S.; Leopoldino E. C.; Tondo D. W.; Dupond J.; Nome F. Imidazolium-based zwitterionic surfactant: a new amphiphilic Pd nanoparticles stabilizing agent Langmuir 28 (1) (2012) 833-840

[35] Corilo Y. E.; Nachtigall F. M.; Abdelnur P. V.; Ebeling G.; Dupont J.; Eberlin M. N. Charge-tagged N-heterocyclic carbens RSC Adv 1 (2011) 73-78

[36] Ott L. S.; Finke R. G. Nanocluster formation and stabilization fundamental studies: investigating "solvent-only"stabilization en route to discovering stabilization by the traditionally weakly coordinationg anion BF4 – plus high dielectric constant solvents Inorg Chem 45 (20) (2006) 8382-8393

[37] Cha S.; Ao M.; Sung W.; Moon B.; Ahlstrom B.; Johansson P.; Ouchi Y.; Kim D. Structures of ionic liquid–water mixtures investigated by IR and NMR spectroscopy Phys Chem Chem Phys 16 (2014) 9591 –9601

[38] Ott L. S.; Cline M. L.; Deetlefs M.; Seddon K. R.; Finke R. G. Nanoclusters in ionic liquids: rom imidazolium-based ionic liquids detected by ^{2}H NMR Evidence for N-heterocyclic carbene formation J Am Chem Soc 127 (16) (2005) 5758-5759

[39] Orita A.; Kamijima K.; Yoshida M. Allyl-functionalized ionic liquids as electrolytes for electric double-layer capacitors Journal of Power Sources 195 (21) (2010) 7471-7479

[40] Pringle J. M.; Golding J.; Baranyai K.; Forsyth C. M.; Deacon G. B.; Scotta J. L.; MacFarlane D. R. The effect of anion fluorination in ionic liquids—physical properties of a range of bis(methanesulfonyl)amide salts New J Chem 27 (2003) 1504-1510

[41] Chiappe C.; Pieraccini D. Ionic liquids: solvent properties and organic reactivity J Phys Org Chem 18 (4) (2005) 275-297

[42] Dzyuba S. V.; Bartsch R. A. Influence of Structural Variations in 1-Alkyl(aralkyl)-3-Methylimidazolium Hexafluorophosphates and Bis(trifluoromethyl-sulfonyl)imides on Physical Properties of the Ionic Liquids Chem Phys Chem 3 (2) (2002) 161-166

[43] Gu Z.; Brennecke J. F. Volume Expansivities and Isothermal Compressibilities of Imidazolium and Pyridinium-Based Ionic Liquids J Chem Eng Data 47 (2) (2002) 339-345

[44] Kole M.; Dey T. K. Thermal conductivity and viscosity of Al_2O_3 nanofluid based on carengine coolant J Phys D: Appl Phys 43 (2010) 315501

[45] Zhou S-Q.; Ni R.; Funfschilling D. J Effects of shear rate and temperature on viscosity of alumina polyalphaolefins nanofluids Appl Phys 107 (2010) 1-6

[46] Ferreira A. G. M.; Simoes P. N.; Ferreira A. F.; Fonseca M. A.; Oliveria M. S. A.; Trino A. S. M. Transport and thermal properties of quaternary phosphonium ionic liquids and Ionanofluids J Chem Thermodyn 64 (2013) 80-92

[47] Wang B.; Wang X.; Lou W.; Hao J. Rheological and tribological properties of ionic liquid-based nanofluids containing functionalized multi-walled carbon nanotubes J Phys Chem C 114 (19) (2010) 8749-8754

[48] Wang B.; Wang X.; Lou W.; Hao J. Ionic liquid based stable nanofluids containing gold nanoparticles J Colloid Interface Sci 362 (1) (2011) 5-14

[49] Keblinski P.; Phillpot S. R.; Choi S. U. S.; Eastman J. A. Mechanisms of heat flow in suspensions of nano-sized particles (nanofluids) Int J Heat Mass Transfer 45 (4) (2002) 855-863.

[50] Nieto de Castro C. A.; Murshed S. M. S., Lourenço M. J. V.; Santos F. J. V.; Lopes M. L. M. and França J. M. P. Enhanced thermal conductivity and specific heat capacity of carbon nanotubes ionanofluids Int. J. Thermal Sciences 62 (2012) 34-39.

[51] França J. M. P'; Vieira S. I. C.; Lourenço M. J. V.; Murshed S. M. S.; Nieto de Castro C. A. Thermal Conductivity of $[C_4mim][(CF_3SO_2)_2N]$ and $[C_2mim][EtSO_4]$ and Their IoNanofluids with Carbon Nanotubes: Experiment and Theory J. Chem Eng. Data 58 (2) (2013) 467-476.

[52] França J. M. P.; Reis F.; Vieira S. I. C.; Lourenço M. J. V.; Santos F. J. V.; Nieto de Castro C. A.; Pádua A. H. Thermophysical properties of ionic liquid dicyanamide (DCA) nanosystems, J. Chem. Thermodynamics 79 (2014) 248-257.

[53] Wang F.; Han L.; Zhang Z.; Fang X.; Shi J.; Ma W. Surfactant-free ionic liquid-based nanofluids with remarkable thermal conductivity enhancement at very low loading of graphene, Nanoscale Research Lett 7 (2012) 1-7.

[54] Prasher R.; Phelan P. E.; Bhattacharya P. Effect of aggregation kinetics on the thermal conductivity of Nanoscale colloidal solutions (nanofluid) Nano Lett 6 (7) (2007) 1529-1534

[55] Buongiorno J.; Venerus D. C.; Prabhat N.; McKrell T.; Townsend J.; Christianson R.; Tolmachev Y. V.; Keblinski P.; Hu L.-W.; Alvarado J. L.; Bang I. C.; Bishnoi S. W.; Bonetti M.; Botz F.; Cecere A.; Chang Y.; Chen G.; Chen H.; Chung S. J.; Chyu M. K.; Das S. K.; Paola R. D.; Ding Y.; Dubois F.; Dzido G.; Eapen J.; Escher W.; Funfschilling D.; Galand Q.; Gao J.; Gharagozloo P. E.; Goodson K. E.; Gutierrez J. G.; Hong H.; Horton M.; Hwang K. S.; Iorio C. S.; Jang S. P.; Jarzebski A. B.; Jiang Y.; Jin L.; Kabelac S.; Kamath A.; Kedzierski M. A.; Kieng L. G.; Kim C.; Kim J.-H.; Kim S.; Lee S. H.; Leong K. C.; Manna I.; Michel B.; Ni R.; Patel H. E.; Philip J.; Poulikakos D.; Reynaud C.; Savino R.; Singh P. K.; Song P.; Sundararajan T.; Timofeeva E.; Tritcak T.; Turanov A. N.; Vaerenbergh S. V.; Wen D.; Witharana S.; Yang C.; Yeh W.-H.; Zhao X.-Z.; Zhou S.-Q. A benchmark study on the thermal conductivity of nanofluids J Appl Phys 106 (9) 094312

[56] M. H.Ghatee; M.Zare; F.Moosavi and A. R. Zolghadr, J Chem Eng Data 55, 3084 (2010).

[57] D. Matkowska, T.Hofman, *J Mol liq* 165, 161 (2011).

[58] Machida, H.; Sato, Y.; Smith, R. L. (2008) *Fluid Phase Equilib.* 264(1), 147-155.

[59] Y.A. Sanmamed, D. Gonzalez-Salgado, J. Troncoso, L. Romani, A. Baylaucq, C.J. Boned, *Chem. Thermodyn*. 42(4), 553-563 (2010).

[60] R.L.Gardas, M.G. Freire, P.J. Carvalho, I.M. Marrucho, I.M.A. Fonseca, A.G.M. Ferreira, J.A.P. Coutinho, *J. Chem. Eng. Data* 52, 80-88 (2007).

[61] R. Gomes de Azevedo, J.M.S. Esperanca, V. Najdanovic-Visak, Z.P.Visak, H.J.R. Guedes, M. Nunes da Ponte, L.P.N. Rebelo, *J. Chem. Eng. Data* 50, 997-1008 (2005).

[62] K. R. Harris, M. Kanakubo, L.A. Woolf, *J. Chem. Eng. Data* 52(6), 2425-2430 (2007).

[63] Q. Zhou, L.S. Wang, H.P. Chen, *J. Chem. Eng. Data* 51(3), 905-908 (2006).

[64] H. Machida, R. Taguchi, Y. Sato, R.L. Smith, *J. Chem. Eng. Data* 56(4), 923-928 (2011).

[65] V. Govinda, P. Attri, P. Venkatesu, P. Venkateswarlu, *Fluid Phase Equilib*. 304(1-2), 35-43 (2011).

[66] R.H. He, B.W. Long, Y.Z Lu, H. Meng, C.X. Li, *J. Chem. Eng. Data* 57(11), 2936-2941 (2012).

[67] J.G. Huddleston, A.E. Visser, W.M. Reichert, H.D. Willauer, G.A. Broker, R.D. Rogers, *Green Chem*. 2001(3), 156-164 (2001).

[68] N.V. Sastry, N.M. Vaghela, P.M. Macwan, *J. Mol. Liq*. 180, 12-18 (2013).

[69] K.S. Kim, B.K. Shin, H. Lee, *Korean J. Chem. Eng*. 21(5), 1010-1014 (2004).

[70] T. Nishida, Y. Tashiro, M. Yamamoto, *J. Fluorine Chem*. 120, 135-141 (2003).

[71] C. Schreiner, S. Zugmann, R. Hartl, H.J. Gores, *J. Chem. Eng. Data* 55(5), 1784-1788, (2010).

[72] H. Tokuda, S. Tsuzuki, M.A.B.H. Susan, K. Hayamizu, M. Watanabe, *J. Phys. Chem. B* 110 (39), 19593-19600 (2006).

[73] E. Rilo, J. Vila, M. Garcia, L.M. Varela, O. Cabeza, *J. Chem. Eng. Data* 55(11), 5156-5163 (2010).

[74] S. Fendt, S. Padmanabhan, H.W. Blanch, J.M. Prausnitz, *J. Chem. Eng. Data* 56(1), 31-34 (2011).

[75] K. R.Seddon, A.Stark and M. J. Torres, *ACS Symposium Series* (2009), Vol. 819, pp 34–49.

[76] A. P. C. Ribeiro, S. I. C.Vieira,P. Goodrich, C.Hardacre, M. J. V. Lourenco and C. A. Nieto de Castro, *J. Nanofluids* 2, 1 (2013).

[77] Migowski P.; Machado G.; Teixeira S. R.; Alves M. C. M.; Morais J.; Traverse A.; Dupont J. Synthesis and characterization of nickel nanoparticles dispersed in imidazolium ionic liquids J Phys Chem Chem Phys 9 (2007) 4814-4821

[78] Schmid G. Nanoparticles, 2nd ed.: Wiley-VCH: Weinheim, Germany, (2004), pp. 185-238.

[79] Shipway A. N., E. Katz, I. Willner, Nanoparticle Arrays on Surfaces for Electronic, Optical, and Sensor Applications Chem Phys Chem 1 (1) (2000) 18-52

[80] Verwey E. J. W.; Overbeek J. Th. G. Theory of the stability of lyophobic colloids, The interaction of sol particles having an electric double layer; Elsevier: Amsterdam; 1948 Dover Publications: Mineola, NY; **(1999)** pp. 1-205

[81] Redel E.; Thomann R.; Janiak C. First correlation of nanoparticle size-dependent formation with the ionic liquid anion molecular volume Inorg Chem 47 (1) 2008 14-16

Chapter 4

Structural and morphological influence of nanoparticles on thermal properties of Ag-nanofluids and Ag-ionanofluids

Chapter 4 presents the investigation of heat transport properties of [Choline][NTf2] ionic liquid and silver nanoparticles of variable morphologies, such as 1dimentional (nanowires), 2 dimentional (nanoplates) and 3 dimentional (nanospheres) in base ILs. The effect of variation in morphology of silver nanoparticles on thermal conductivity, density and viscosity of INFs is demonstratded in this chapter.

4.1 INTRODUCTION

It is current need of the society to develop more efficient heat transfer fluids for use in cars and industrial equipment. Novel fluids are needed with improved thermal properties as well as with improved economics [1]. Such oils and coolants would make possible more efficient engine with smaller size, cheaper cost having their fuel demand at a much lower level causing emissions with less damage to the environment. Addition of nanosize materials in conventional fluids were investigated to improve thermal properties of the fluids [2]. The traditional fluids like water, ethylene glycol and synthetic oil containing nanoparticles of different materials utilize as a heat transfer media have some drawbacks like low operating tempearature, high vapor pressure and poor thermal stability [3-5]. To overcome these obstacles researchers have been studying ILs which can be employed as a new generation heat transfer fluids due to their low vapor pressure, improved thermal conductivity, which make it possible to apply them at high temperature operating conditions [6]. To utilize ILs as a new genearation heat transfer fluids it is necessary to investigate first their various properties such as density, viscosity and more particularly, their thermal conductivity. The combination of nanoparticles and ILs further showed more improved thermal properties as compared to IL itself, to be utilized in small volume heat exchangers and microchannels [7].

Now a days with improved thermophysical properties, we can imrove the economy of process designing but simultaneously it is necessary that dsigned or developed materials should be more ecofriendly. With fascinating properties of ILs and to develop more environmentally benign IL choline is utilized in the development of ILs. In addition, the presence of hydroxyl group in choline cation for example, further improves the biodegradability of the respective IL [8]. Silver (Ag) is well known metal for it's highest thermal conductivity. Silver metal nanoparticles in conventional solvents has previously shown the enhacement in thermal conductivity [9]. Among the ammonia based ILs, due to its bioderived nature choline [NTf2] IL, was screened as a suitable IL in the application of IL in NH_3 absorbtion system [10]. To develop new class ionanofluids (INFs) it is necessary to investigate their essential properties such as density, viscosity and thermal conductivity.

In near future the heat transfer fluids will be developed with the available nanoparticles in combination with base ILs. However, it is necessary to explore the effect of variation in particle morphology on various properties of such fluids. Eventhough the dispersing materials with higheser thermal conductivity and also a variety of ionic liquds are available it is difficult to disperse the desired nanoparticles in the desired base ionic liquids. With this background, we developed a protocol for dispersion of silver nanoparticles with one dimentional (1D), two dimentional (2D) and three dimentional (3D) nanostructures of silver in Choline [NTf2] IL with the aim to develop new generation ionanofluids with improved thermal properties. The effect of variation in nanoparticle morphology on density, viscosity and thermal conductivity of silver nanofluids and silver ionanofluids were studied to explore the role of nanoparticle morphology on heat transfer properties of INFs.

4.2 EXPERIMENTAL

In order to develop INFs specifically, transition metal nanoparticles in base ionic liquids choline [NTf2] IL was studied in this work. More particularly, silver nanoparticles with three different morphologies namely, nanospheres, nanowires and nanoplates were investigated. Material specifications of the purchased IL and silver nanofluid (NF) and silver nanoparticles are given in section 2.1 of chapter 2. Silver NFs and silver INFs were developed in our laboratory. The preparation protocol and schematic of development are described in detail in section 2.1 and sub section 2.1.2 of chapter 2. Freshly prepared silver NFs, vacuum dried choline [NTf2] IL and silver INFs further utilized for structural, morphological, optical absorption, thermal stability characterization with various characterization tools and techniques. Details for material characterization and characterization techniques utilized for analysis of Ag NFs and Ag INFs are given in detail in section 2.2 of chapter 2. Equipments procedures utilized for the measurement of density, viscosity and thermal conductivity of silver NFs and silver INFs are mentioned in section 2.3 of chapter 2.

4.3 EFFECT OF NANOPARTICLE MORPHOLOGY ON STRUCTURES OF Ag-INFs

Structural characterization of Choline bis(trifluromethylsulfonyl)imide ionic liquid was analyzed with ^{1}H and ^{13}C NMR spectroscopy to ensure the purity of purchased ionic liquid. Samples of silver INFs with silver nanoparticles of three different morphologies in base ionic liquids were also studied with NMR to detect the structural variation in ionic liquids after interactions with nanoparticle surfaces.

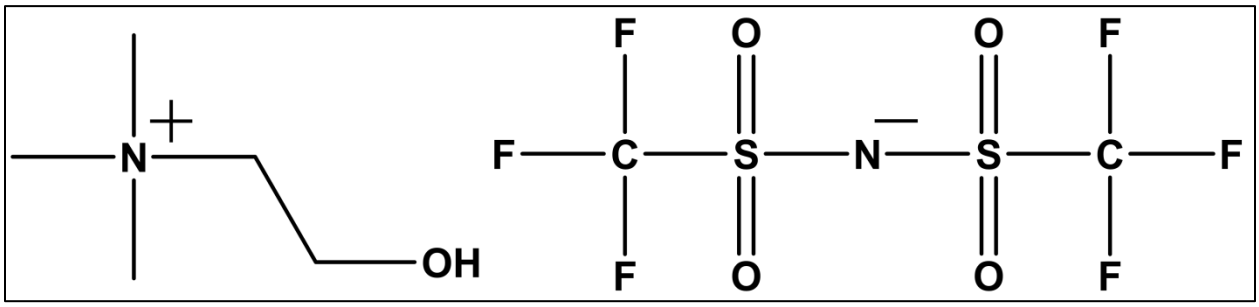

Figure 4. 1 *Chemical structure of Choline bis(trifluromethylsulfonyl) imide ionic liquid*

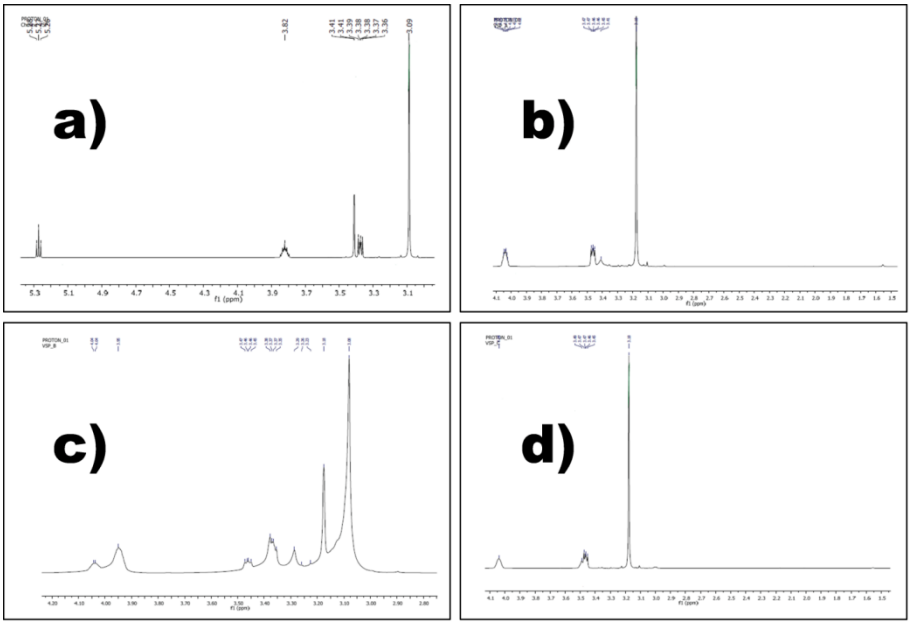

Figure 4.2 *^{1}H NMR spectrum of a) Choline [NTf2] IL, b) Ag-spheres-INF, c) Ag-nanowires-INF, d) Ag-nanoplates-INF*

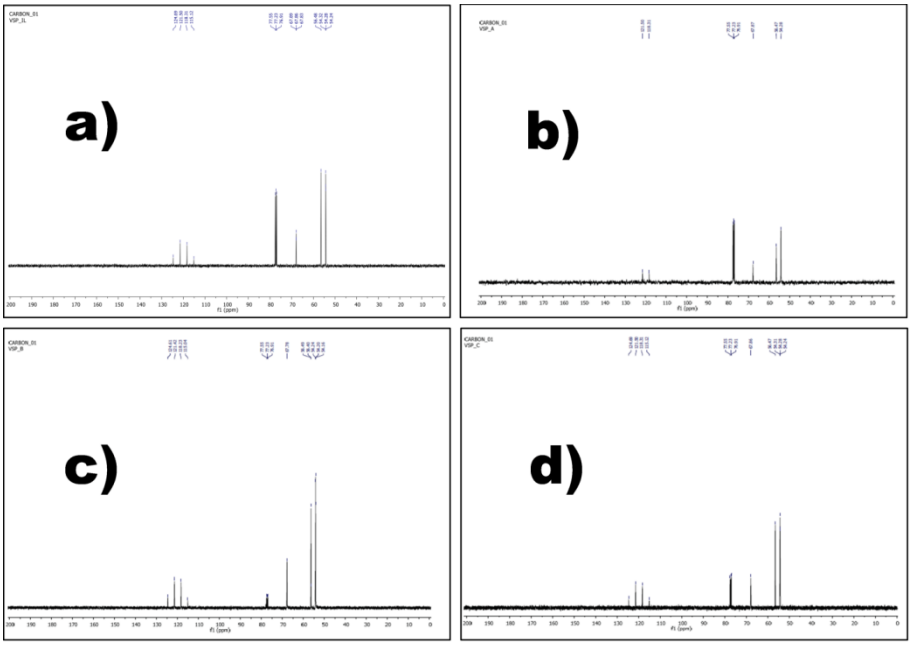

Figure 4.3 *^{13}C NMR spectrum of a) Choline [NTf2] IL, b) Ag-spheres-INF, c) Ag-nanowires-INF, d) Ag-nanoplates-INF*

Structural elucidation of ionic liquid was done by ^{1}H and ^{13}C NMR and obtained peak assignments shown in Figure 4.2 a) and Figure 4.3 a). The obtained ^{1}H NMR peak assignments are in good agreements with the literature data [11]. However one peak at 3.41 ppm obtained in the spectrum was due to traces of water present in IL. With curiosity to understand the structural variation in the structure of IL we analyze the silver ionanofluids (Ag-INF) namely Ag-spheres-INF, Ag-nanowires-INF, Ag-nanoplates-INF. It was observed that in case of all three INFs the peak obtained at 5.23 ppm of hydroxyl proton (-OH) in case of choline [NTf2] was disappeared which reveals that there is an interaction of (-OH) group from ionic liquid cation in the solvation and stabilization of dispersion of Ag-nanoparticles in ionic liquid medium. All neat NMR spectral assignments of base ionic liquid and silver ionanofluids are shown in Table 4.1. For ^{13}C NMR no any major changes observe which is remarkable that in the stabilization of nanoparticles in IL medium major role played by hydrogen bonding from choline cation.

Table 4.1 *^{1}H and ^{13}C NMR assignments of IL and silver INFs*

Entry	Sample Name	^{1}H and ^{13}C NMR spectroscopy (400 MHz CDCl3) (shift ppm)
1	[Choline][NTf2]	^{1}H NMR: 3.09 (s, 6H, N(C**H**$_3$)3,-CH$_2$-CH$_2$-OH), 3.37 (t, 2H, N(CH$_3$)3,-C**H**$_2$-CH$_2$-OH), 3.82 (m, 2H, N(CH$_3$)3,-CH$_2$-C**H**$_2$-OH), 5.27 (t, 1H, N(CH$_3$)3,-CH$_2$-CH$_2$-O**H**) ^{13}C NMR: 54.28 (s, 6H, N(**C**H$_3$)3,-CH$_2$-CH$_2$-OH), 67.86 (s, 2H, N(CH$_3$)3,-**C**H$_2$-CH$_2$-OH), 56.48 (s, 2H, N(CH$_3$)3,-CH$_2$-**C**H$_2$-OH)
2	Ag-nanospheres-INF	^{1}H NMR: 3.18 (s, 6H, N(C**H**$_3$)3,-CH$_2$-CH$_2$-OH), 3.47 (t, 2H, N(CH$_3$)3,-C**H**$_2$-CH$_2$-OH), 4.05 (m, 2H, N(CH$_3$)3,-CH$_2$-C**H**$_2$-OH) ^{13}C NMR: 54.28 (s, 6H, N(**C**H$_3$)3,-CH$_2$-CH$_2$-OH), 67.87 (s, 2H, N(CH$_3$)3,-**C**H$_2$-CH$_2$-OH), 56.47 (s, 2H, N(CH$_3$)3,-CH$_2$-**C**H$_2$-OH)
3	Ag-nanowires-INF	^{1}H NMR: 3.18 (s, 6H, N(C**H**$_3$)3,-CH$_2$-CH$_2$-OH), 3.46 (t, 2H, N(CH$_3$)3,-C**H**$_2$-CH$_2$-OH), 4.04 (m, 2H, N(CH$_3$)3,-CH$_2$-C**H**$_2$-OH) ^{13}C NMR: 54.20 (s, 6H, N(**C**H$_3$)3,-CH$_2$-CH$_2$-OH), 67.78 (s, 2H, N(CH$_3$)3,-**C**H$_2$-CH$_2$-OH), 56.49 (s, 2H, N(CH$_3$)3,-CH$_2$-**C**H$_2$-OH)
4	Ag-nanoplates-INF	^{1}H NMR: 3.18 (s, 6H, N(C**H**$_3$)3,-CH$_2$-CH$_2$-OH), 3.47 (t, 2H, N(CH$_3$)3,-C**H**$_2$-CH$_2$-OH), 4.05 (m, 2H, N(CH$_3$)3,-CH$_2$-C**H**$_2$-OH) ^{13}C NMR: 54.28 (s, 6H, N(**C**H$_3$)3,-CH$_2$-CH$_2$-OH), 67.86 (s, 2H, N(CH$_3$)3,-**C**H$_2$-CH$_2$-OH), 56.47 (s, 2H, N(CH$_3$)3,-CH$_2$-**C**H$_2$-OH)

4.4 INFLUENCE OF NANOPARTICLES MORPHOLOGY ON OPTICAL ABSORPTION

The UV-Visible absorption spectrum of silver NFs, base ionic liquid and silver INFs with three different geometries nanospheres, nanorods and nanoplates are shown in Figure 4.4. The UV-Visible absorptions of all silver NFs and INFs samples were recorded without further dilution of the samples. The colors of silver nanoparticle colloids in water as a solvent media are distinct from each other. It is clearly observed in inset photograph of Figure 4.4 a). UV-Visible optical absorption spectrum of Choline [NTf2] IL and silver INFs with various geometries is shown in Figure 4.4 b).

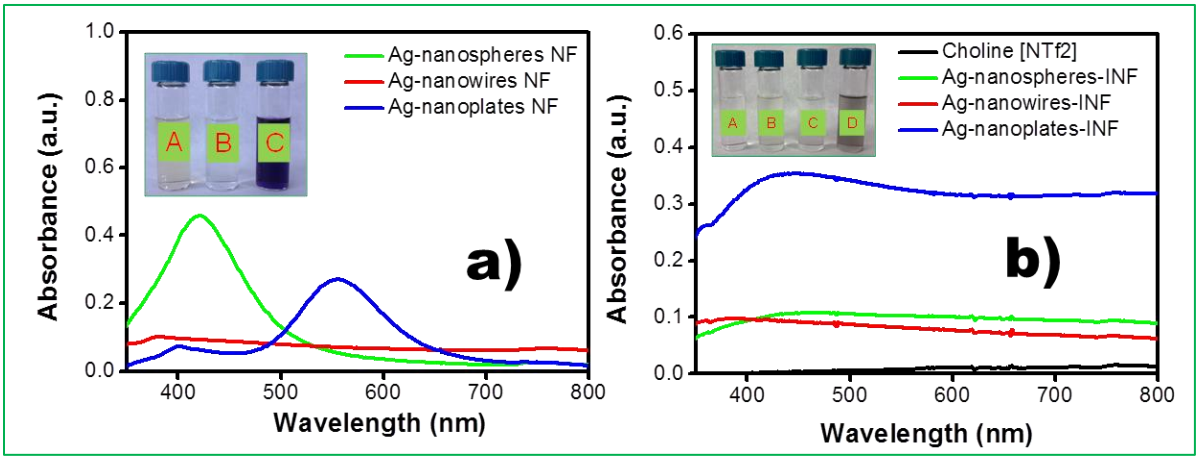

Figure 4.4 *UV-Visible absorption spectra of a) silver nanofluids b) [Choline][NTf2] IL and silver INFs with various geometries*

Silver colloidal solution containing nanospheres displays yellow color while silver colloidal solution containing nanowires and silver nanoplates colloidal solution show transparent white and blue color, respectively in water as a base solvent. It is well known that metal nanoparticles show localized surface plasmon resonance (LSPR) due to the coherent oscillation of conduction electrons on the surface of metal nanoparticles in resonance with the electromagnetic waves at the metal–dielectric interface [12-13]. Surface plasmonic resonance of silver nanoparticles is well-known at 400 nm. However absorption of silver nanoparticle colloids varies with variation of particle size or morphology [14]. Silver nanospheres nanofluids (Ag-nanospheres-NF) shows absorption maximum at 421.91 nm. While silver nanowires nanofluids (Ag-nanowires-NF) shows small absorption maximum at 375.40 nm and long tail absorption peak above 400 nm. Silver nanoplates nanofluids (Ag-nanoplates-NF) has two distinct optical absorptions one at 398.75 nm and another at 555.34 nm which is due to resonant silver nanoplates. Small absorption at 398.75 corresponds to presence of few small size of silver nanoplates. Choline cation has no any aromatic character or conjugation whereas [NTf2] anion has no chromophores in the structure which is resulted into no absoption for Choline [NTf2] IL in UV-Visible region. Also IL do not have any color as clearly observes in the inset photograph of the Choline [NTf2] ionic liquid [15]. After dispersion of silver nanoparticles into IL phase from water phase it is found that UV-Visible absorptions are more shifted towards the red shift after interactions with ionic

liquids. Silver nanospheres ionanofluid (Ag-nanospheres-INF) shows red shift from 421.91 nm to 432.42 nm. Silver nanowires ionanofluid (Ag-nanowires-INF) shows shit from 375.40 nm to 380.46 nm and silver nanoplates ionanofluids (Ag-nanoplates-INF) indicates red shift from 398.75 nm to 431.35 nm compare to Ag-nanoplates-NF. The Ag-nanoplates-NF was resonant in nature after interaction of silver nanoplates with ionic liquids it changes it's color from blue to black as clearly observe from the inset photograph of Figure 4.4 a) and b). However in case of Ag-nanospheres-INF its color becomes faint yellow compare to Ag-nanospheres-NF. Ag-nanowires-INF show similar color with negligible turbidity due to viscous IL, compare to Ag-nanowires-NF.

4.5 EFFECT OF NANOPARTICLE MORPHOLOGY ON BONDING OF ILS AND INFs

Effect of silver nanoparticles morphologies on bonding of silver NFs and INFs was studied with the help of ATR-IR analysis. ATR-IR spectra of silver NFs are given in Figure 4.5 a). ATR-IR spectra of neat choline [NTf2] IL and its respective silver INFs are shown in Figure 4.5 b).

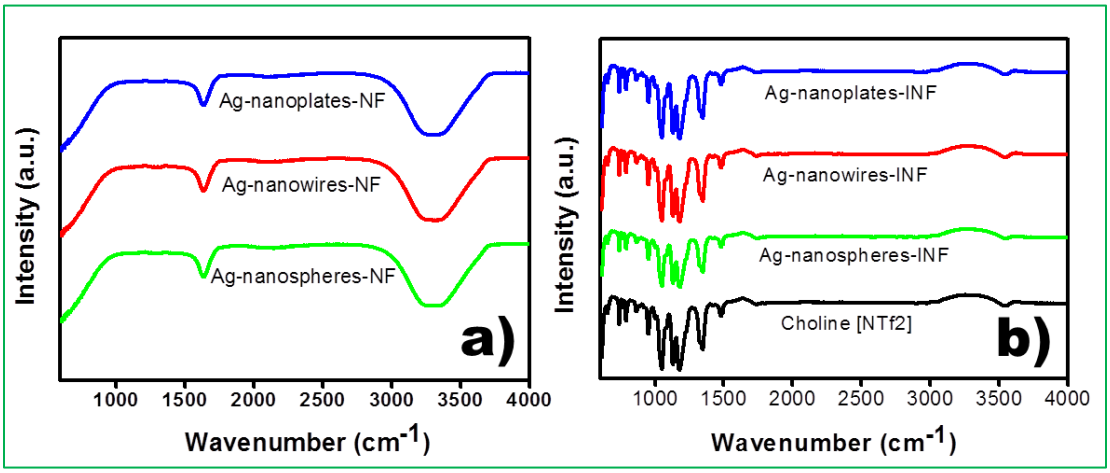

Figure 4.5 *ATR-IR spectra of a) silver nanofluids b) [Choline][NTf2] IL and silver INFs with various geometries*

The sharp peak obtained at 1638 cm^{-1} (Figure 4.5 a)) was originated from silver nanoparticles stabilized with PVP as a stabilizing agent. N. giri et. al reported the single peak at 1645 cm^{-1} in

case of PVP nano silver matrix [16]. We observe same peak at 1638 cm^{-1} in case of all three nanofluids of silver nanoparticles for three different morphologies. Ag nanoparticles namely nanospheres, nanowires and nanoplates were dispersed in the water as a solvent. The IR peak observed in the range of (3200-3500 cm^{-1}) generated for the water molecule [17]. In case of choline [NTf2] IL the strong and sharp peak at 3550 cm^{-1} was assigned to (-OH) group present in choline cation. In case of Ag-nanospheres-INF and Ag-naowires-INF the present peak shows displacement towards 3545 cm^{-1} and Ag-nanoplates-INF show same peak at 3540 cm^{-1}. These results are consistent with ^{1}H NMR results of silver INFs (Figure 4.2). Both results reveal that the (-OH) group from choline cation has crucial role in stabilization and dispersion of silver nanoparticles in IL medium. The common peaks for IL and INFs at 1476 cm^{-1} and 737 cm^{-1} was due to small structural chain of alkane present in choline cation. The another common peaks observed in Figure 4.5 b) at 1174 cm^{-1} , 1132 cm^{-1} and 1048 cm^{-1} was for (C-N strech). Other peaks observe in all IR spectra of Figure 4.5 b) at 657 cm^{-1} and 867 cm^{-1} is for C-F stretch present in [NTf2] anion.

4.6 THERMAL STABILITY STUDY

Figure 4.6 shows thermal stabilities of IL, water based silver NFs and Choline [NTf2] IL based silver ionanofluids with silver nanoparticles of various morphologies (spheres, wires, plates).

The temperates at which the degradation of sample starts (T (onset)) and temperatures at which the compound degrade totally (T (deg)) are displayed in Table 4.3.

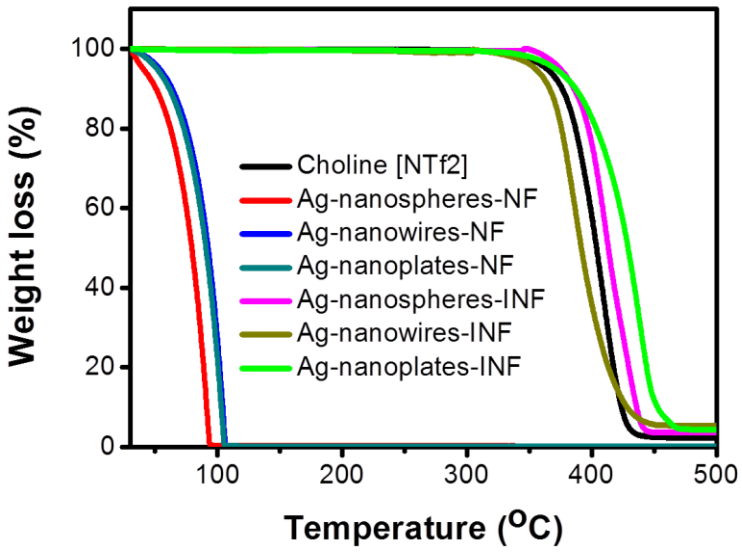

Figure 4.6 *Thermal gravimetric analysis of [Choline][NTf2] IL, silver NFs and silver INFs*

Table 4.2 *Thermal stabilities of IL, silver nanofluids and silver ionanofluids*

Entry	Sample Name	T(onset)	T (deg)
1	[Choline][NTf2]	376.67 °C	428.00 °C
2	Ag-nanospheres-NF	59.78 °C	93.84 °C
3	Ag-nanowires-NF	74.73 °C	106.75 °C
4	Ag-nanoplates-NF	70.46 °C	104.21 °C
5	Ag-nanospheres-INF	391.62 °C	443.67 °C
6	Ag-nanowires-INF	365.29 °C	430.46 °C
7	Ag-nanoplates-INF	399.04 °C	460.00 °C

Nowaday's metal nanoparticle in conventional solvents like water becomes point of attention from scientific communities due to the advantages such as reduced pumping power and enhanced heat conduction in heat transfer technologies [18]. An especially metal nanoparticles in water as a fluid has thermal volatility above 100 °C is the major problem to apply those nanofluids where heat transfer requires at elevated temperatures. The water as a solvent based

Ag-nanospheres-NF, Ag-nanowires-NF and Ag-naoplates-NF has similar trend and instability above 100 ^{o}C as clearly observe for their thermogram in Figure 4.6. The various morphologies of these NFs affect the thermal stability of NFs. Thermal stability of NFs are observed in this trend Ag-nanowires-NF > Ag-naoplates-NF > Ag-nanospheres-NF. Ionic liquids are well known for their thermal stability. We found that the Choline [NTf2] IL is thermally stable up to 376.37 ^{o}C in N_2 environment for thermal gravimetric analysis. When we dispersed same amount of commercially available silver nanoparticles with various morphologies in Choline [NTf2] ionic liquid after interaction of nanoparticles with ionic liquids it shows difference in their thermal stabilities compare to base IL. Ionic liquid and its respective ionanofluids show thermal stability in the trend as follows:

Ag-naoplates-INF > Ag-nanospheres-INF > Choline [NTf2] > Ag-nanowires-NF. In case of silver INFs and Choline [NTf2] IL we found that the small amount of residues remains in a sample pan from 2-5 weight % which was not degrade near to 400 ^{o}C temperature we continued the scan upto 500 ^{o}C but it remains same without any weight loss afterwords.

4.7 MORPHOLOGY STUDY OF SILVER NANOPARTICLES FLUIDS IN WATER AND IL

The scanning electron microscopy and transmission electron microscopy techniques were employed to characterize the dispersion, clustering and morphological variation in nanoparticle structures after dispersion in water and IL medium.

Scanning electron microscopy analysis

Figure 4.7 presents results of dipersions of commersially purchased silver NPs in water and Choline [NTf2] ionic liquid as a solvents.

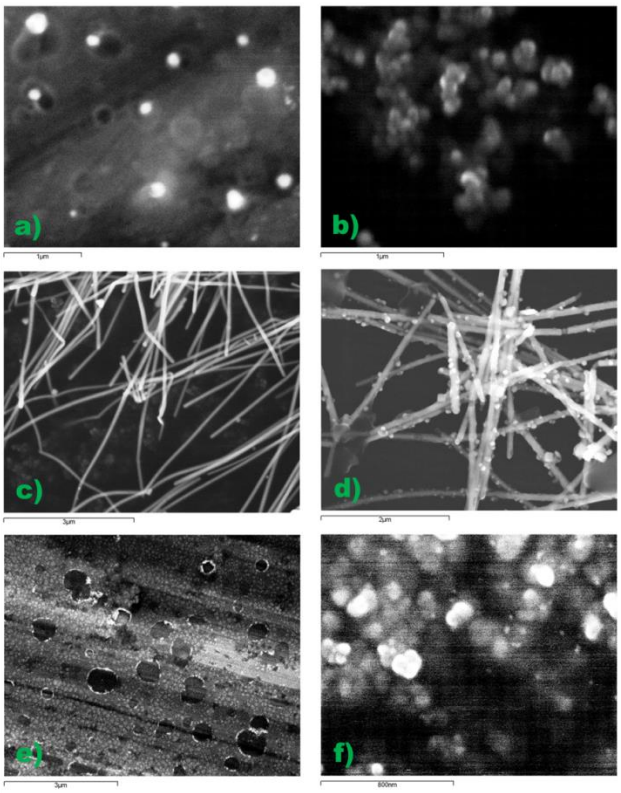

Figure 4.7 *SEM micrograph of a) Ag-nanospheres-NF, b) Ag-nanowires-NF, c) Ag-nanoplates-NF, d) Ag-nanospheres-INF, e) Ag-nanowires-INF and f) Ag-nanoplates-INF*

The sample of colloidal suspension of silver NPs was used to form a very thin layered film on the surface of the SEM sample holder stud. For silver nanospheres when it dispersed in water it is found that they show very good dispersion (Figure 4.7 a)) while in case of ionic liquid silver nanospheres are embedded in ionic liquid matrix as observed from (Figure 4.7 b)). The nanowires again show the dispersion in an ionic liquid medium a thick layer of ionic liquid over the surface of silver nanowires clearly observed from Figure 4.7 d). The SEM micrograph of silver nanoplates in water and ionic liquid are shown in Figures 4.7 e) and Figure 4.7 f). After dispersion of silver nanoplates in water, it is found that they are very well dispersed in water and their morphology remain the same. However in SEM micrograph of silver nanoplates in IL did not resolve very well as observed from Figure 4.7 f). In order to study the morphologies of silver nanoparticles in water and IL in more details, trasmission electron microscopy characterization was also performed.

Transmission electron microscopy analysis

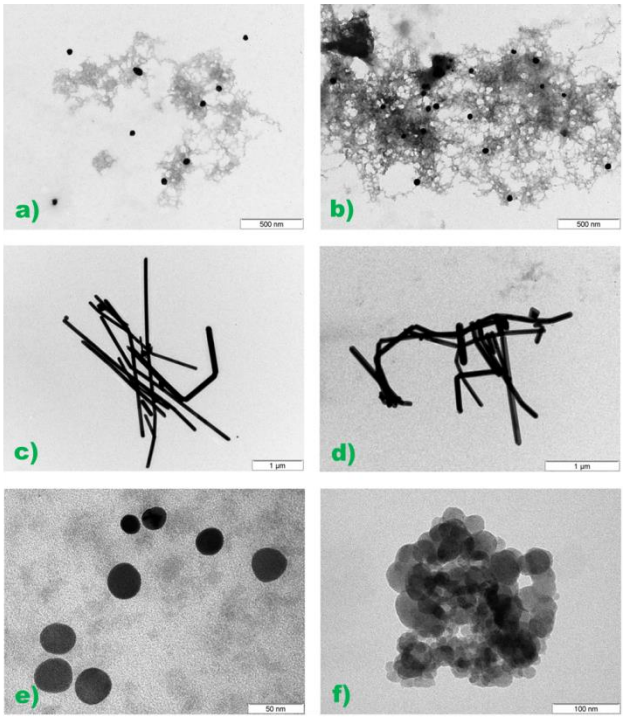

Figure 4.8 *TEM micrograph of a) Ag-nanospheres-NF, b) Ag-nanowires-NF, c) Ag-nanoplates-NF, d) Ag-nanospheres-INF, e) Ag-nanowires-INF and f) Ag-nanoplates-INF*

For TEM analysis, one drop of silver NF diluted in 3 mL of millipore water and silver INF solution diluted in 3 mL of acetone was dropcasted on a carbon coated copper grid. The sample loaded TEM grids were dried at ambient temperature conditions for 24 hrs and futher utilized for TEM analysis. For Ag nanopheres in water and choline [NTf2] ionic liquid (Figure 4.8 a) and b)) the silver nanospheres particles are well dispersed in both the solvents. Only in case of silver nanospheres in IL, the ionc liquid matrix is observed as shown in Figure 7 b). For Ag-nanowires-NF, a good dispersion of nanowires in a water was observed. While TEM micrographs of Ag-nanowires-INF as shown in Figure 4.8 d) found to have similar morphology in water and in IL phase. Ag-nanoplates-NF shows very good dispersion of nanoplates but sizes of nanoplates were found to vary in the range of 30 nm-50 nm. This may be the effect of ultrasonication used for dispersing the nanoparticles in a solvents. While in case of Ag-nanoplates-INF particles are agglomerated which is clearly observed in Figure 4.8 f). This

agglomeration results into more red shift of Ag-nanoplates-INF in UV-visible spectrum observed in Figure 4.4 b)

4.8 XPS AND EDAX STUDY OF SILVER NFs AND SILVER INFs

Electronic environment of the dispersions of silver nanoparticles with various morphologies in water and IL solvents were studied with X-ray photoelectron spectroscopy study. For analysis of samples fluid samples dropcast on sample mounting stud of XPS which forms thin film of NF and INF sample. After mounting sample immediately introduced into high vaccum sample chamber of XPS. The samples scanned for the Ag metal with in binding energies of 361-379 eV. XPS spectra of Ag 3d spectra for Ag nanofluids, base IL and Ag INFs are shown in Figure 4.9 below.

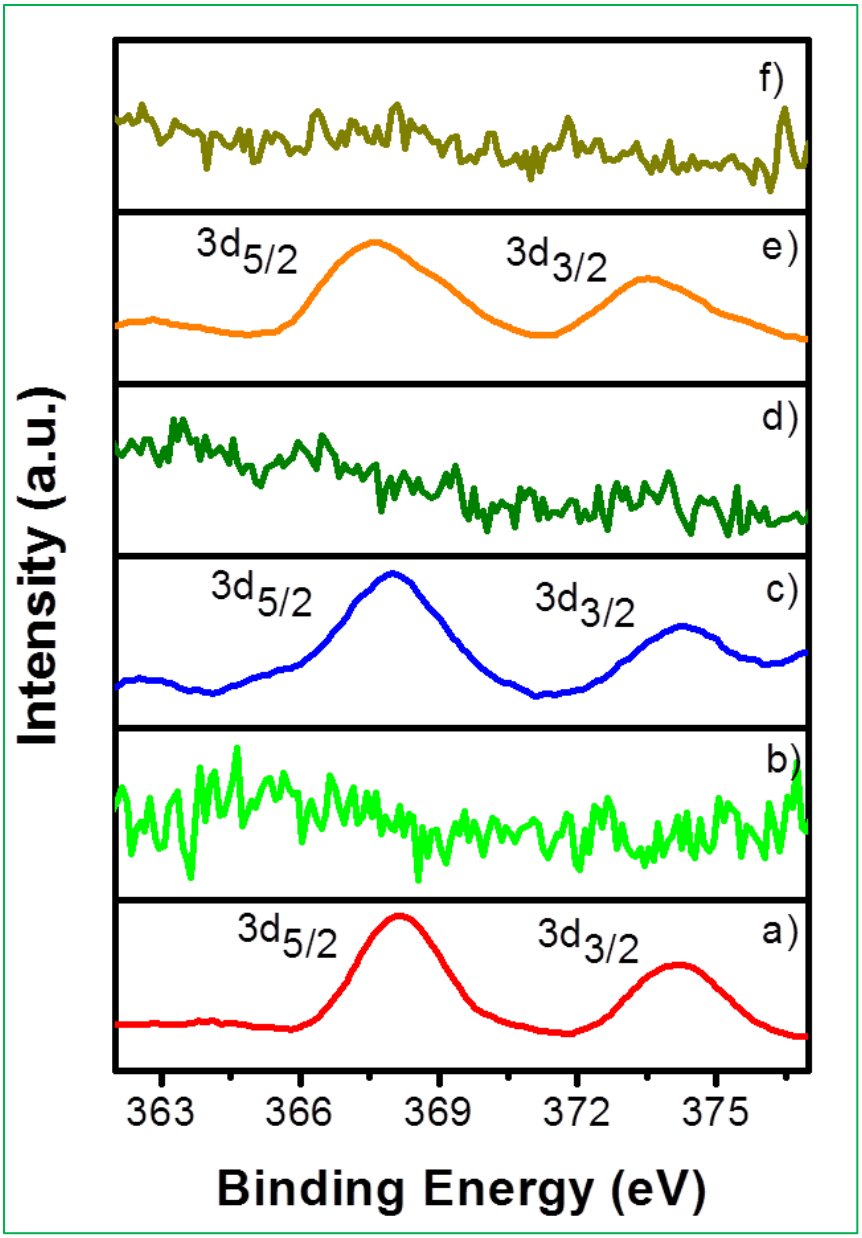

Figure 4.9 *XPS Ag 3d spectra of a) Ag-nanospheres-NF, b) Ag-nanowires-NF, c) Ag-nanoplates-NF, d) Ag-nanospheres-INF, e) Ag-nanowires-INF, f) Ag-nanoplates-INF*

Table 4.3 *Binding energy assignments for silver NFs*

Entry	Sample	Ag 3d $_{5/2}$	Ag 3d $_{3/2}$
1	Ag-nanospheres-NF	374.18 eV	368.18 eV
2	Ag-nanowires-NF	374.31 eV	368.17 eV
3	Ag-nanoplates-NF	373.56 eV	367.69 eV

It is observed that for silver NFs the Ag $3d_{5/2}$ and Ag $3d_{3/2}$ peaks could be attributed to Ag^{o}. In case of silver INFs the metal surface was covered with one layer thick IL. XPS is a surface sensitive technique in which because of IL covering the nanoparticles surface, it is not possible to reach the X-rays upto silver metal surface due to less penetration depth of X-rays. Hence, to confirm the presence of silver in INFs, we employed EDAX mapping. From EDAX mapping results, it is clearly observed that silver was present in INF samples (Figure 4.9) which ensured the successful transfer of silver nanoparticles from water phase to IL phase.

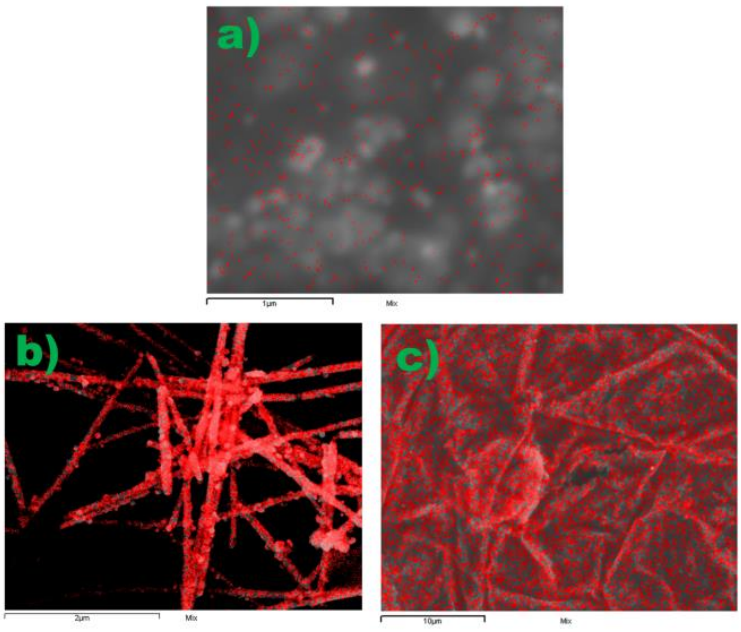

Figure 4.10 *EDAX mapping of a) Ag-nanospheres-INF, b) Ag-nanowires-INF, c) Ag-nanoplates-INF*

4.9 EFFECT OF MORPHOLOGIES OF NANOPARTICLES ON THERMAL PROPERTIES

Water impurity appears to have adverse effect on thermo physical properties of ILs and INFs [7]. Considering the adverse impact of water content on measurement of thermal properties of ILs and INFs, we checked the water content of [Choline][NTf2] IL and respective silver INFs samples before and after measurement of density, viscosity and thermal conductivity which gave more accuracy in measurement. All samples were vacuum dried for 2 days prior to measurement of their thermal properties. The water content of samples was measured with Karl Fisher equipment. The water contents of IL and INFs samples before and after measurements are given in Table 4.4.

Table 4.4 *Measurement of water content*

Entry	Sample Name	Measured property	Water content before measurement (ppm)	Water content after measurement (ppm)
1	[Choline][NTf2]	Density	50.95	746.8
2	Ag-nanospheres-INF		43.4	847.3
3	Ag-nanowires-INF		36.05	765.1
4	Ag-nanoplates-INF		65.65	743.9
5	[Choline][NTf2]	Viscosity	47.85	785.2
6	Ag-nanospheres-INF		41.9	801.3
7	Ag-nanowires-INF		30.9	799.1
8	Ag-nanoplates-INF		39.1	736.5
9	[Choline][NTf2]	Thermal conductivity	36.7	646.65
10	Ag-nanospheres-INF		40.7	888.4
11	Ag-nanowires-INF		30.12	793.1
12	Ag-nanoplates-INF		35.3	734.0

Effect on density

Density of freshly prepared silver NFs was measured in the range of 20 ^{o}C to 70 ^{o}C with Anton Paar DSA 5000 measuring unit and the results are shown in Figure 4.11 a) below.

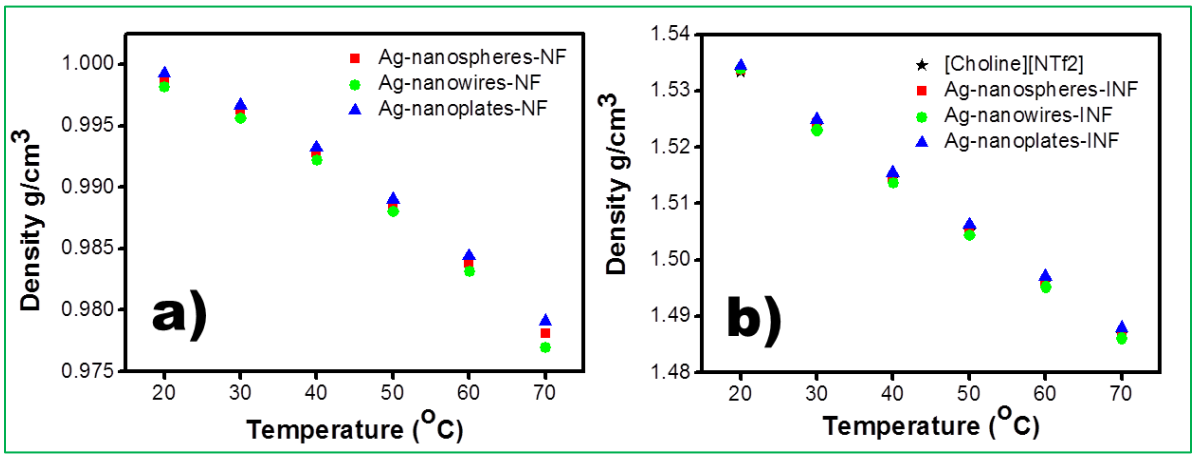

Figure 4.11 *Density measurement of a) silver NFs and b) silver INFs with various morphologies from 20 ^{o}C to 70 ^{o}C*

Each NF sample contain equal amount of silver nanoparticles which were dispersed in an equal amount of water as a solvent. The variation in morphology displays considerable variation in density of NFs (Figure 4.11a)). It was found that Ag-nanowires-NF which is one dimensional in nature shows less compactness between nanoparticle surfaces which results into decrease in density compared to the other two morphologies of silver nanoparticles. While silver nanoplates NFs which are two dimensional in nature show highest density among all three morphologies of silver nanoparticles. While three dimensional structures of silver Ag-nanospheres-NFs show density in between the Ag-nanowires-NF and Ag-nanoplates-NF. To study the effect of nanoparticles morphology on base IL, we first measured the density of dried [choline][NTf2] IL. Obtained results are in a good agreement with the reported values of density for [choline][NTf2] IL [11]. Silver NFs showed similar trend for the silver INFs.The trend of density observed for Ag nanoparticles density trend with respect to morphology as seen from in Figure 10 b) is found to be 1D < 3D < 2D structures of silver nanoparticles in [Choline] [NTf2] IL.

Effect on viscosity

Viscosity is one of the important properties to apply NFs and INFs for designing of instrument. Less viscous fluids can reduce the pumping cost of the instrument to flow the liquid through heat transfer based equipments. We measured the viscosities of silver NFs and silver INFs in temperature range of 20 ^{o}C to 70 ^{o}C.

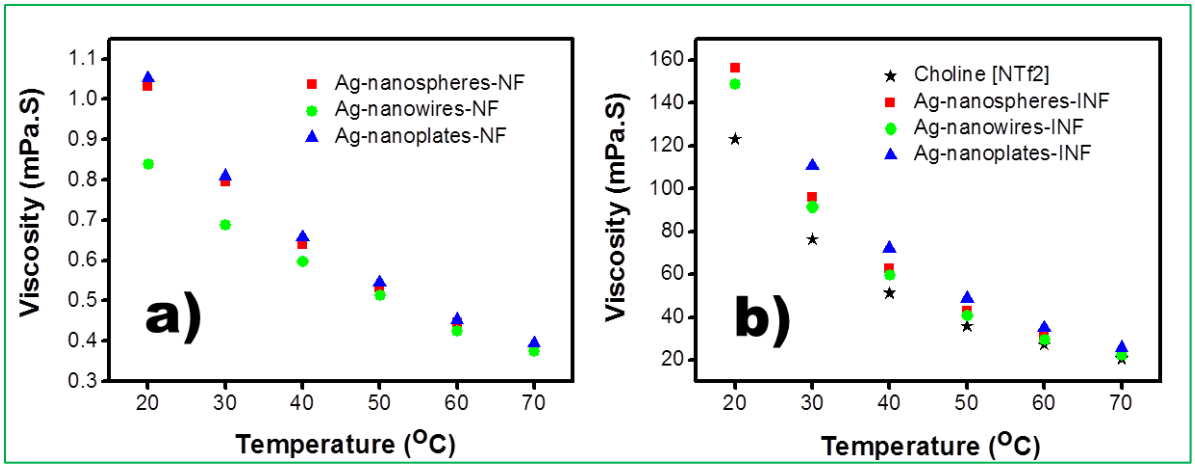

Figure 4.12 *Viscosity measurement of a) silver NFs and b) silver INFs with various morphologies from 20 ^{o}C to 70 ^{o}C*

We studied the effect of nanoparticle morphology on viscosity of base solvents used for dispersion of nanoparticles with different morphologies as shown in Figure 4.12 a) and b). For silver NFs the Ag-nanowires-NF shows very less viscosity compared to the Ag-nanospheres-NF, while Ag-nanoplates-NF shows highest viscosity. The obtained results demonstrated that 2D structures responsible for increase in viscosity of NFs. ILs and INFs are more viscous compared to NFs but the thermal stability is the considerable advantage of INFs as observe in Figure 5. We found that all three silver INFs displays increase in viscosity of base IL after addition of nanoparticles, as thess results are consistant with the addition of SiO_2 and TiO_2 nanoparticles in silicon oil as a base fluid reported by murshed et al [19]. Ag-nanospheres-INF and Ag-nanowires-INF shows similar viscosities with negligible difference. Among IL and INFs 2D silver nanoplates shows highest viscosity while at 20 ^{o}C it is too high that we not obtain data point at this temperature. The TEM image of Ag-nanoplates-INF also shows the agglomeration

of nanoparticles in base ionic liquids which resulted into increase in viscosity for Ag-nanoplates-INF as observe in Figure 4.8 f).

Effect on thermal conductivity

Thermal conductivity of silver NFs samples and silver INFs samples were measured in the temperature range of 20 ^{o}C to 60 ^{o}C. Compared to all NFs samples thermal conductivity of choline [NTf2] IL and silver-INFs was found to be almost double. As observed from Figure 4.12 a) and b), the Ag-nanowires-NF sample show the highest thermal conductivity compared to other morphologies of silver like Ag-nanospheres-NF and Ag-nanoplates-NF. Simillar trend was observed for silver-INFs. After dispersion of silver nanoparticles in base ionic liquids, for all the INFs the enhancement in thermal conductivity was observed.

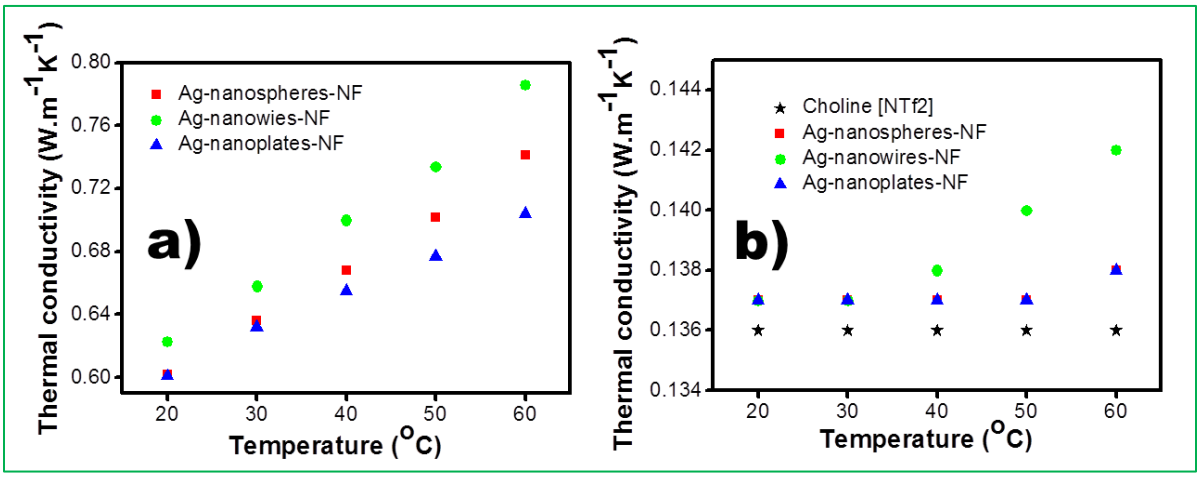

Figure 4.13 *Thermal conductivity measurement of a) silver NFs and b) silver INFs with various morphologies from 20 ^{o}C to 60 ^{o}C*

4.10 CONCLUSIONS

The NMR study shows that the –OH functional group present in cation has played crucial role in the dispersion of silver nanoparticles in ionic liquid medium. IL and Ag-INFs are found to be more thermal stable than that of silver NFs samples. Silver nanoplates 2D structures shows highest density and viscosity due to agglomeration of nanoplates during phase transformation of nanoparticles from water to IL phase. One dimentional silver nanowires has highest thermal conductivity compare to two dimentional silver nanoplates and three dimentional silver

nanospheres. Enhanced thermal conductivity, reduced viscosity of Ag-nanowires-INF make this fluid as a potential heat transfer fluid .

4.11 REFERENCES

[1] Moens L. and Blake D. M. Advanced Heat Transfer and Thermal Storage Fluids, Conference Paper January (2005) NREL/CP-510-37083

[2] Bhatt R. J.; Patel H. J.; Vashi O. G. Nano fluids: A New Generation Coolants, IJRMET 4 (2) (2014) 16-22

[3] Mintsa H. A.; Roy G.; Nguyen C. T.; Doucet D. New temperature dependent thermal conductivity data for water-based nanofluids Int J Therm Sci 48 (2009) 363-371

[4] Hwang Y.; Ahn Y.; Shin H.; Lee C.; Kim G.; Park H.; Lee J. Investigation on characteristics of thermal conductivity enhancement of nanofluids Curr Appl Phys 6 (6) (2006) 1068-1071

[5] Li D.; Hong B.; Fang W.; Guo Y.; Lin R preparation of well-dispersed silver nanoparticles for oil-based nanofluids Ind Eng Chem Res 49 (2010) 1697-1702

[6] Michael E.Van Valkenburg, Robert L. Vaughn, Margaret Williams, John S. Wilkes, Thermochemistry of ionic liquid heat-transfer fluids, Thermochimica Acta 425 (2005) 181–188

[7] França J. M. P; Reis F.; Vieira S. I. C.; Lourenço M. J. V.; Santos F. J. V.; Nieto de Castro C. A.; Pádua A. A. H.; Thermophysical properties of ionic liquid dicyanamide (DCA) nanosystems, J. Chem. Thermodynamics 79 (2014) 248–257

[8] Gathergood N., Garcia M. T., Scammells P. J., Biodegradable ionic liquids: Part I. Concept, preliminary targets and evaluation Green Chem. 6 (2004) 166 –175

[9] Warrier P.; Teja A. Effect of particle size on the thermal conductivity of nanofluids containing metallic nanoparticles, Nanoscale Research Letters 247 (2011) 1-6

[10] Bedia J.; Palomar J.; González-Miquel M.; Rodriguez F.; Rodríguez J. J. Screening ionic liquids as suitable ammonia absorbents on the basis of thermodynamic and kinetic analysis Sep Purif Technol 95 (2012) 188-195

[11] Costa A. J. L.; Soromenho M. R. C.; Shimizu K.; Marrucho I. M.; Esperanca J. M. S. S.; Lopes J. N. C. and Rebelo L. P. N. Density, Thermal Expansion and Viscosity of

Cholinium-Derived Ionic Liquids 13 (2012) 1902-1909

[12] Mie G. Contributions to the optics of turbid media, particularly of colloidal metal solutions. J Ann Phys 25 (1908) 377-445

[13] Renteria V.M.; Garcia-Macedo J. Modeling of optical absorption of silver prolate nanoparticles stabilized by Gemini surfactant Colloids Surf A 273 (2006) 1-3

[14] Preparation and Size Characterization of Silver Nanoparticles Produced byFemtosecond Laser Ablation in Water Chin Phys Lett 25 (12) (2008) 4463-

[15] Temperature-Driven Mixing-Demixing Behavior of Binary Mixtures of the Ionic Liquid Choline Bis(trifluoromethylsulfonyl)imide and Water J Phys Chem B 113 (2009) 1429-1437

[16] Giri N.; Natarajan R. K.; Gunasekaran S.; Shreemathi S. 13C NMR and FTIR spectroscopic study of blend behavior of PVP and nano silver particles Archives of Applied Science Research 3 (5) (2011) 624-630

[17] Manna S. C.; Mistria S.and Jana A. D. A rare supramolecular assembly involving ion pairs of coordination complexeswith a host–guest relationship: synthesis, crystal structure, photoluminescenceand thermal study Cryst Eng Comm 14 (2012) 7415–7422

[18] Cheng L. Nanofluids heat transfer technologies Recent patents on engineering 3 (2009) 1-7

[19] Murshed S. M. S.; Santos F. J. V.; and Nieto de Castro C. A. Investigations of Viscosity of Silicone Oil-Based Semiconductor Nanofluids J Nanofluids 2 (2013) 261-266

Chapter 5

Selective hydrogenation of levulinic acid to γ-valerolactone over ionic liquid assisted Ru/C catalyst

Chapter 5 deals with a novel combination of 5% Ru/C and acidic Brønsted ionic liquids developed for the selective hydrogenation of bioderived levulinic acid to γ–valerolactone. Effect of variation in acidic anion and its chain length on acidity of ionic liquid is investigated with Hammet acidity function. Further correlation of IL Brønsted acidity and catalytic activity study is discussed in this chapter. Effect of process parameters is investigated for optimization of the reaction conditions.

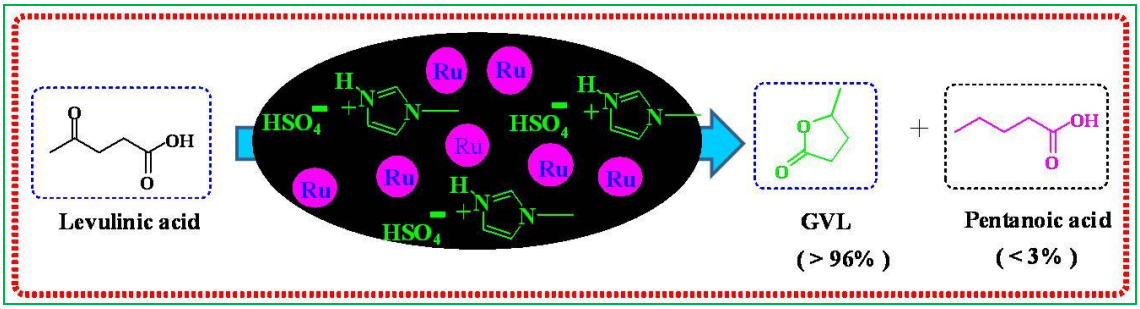

5.1 INTRODUCTION

Replacing petroleum feedstock with renewable resources such as lignocellulosic biomass is inevitable in near future for sustainable process development. Lignocellulosic biomass is composed of cellulose, hemicellulose and lignin [1-2] among which pentoses as well as hexoses derived from carbohydrate feedstock are processed to obtain important C5-C6 platform molecules such as levulinic acid (LA) and/or furfural [3-5]. Considerable research over the past few years has been focused on the catalytic conversion of biomass to LA by both batch and continuous technologies, which resulted into potential commercial production of LA. Further downstream processing of levulinic acid (LA) involves its selective hydrogenation to γ-valerolactone (GVL) which is a much more value-added having applications in the production of perfumes, food additives, as a solvent and precursor for other green solvents [5-6]. Additionally, GVL can be used as fuel additive to current fuels derived from petroleum in similar way as ethanol. For instance, Horvath et al. [4] have compared mixtures of 90 vol% gasoline with 10 vol% ethanol or 10 vol% GVL that shows similar octane numbers. It has combustion energy similar to ethanol (35 MJ L^{-1}) and a higher energy density which confers GVL potential as a liquid fuel.

Levulinic acid (LA) hydrogenation proceeds through the formation of an intermediate, 4-hydroxy LA which then undergoes cyclization to give GVL. LA has been hydrogenated to GVL under relatively mild conditions using homogeneous Ru complexes such as $RuCl_2(PPh_3)_3$,[7] $Ru(acac)_3$ ligated with PBu_3 or tris(3-sulfonatophenyl) phosphine (TPPTS) [8] and $RuCl_3$ combined with TPPTS [9] or PPh_3 [10] in excellent yields of 99%. Nevertheless, homogeneous catalysts obviously have the practical disadvantage of their separation and recyclability along with multistep ligand synthesis which discourage their commercial exploitation. Therefore, LA to GVL hydrogenation has been attempted on various supported noble metal catalysts such as Ru, Pd, Pt, Ni, Rh, Ir and Au. Among these metals, reasonable success was achieved over 5 wt% Ru/C catalyst with GVL yield as high as 97% at 423 K [11]. While in a continuous process in supercritical CO_2 over a Ru/SiO_2 catalyst, 99% yield of GVL could be obtained [12]. Selective hydrogenation of levulinic acid to GVL has been efficiently performed in 1, 4-dioxane with Ru, Pt and Pd supported on carbon among which, 5 wt% Ru/C gave complete conversion with 100%

selectivity to GVL [13]. The higher catalytic activity and selectivity of the Ru/C catalyst was attributed to the higher dispersion of nano-metallic Ru particles over carbon compared to Pt and Pd catalysts. However, few systems involved other metal catalysts in combination with acidic co-catalyst achieving better activity and catalyst stability for hydrogenation of LA with highest selectivity to GVL under mild reaction conditions [14-15]. Some of these include use of TiO_2 or ZrO_2, Sn, Amberlyst 15, niobium phosphate/oxide or use of supercritical CO_2 medium [14,16-18]. Recently, Nadgeri *et al*. reported the addition of solid acid catalysts to Ru/graphite enhanced the formation of GVL from methyl 4-hydroxyvalerate [19]. Our own efforts in this direction proved that non-noble metal catalyst in combination with ZrO_2 having acidic characteristic could afford quantitative hydrogenation of LA and its methyl ester with complete selectivity to GVL [20]. In another variations also where H-donors have been employed in place of external hydrogen for LA to GVL conversion, use of acidic catalyst was inevitable for the step of ring closure of the intermediate to form GVL [21-23]. In continuation of our work on LA hydrogenation, we found that in aqueous medium; imidazole based Brønsted acidic ionic liquid (IL) as a co-catalyst with 5% Ru/C catalyst gave > 90% LA conversion with 98% selectivity to GVL and 2% pentanoic acid (valeric acid). The later also has wide spread applications in flavors, perfumes and cosmetics.

In this work, we systematically varied the acidity of imidazole based IL by varying the anions which dramatically affected both LA conversion and GVL selectivity. The acidity of various ILs was determined using the Hammet method with UV-visible spectroscopy. In addition, effects of process parameters like, concentration of ILs and catalyst and H_2 pressure have been studied to achieve maximum LA conversion and GVL selectivity. IL and Ru/C are easily separable by means of simple filtration and can be reused up to several cycles with consistent results.

5.2 EXPERIMENTAL

5.2.1 Preparation of 5% Ru/C catalyst

Ru supported carbon catalyst was prepared by impregnation method. In a typical procedure, 2 g of the carbon support was suspended in aqueous medium containing calculated amount of

$RuCl_3.6H_2O$ for 5% loading under stirring for 1h. It was subsequently reduced using 5 mL (1M solution in water) of $NaBH_4$. Then suspension was filtered and dried at 110 ^oC for 12h.

5.2.2 Synthesis of imidazole based Brønsted acidic ILs

All four imidazole based Brønsted acidic ILs *viz*. 1-methyl imidazolium formate ([Hmim][HCOO]), 1-methyl imidazolium acetate ([Hmim][CH_3COO]), 1-methyl imidazolium propionate ([Hmim][CH_3CH_2COO]), 1-methyl imidazolium hydrogen sulfate ([Hmim][HSO_4]) were synthesized by mixing equimolar amounts of acid and base [24]. In a typical synthesis, dropwise addition of base to acid was carried out for complete neutralization in an ice bath in order to avoid heat generation. The reaction mixture was stirred for 6 h at room temperature. The water formed in the neutralization was removed by rotavapour at 80 ^oC for 6 h. The last traces of water and volatile impurities were removed from ILs under reduced pressure at 70 ^oC for 10 h [25].

5.2.3 Procedure for hydrogenation of levulinic acid and product analysis

In a typical hydrogenation reaction, levulinic acid (1.25 g), 5% Ru/C catalyst (0.1 g), IL (0.025 - 0.1 g) and solvent (23.75 mL), were mixed together in a 50 mL capacity autoclave (Parr Instruments Co., USA). The autoclave was heated at 100 ^oC under H_2 pressure of about 500 psi, the reaction were maintained under stirring at 1000 rpm for 5 h. Samples were withdrawn periodically with 1 h. interval and analyzed by GC (Shimadzu GC 2025) having an AB-FFAP (30m, 0.53 mm Id, 1um) column coupled with a FID detector.

5.2.4 Catalyst recycling

To test the recyclability, the catalyst combination was reused for four subsequent runs. After each experiment, the catalyst combination was separated from the mixture by simple filtration and the residue containing Ru/C was dried in oven at 120 ^oC for 2 h prior to reuse and mother liquor was extracted with ethyl acetate (25mL x 2). The aqueous layer separated was concentrated on a rotavapor at 80 ^oC for 2 h to remove water and was then used for the next reaction. The reaction condition for each cycle was identical, as follows: levulinic acid (1.25 g), 5% Ru/C catalyst (0.1 g), [Hmim][HSO_4] (0.1 g) and H_2O (23.75 mL), were mixed together in a 50 mL capacity autoclave (Parr Instruments Co., USA). The autoclave was heated at 100 ^oC

under H_2 pressure of about 500 psi, the reaction was maintained under stirring at 1000 rpm for 5 h.

5.3 RESULTS AND DISCUSSION

Selectivity to GVL could be improved by the stronger acidity of ILs which protonates the ketonic functional group of LA making it facile for ring closing by intramolecular esterification. The subsequent dehydration leads to the formation of α- angelica lactone which on hydrogenation forms GVL. If hydrogenation function dominates, it hydrogenate ketonic group to form unstable intermediate 4- hydroxy pentanoic acid which converted into GVL by ring closing via intramolecular esterification and eliminate water molecule. 4-hydroxy pentanoic acid furthermore converted to pentanoic acid via dehydration to olefinic acid (3-pentenoic acid) in acidic medium and subsequent hydrogenation (Scheme 5.1).

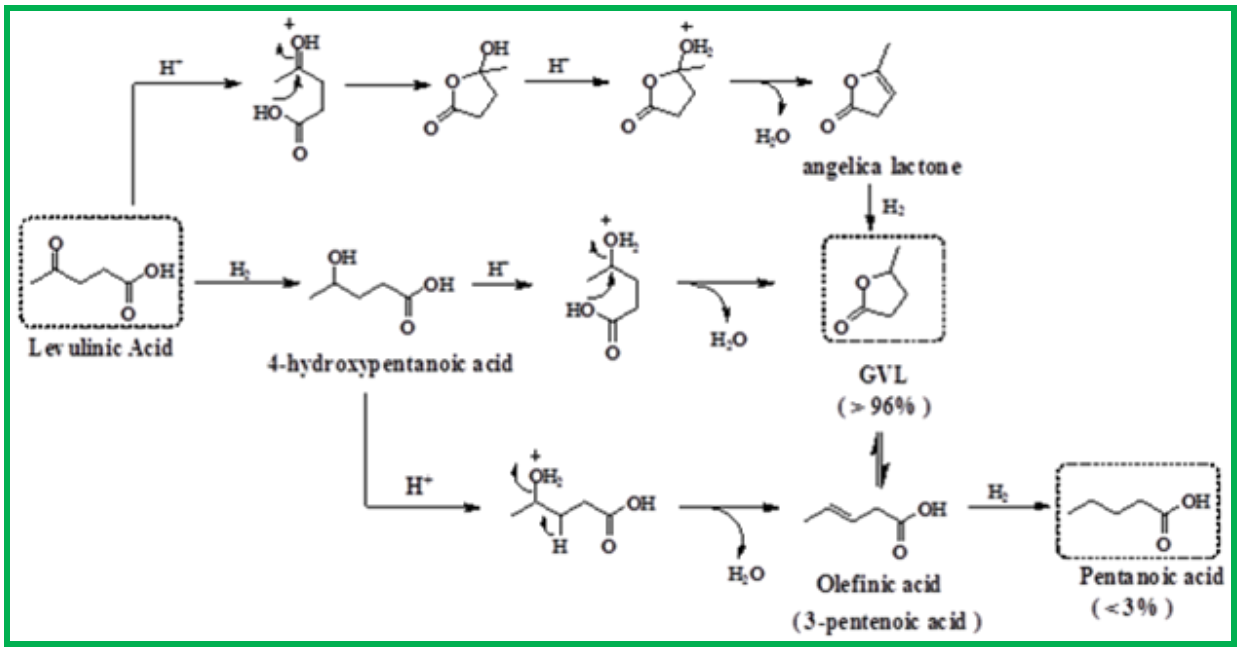

Scheme 5.1 *Reaction pathways to GVL and Pentanoic acid (Valeric acid)*

5.3.1 Activity measurement

LA hydrogenation reaction in absence of IL gave 99% conversion but selectivity to GVL was only 62% and remaining 38% was the intermediate, 4-hydroxy pentanoic acid (entry 1, Table

5.1). Thus, the role of IL was crucial in achieving selective formation of GVL in LA hydrogenation. In order to understand the role of acid sites in the LA hydrogenation several Brønsted acidic ILs (Table 5.1, entries 2-6). [Hmim][HSO_4], [Hmim][CH_3CH_2COO], [Hmim][CH_3COO] and [Hmim][HCOO] ILs were tested along with 5% Ru/C. To understand the role of only [Hmim][HSO_4] IL as a catalyst a control experiment was perfomed with only IL without 5% Ru/C catalyst (entry 7, Table 5.1). The results of this run showed that conversion of LA was very poor 26% while selectivity to GVL was 64.23% which was much less than that for the combination of 5% Ru/C and [Hmim][HSO_4] IL catalyst (entry 5, Table 5.1). While selectivity to PA marginally increased upto 22% but the selectivity to other products increased to 13.24% .

***Table 5.1**. IL Screening results for hydrogenation of LA*

Entry	IL	Hammet Acidity (Ho)	Conversion (%)	(%) Selectivity GVL	PA	Other
1	Without IL	-----	99.92	61.93	0.05	38.00
2	[Hmim][HCOO]	-0.036	19.38	22.28	55.57	22.14
3	[Hmim][CH_3COO]	-0.17	82.68	86.21	7.46	6.32
4	[Hmim]][CH_3CH_2COO]	-0.224	74.69	86.25	8.01	5.72
5	[Hmim][HSO_4]	-0.708	89.84	96.90	2.18	0.90
6	[Hmim][HSO_4]*	-0.708	86.57	92.52	5.73	1.74
7	Without 5% Ru/C**	-0.708	26.77	64.23	22.51	13.24

***Reaction conditions:** levulinic acid, 1.25 g; 5% Ru/C, 0.2 g ; [Hmim][HSO_4],0.075 g ; H_2O, 23.75 mL; H_2 pressure, 500 psi; temperature, 100 ^oC, *200 ^oC; reaction time, 5 h.,** Only IL [Hmim][HSO_4]*

Among all four ILs studied in this work, [Hmim][HSO_4] showed the best performance in terms of 90% LA conversion and 97% selectivity to GVL (entry 5, Table 5.1) at 100 ^oC. However, as the temperature increased to 200 ^oC for the same IL, both LA conversion and GVL selectivity marginally decreased to 86% and 92%, respectively. For [Hmim][HCOO] conversion dropped down to 20% but surprisingly selectivity to PA enhanced to 55% at the cost of GVL (22%;

entry 2, Table 5.1). Chain length increment in anionic counterpart of ILs influenced their acidity and substantially improved conversion of LA upto 83% and selectivity of GVL upto 86%. [Hmim][CH_3CH_2COO] and [Hmim][CH_3COO] ILs showed almost the same acid strength and GVL selectivity (entries 2, 3; Table 5.1). In order to further enhance the acidity of IL, the anion contrepart was changed to HSO_4 and the resulting IL, [Hmim][HSO_4] gave the highest activity of ~ 90% LA conversion and maximum selectivity of 97% to GVL.

The catalytic activity observed for various ILs was found to be consistent with their Brønsted acidity which was determined in terms of Hammet acidity function as given below [26].

$$Ho = pK\,(I)\,aq + \log([I]/[IH^+]) \quad \text{(5.1)}$$

Where, pK (I) aq is the pKa value of the indicator which is (0.99), $[IH^+]$ is the protonated form of indicators, [I] is the molar concentration of unprotonated form of indicator, $[IH^+]$ is molar concentration of protonated form of indicator. UV-Vis spectra of both unprotonated and protonated forms of indicator showed a specific absorption at 360 nm in ethanol however, the intensity increases for the protonated form. The measured values of absorbance were used to determine $[I]/[IH^+]$ ratio from which value of Ho was calculated for all four ILs. As shown in Table 1, acidity trend of ILs was in the following order, [Hmim][HSO_4] > [Hmim]][CH_3CH_2COO] > [Hmim][CH_3COO] > [Hmim][HCOO] which was also consistent with their catalytic activity.

5.3.2 Characterization of ILs

Thermal stability of the prepared Brønsted acidic ILs was studied by thermal gravimetric analysis over a temperature range from of 30 ^oC – 500 ^oC (Figure 5.1). This thermo gravimetric analysis of ionic liquids conducted in N_2 atmosphere with an heating rate 5 ^oC/min. The onset of thermal decomposition varied with different ILs such that for [Hmim][HCOO] decomposition started at 98 ^oC, [Hmim][CH_3COO] at 80 ^oC, [Hmim][CH_3CH_2COO] at 82 ^oC and [Hmim][HSO_4] at 230 ^oC, respectively. Total degradation temperatures also varied for all the ILs as follows: [Hmim][HCOO] at 172 ^oC, [Hmim][CH_3COO] at 154 ^oC, [Hmim][CH_3CH_2COO] at 153 ^oC, while [Hmim][HSO_4] at 363 ^oC. It was observed that increased chain length reduced the thermal stability of IL. [HSO_4] anion based IL showed the

highest thermal stability. The first weight loss occured up to 11%, 4%, 4%, and 4% for formate, acetate, propionate and hydrogen sulphate anions, respectively which was because of evaporation of water absorbed at the time of sample mounting before the measurement. [Hmim][HSO_4] IL that showed the highest activity and selectivity was also found to be the most stable IL.

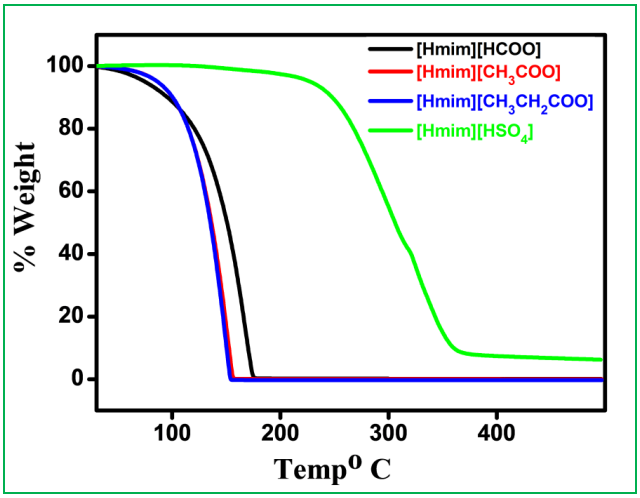

Figure 5.1 *Thermo gravimetric analysis of ILs*

The structural elucidation of the prepared ILs was done by ^{1}H and C^{13} NMR. ^{1}H and C^{13} NMR spectra of the prepared ILs are shown in Figure 5.2 and 5.3. NMR spectroscopic data is given as follows:

N-Methyl imidazolium formate. ^{1}H NMR ($CDCl_3$, 200 MHz, δ): 3.75 (m, 3H, N-CH_3), 6.96 (t, 1H, CH, *J*=6.19 Hz), 7.10 (t, 1H, CH, *J*=6.19 Hz), 7.75 (t, 1H, CH), 8.37 (m,1H, HCOO), 11.83 (t, 1H, NH), (Figure 5.2 a)). ^{13}C NMR (δ): 33.58, 120.48, 125.86, 136.56, 165.39, (Figure 5.3 a)).

N-Methyl imidazolium acetate. ^{1}H NMR ($CDCl_3$, 200 MHz,δ): 2.06 (t, 3H, CH_3COO), 3.71 (m, 3H, N-CH_3), 6.9 (t, 1H, CH, *J*=8.97Hz), 7.09 (t, 1H, CH, J=8.97Hz), 7.67 (t, 1H, CH), 13.52 (t, 1H, NH), (Figure 5.2 b)). ^{13}C NMR (δ): 21.23, 33.27, 119.94, 126.96, 137.00, 174.66, (Figure 5.3 b)).

N-Methyl imidazolium propionate. ^{1}H NMR ($CDCl_3$, 200 MHz,δ): 1.15 (t, 3H, CH_3CH_2COO), 2.37 (q, 2H, CH_3CH_2COO), 3.70 (s, 3H, N-CH_3), 6.89 (t, 1H, CH), 7.08 (t, 1H,CH), 7.64 (s, 1H,

CH) 13.59 (s, 1H, NH), (Figure 5.2 c)). ^{13}C NMR (δ): 9.36, 28.07, 33.68, 120.31, 127.70, 137.53, 178.28, (Figure 5.3 c)).

N-Methyl imidazolium hydrogen sulfate: ^{1}H NMR ($CDCl_3$, 200 MHz, δ): 3.77 (s, 3H, N-CH_3), 7.19 (s, 1H, CH), 7.24 (s, 1H, CH), 8.28 (s, 1H, CH), 11.15 (s, 1H, NH), (Figure 5.2 d)). ^{13}C NMR (δ):134.72, 123.24, 119.84, 35.87, (Figure 5.3 d)).

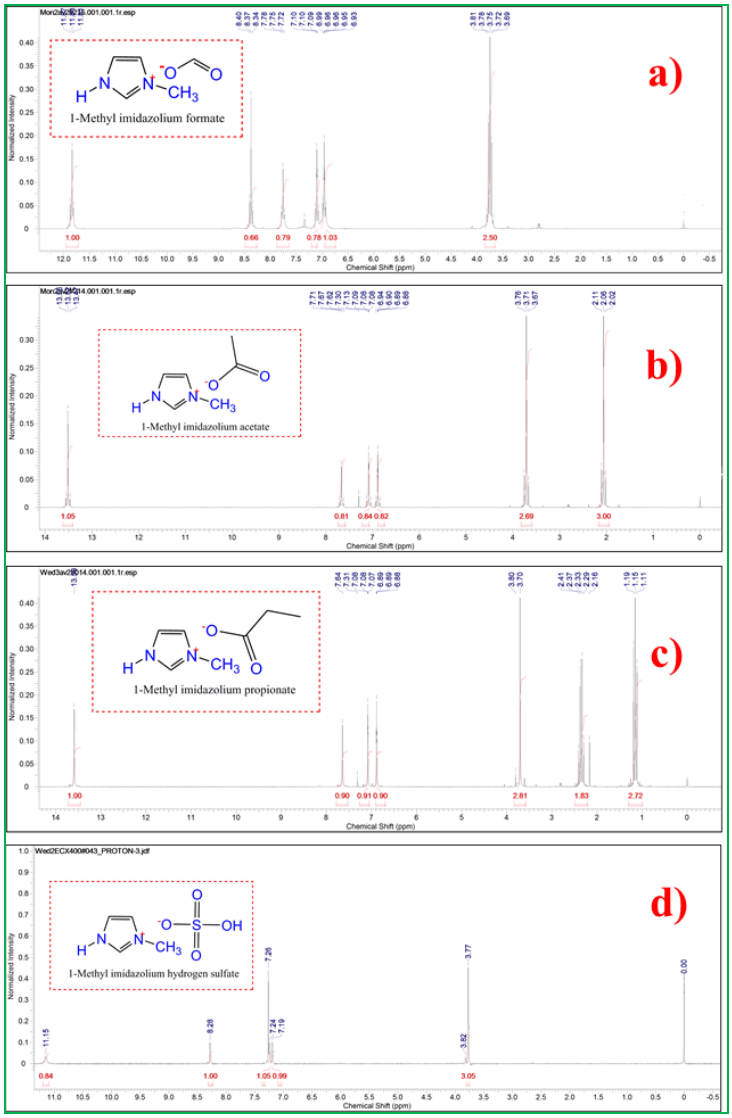

Figure 5.2 *^{1}H NMR of a) 1-Methyl imidazolium formate b) 1-Methyl imidazolium acetate, c) 1-Methyl imidazolium propionate, d) 1-Methyl imidazolium hydrogen sulfate*

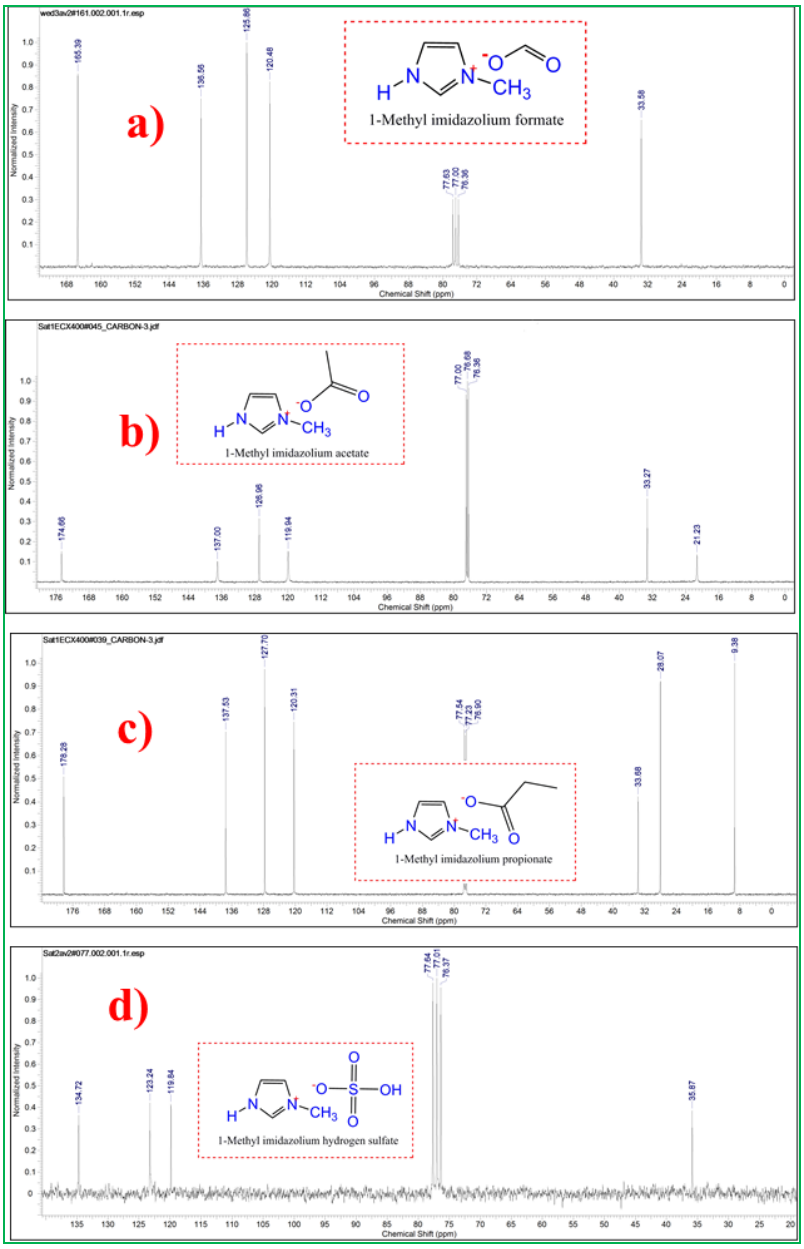

Figure 5.3 *^{13}C NMR of a) 1-Methyl imidazolium formate b) 1-Methyl imidazolium acetate, c) 1-Methyl imidazolium propionate, d) 1-Methyl imidazolium hydrogen sulfate*

5.3.3 Catalyst characterization

The hydrogenation catalyst, 5% Ru/C was prepared in our laboratory hence, its characterization was also carried to study the extent of metallic phase formation and the particle size. XRD pattern of as prepared 5% Ru/C catalyst showed an average crystallite size of Ru to be ~ 2 nm (Figure 5.4). Two peaks at $2\theta = 24.95^{o}$ and at $2\theta = 72.6^{o}$ represented the (4 0 0), (10 4 2) planes, respectively of carbon support with *fcc* structure (JCPDS File No. 82-0505). A reflection at $2\theta = 44^{o}$ represented (1 0 1) plane from hexagonal primitive structure of metallic ruthenium (JCPDS File No. 06-0663) confirming the complete reduction of ruthenium precursor to its metallic form.

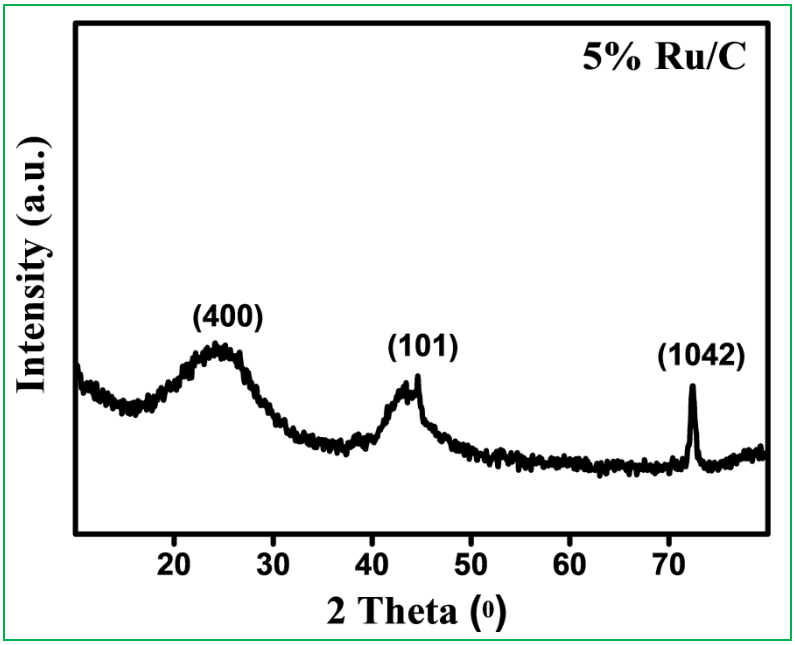

Figure 5.4 *XRD pattern for 5% Ru/C Catalyst*

HR-TEM of 5% Ru/C shows that Ru nanoparticles were spherical in shape with a particle size of 1.7-4.2 nm (Figure 5.5). Inset particle size histogram in Figure 5.5 shows that Ru nanoparticles were very well dispersed over the surface of carbon.

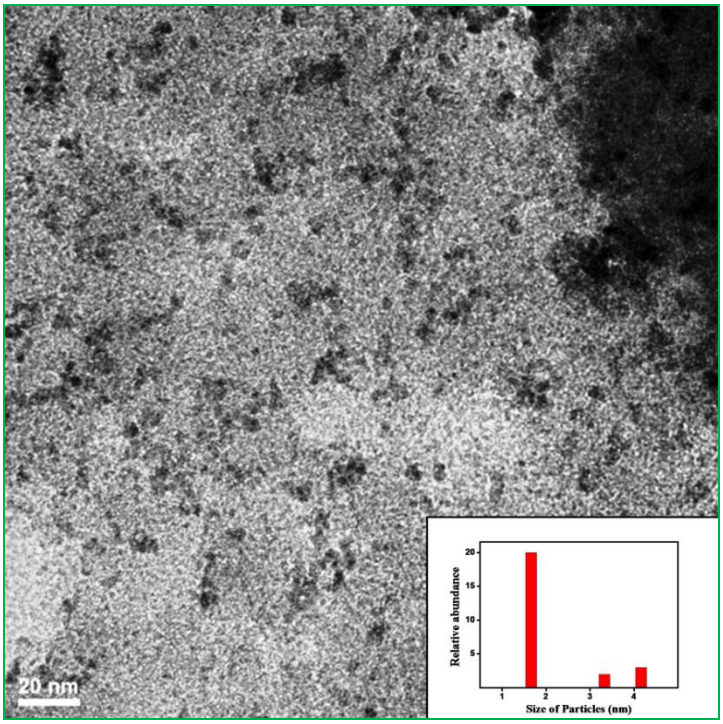

Figure 5.5 *HR-TEM micrograph and histogram of 5% Ru/C catalyst*

Elemental composition of as prepared catalyst characterized with the Energy Dispersive X-ray Spectroscopy (EDS) technique. Chemical composition of 5% Ru/C catalyst presented in Figure 5.6 shows peaks for carbon, ruthenium and copper. Copper peak was obtained from copper grid used to mount sample of catalyst.

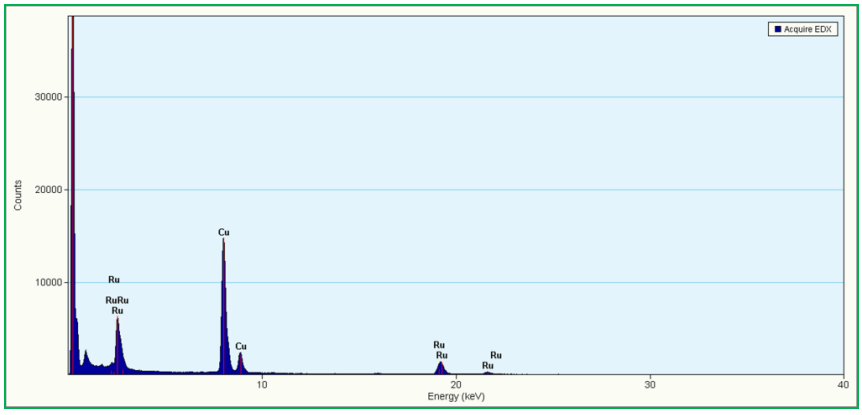

Figure 5.6 *EDS spectrum of 5% Ru/C catalyst*

5.4 PARAMETERS EFFECT STUDY

5.4.1 Effect of time

To achieve the maximum conversion of levulinic acid and GVL selectivity effect of reaction time on LA conversion and selectivity to hydrogenation products of LA was studied in water as a solvent. Within first h of the reaction, LA conversion observed was 73% with ~ 95% selectivity to GVL both of which increased to 89.84% and 96.90%, respectively, as shown in Figure 5.7. While the selectivity to PA decrease from 3.17% to 2.18% with increase in reaction time to 5h. Formation of other products also decreased from 2.23% to 0.90% with increased reaction time.

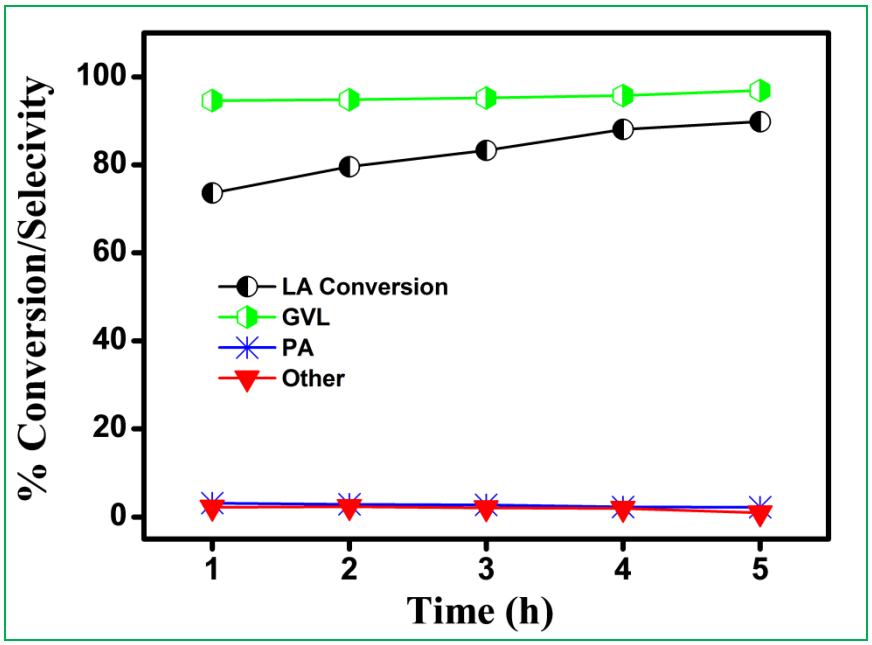

Figure 5.7 *Conversion and selectivity vs. time profile for LA hydrogenation*

Reaction conditions: *levulinic acid, 1.25 g; catalyst, 5% Ru/C, 0.2 g; ionic liquid, [Hmim][HSO$_4$], 0.1 g; solvent, H_2O, 23.75mL; H_2 pressure, 500 psi; temperature, 100 ^oC; reaction time, 1-5h.*

5.4.2 Effect of IL concentration

Since [Hmim][HSO_4] IL was found to be the best among others, effect of its concentration on conversion and selectivity results is presented in Figure 5.8. Dependence of LA conversion and GVL selectivity was studied by varying the concentration of [Hmim][HSO_4] in the range of 0.025g to 0.1g at 100^oC with H_2 pressure of 500 psi. LA conversion decreased from 99.9 to 89.84 % with increase in IL concentration from 0.025g to 0.1g. Selectivity to GVL marginally decreased from 98.34 to 96.9% with simultaneous increase in selectivity to PA (from 0.03 to 2.18%) with increase in concentration of IL. Increase IL concentration increased the acidic sites available for reaction which resulted in increase in PA selectivity. At the same time, selectivity to other byproducts decreased substantially from 1.54 to 0.9%.

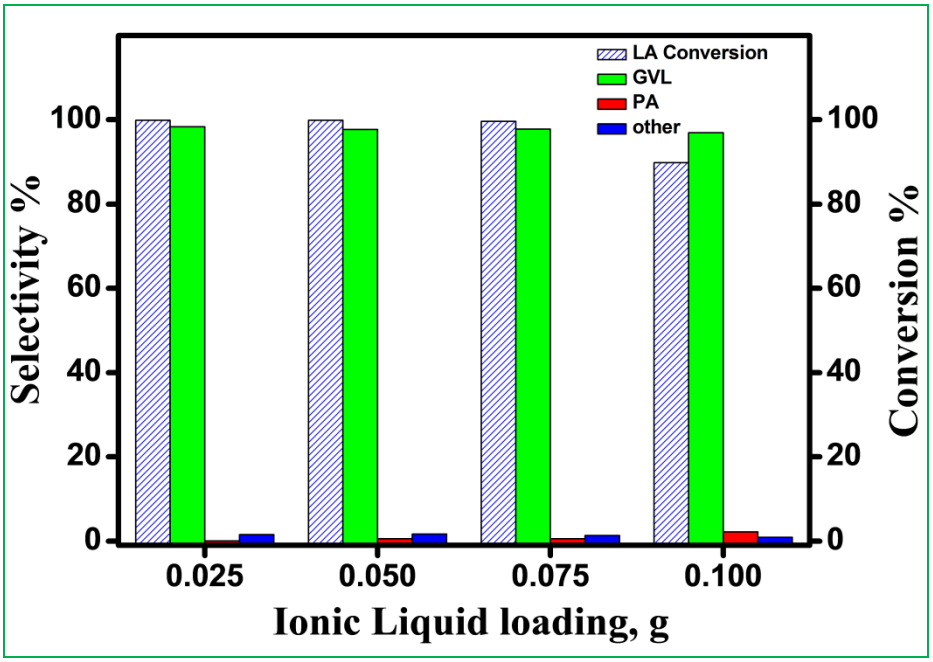

Figure 5.8 *Effect of IL concentration on hydrogenation of LA*

Reaction conditions: *levulinic acid, 1.25 g; catalyst, 5% Ru/C, 0.2 g; ionic liquid, [Hmim][HSO_4], 0.025-0.1 g;, solvent, H_2O, 23.75mL; H_2 pressure, 500 psi; temperature, 100 ^oC; reaction time 5 h.*

5.4.3 Effect of catalyst concentration

The effect of 5% Ru/C catalyst concentration on the conversion of LA and GVL selectivity was studied in the range of 0.05 to 0.2g at 100 ^{o}C (Figure 5.9). It was found that conversion of LA decreased from 99.8 to 89.84% with increase in catalyst concentration from 0.05 to 0.1g while, the conversion again enhanced from 89.84 to 99.52% with further increase in catalyst concentration from 0.1 to 0.2g. Selectivity to GVL increased marginally from 96.37 to 97.24% with an increase in catalyst concentration. Increasing the catalyst concentration from 0.05 to 0.1g caused an increase in PA selectivity from 1.18 to 2.18% while further increase in catalyst concentration decreased the PA selectivity up to 0.55% with increase in selectivity toother byproducts (up to 2.19%).

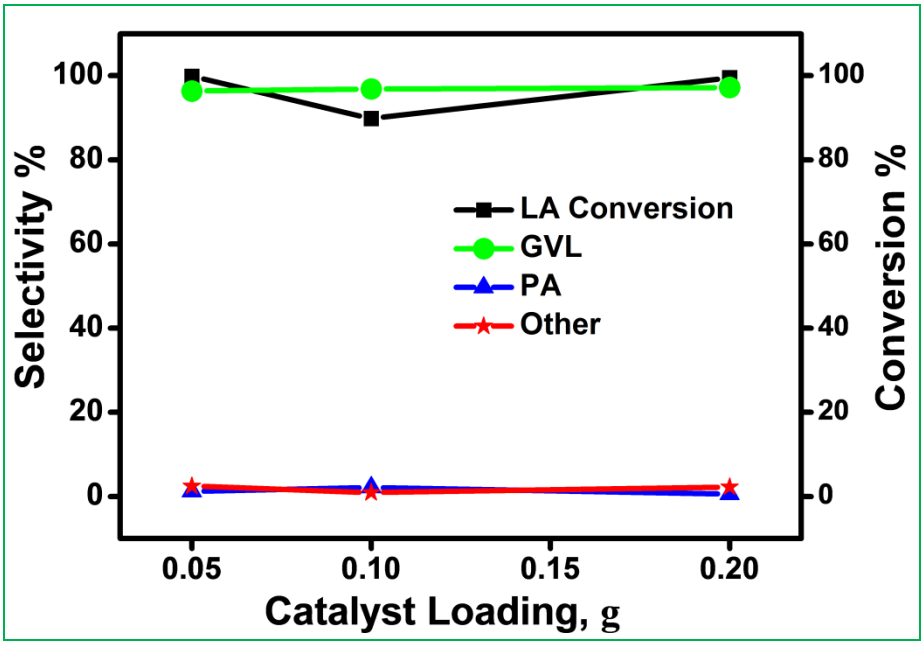

Figure 5.9 *Effect of catalyst concentration on hydrogenation of LA*

Reaction conditions: *levulinic acid, 1.25 g; catalyst, 5% Ru/C, 0.05-0.20 g; ionic liquid, [Hmim][HSO$_4$], 0.075 g; solvent, H_2O, 23.75 mL; H_2 pressure, 500 psi; temperature 100 ^{o}C, reaction time 5 h.*

5.4.4 Effect of H_2 pressure

Figure 5.10 shows the effect of hydrogen pressure on LA hydrogenation at 100 ^oC. The conversion of LA first decreased from 99 to 89 % for the initial increase in H_2 pressure from 250 psi to 500 psi beyond which it increased noticeably up to 100% at 750 psi of H_2 pressure. The selectivity to GVL hardly varied with increase in hydrogen pressure. Increase in activity with increase in hydrogen pressure beyond 500 psi was obviously due to higher dissolved concentration of hydrogen according to Henry's law [27]. The selectivity to PA increased first from 1.47 to 2.18% and then decreased to 0.91% with increase in hydrogen pressure from 250 to 750 psi. However, selectivity to other products first decreased from 2 to < 1% and then increased to > 1 %.

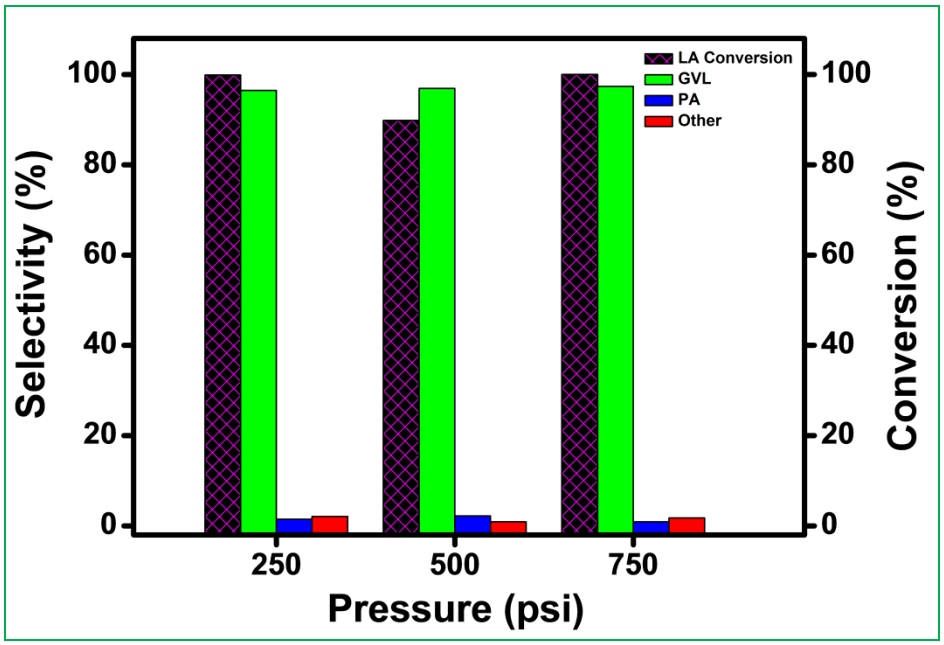

Figure 5.10 *Effect of hydrogen pressure on hydrogenation of LA*

Reaction conditions: *levulinic acid, 1.25 g; solvent H_2O, 23.75 ml; H_2 pressure, 250-750 psi; catalyst, 5% Ru/C, 0.1g; ionic liquid [Hmim][HSO_4], 0.1g; reaction time, 5 h; temperature, 100 ^oC.*

5.4.5 Effect of solvent

Figure 5.11 shows the effect of different solvents on hydrogenation of levulinic acid. In polar solvent like methanol, higher conversion of LA and higher selectivity to GVL were obtained. While in case of non-polar solvent like toluene both LA conversion and GVL selectivity were affected adversely due to formation of other products to the extent of > 21%. For methanol and water solvents, selectivity to other products was only 1.21% and 0.90 %, respectively. Methanol solvent gave 98% LA conversion while GVL selectivity was 97% compared to water and toluene solvents. In methanol solvent selectivity to PA was 1.62 % while selectivity to other products was 1.21%. In case of water as a solvent, selectivity to PA increased from to 2.18% while that to other product slightly decreased to 0.90 %. Considering the less selectivity to other products water was considered as more efficient solvent for LA hydrogenation than methanol.

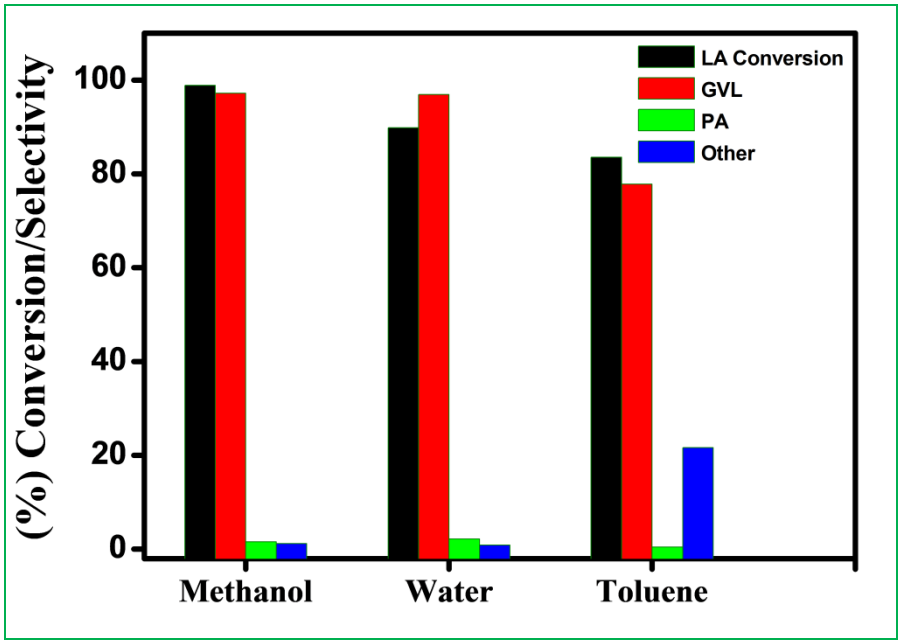

Figure 5.11 *Effect of solvent on hydrogenation of LA*

Reaction conditions: *levulinic acid, 1.25 g; solvent, 23.75 mL; H_2 pressure, 500 psi; catalyst, 5% Ru/C, 0.1g; ionic liquid, [Hmim][HSO_4], 0.1g; temperature 100 ^oC; reaction time, 5 h.*

5.5 CATALYST RECYCLE STUDY

In order to establish the stability of the catalyst, a series of recycle experiments were also conducted with 5% Ru/C and [Hmim][HSO_4] combination (Figure 5.12). Fresh catalytic combination showed 90% LA conversion and GVL selectivity of 97%. There was slight decrease in the conversion of LA from 90% to 86 % at the end of the 4th reuse. However LA conversion marginally decreased below 80% after the 4th cycle, but selectivity of GVL (97%) remained same. As the catalyst loading was 0.2 g, there could be considerable handling losses for the subsequent recycles which caused the decrease in activity after the 4th recycle experiment.

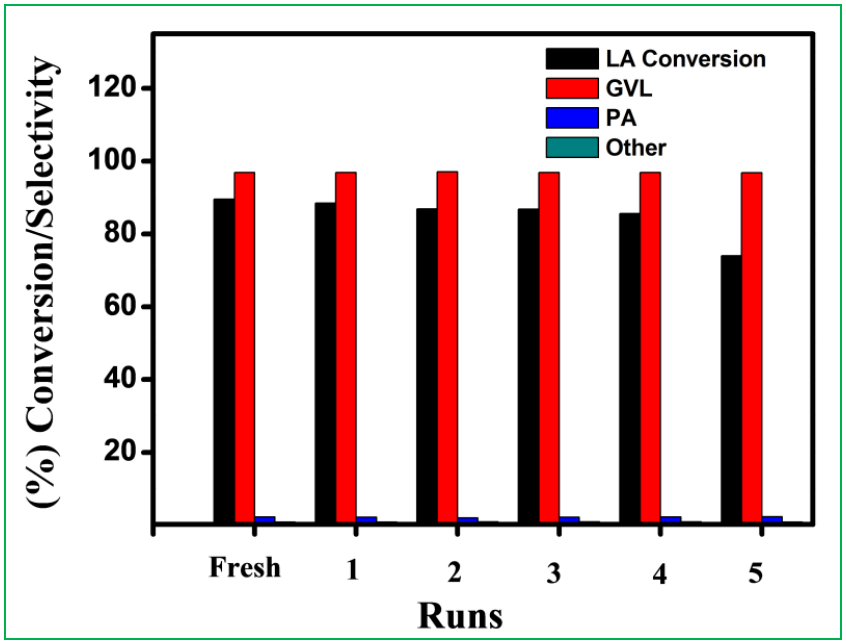

Figure 5.12 *Recycling experiments catalyzed by 5% Ru/C and [Hmim][HSO_4]*

Reaction conditions: *levulinic acid, 1.25 g; catalyst, 5% Ru/C, 0.2 g; ionic liquid, [Hmim][HSO_4], 0.075 g; solvent, H_2O, 23.75mL; H_2 pressure, 500 psi; temperature 100 ^oC; reaction time 5 h.*

5.6 CONCLUSIONS

A combination of 5% Ru/C and [Hmim][HSO_4] was found to be highly efficient for the selective hydrogenation of LA to GVL in a aqueous medium. Variation in anion and the chain length influenced the acidities of ILs as shown by Hammet acidity function. Increase in IL acidity resulted in the enhancement in both LA conversion and GVL selectivity. The optimum concentrations of both IL and Ru/C catalyst were determined to give 90% LA conversion with > 96% selectivity to GVL. Combination of 5% Ru/C and [Hmim][HSO_4] catalyst effectively used up to four recycles with same selectivity to GVL.

5.7 REFERENCES

[1] Climent M. J.; Corma A.; Iborra S. Converting carbohydrates to bulk chemicals and fine chemicals over heterogeneous catalysts Green Chem 13 (2011**)** 520-540

[2] Huber G. W.; Chheda J. N.; Barrett C. J.; Dumesic J. A. Production of Liquid Alkanes by Aqueous-Phase Processing of Biomass-Derived Carbohydrates Science 308 **(**2005) 1446-1450

[3] Bozell, J. J.; Petersen, G. R. Technology development for the production of biobased products from biorefinery carbohydrates—the US Department of Energy's "Top 10"revisited. Green Chem 12 (2010) 539-554

[4] Horvath I. T.; Mehdi H.; Fabos V.; Boda L.; Mika L. T. γ -Valerolactone - a sustainable liquid for energy and carbon-based chemicals Green Chem 10 (2008) 238-242

[5] Fegyverneki D.; Orha L.; Lang G.; Horvath I. T; Gamma-valerolactone-based solvents. Tetrahedron 66 (2010) 1078-1081

[6] Alonso D. M.; Wettstein S.G.; Dumesic J. A. Gamma-valerolactone, a sustainable platform molecule derived from lignocellulosic biomass Green Chem 15 (2013) 584-595

[7] Osakada K.; Ikariya T.; Yoshikawa S. Preparation and properties of hydride triphenyl phosphine ruthenium complex with 3-formyl (or acyl) propionate [RuH(OCOCHRCHRCOR')(PPh_3)$_3$] (R=H,CH_3,C_2H_5; R'=H,CH_3,C_6H_5) and with 2-formyl (or acyl) benzoate [RuH(o-$OCOC_6H_4$COR')(PPh_3)$_3$] (R=H, CH_3) J Organomet Chem 231 (1982) 79-90

[8] Mehdi H.; Fabos V.; Tuba R.; Bodor A.; Mika L.T.; Horvath I. T. Integration of homogeneous and heterogeneous catalytic process for a multistep conversion of biomass: From sucrose to levulinic acid, γ -Valerolactone 1,4-pentane diol, 2-Methyl tetrahydrofuran and alkanes Top Catal 48 (2008) 49-54

[9] Chalid M.; Broekhuis A. A.; Heeres H. J. Experimental and kinetic modeling studies on biphasic hydrogenation of levulinic acid to γ -Valerolactone using a homogeneous water – soluble Ru-(TPPS) catalyst J Mol Catal A Chem 341 (2011) 14-21

[10] Deng L.; Li J.; Lai D.; Fu Y.; Guo Q. Catalytic conversion of biomass-derived carbohydrates into γ -Valerolactone without using an external H_2 supply Angew Chem Int Ed 48 (2009) 6529-6532

[11] Manzer L. E. Catalytic synthesis of α-methylene-γ-valerolactone: a biomass-derived acrylic monomer Appl Catal A Gen 272 (2004) 249-256

[12] Yan Z.P.; Lin L.; Lu S. Synthesis of γ‑valerolactone by hydrogenation of biomass-derived levulinic acid over Ru/C catalyst Energy & Fuels 23 (2009) 3853-3858

[13] Upare P. P.; Lee J. M.; Hwang D.W.; Halligudi S. B.; Hwang Y. K.; Chang J . S. Selective hydrogenation of levulinic acid to γ -Valerolactone over carbon-supported noble metal catalysts. J Ind Eng Chem 17 (2011) 287-292

[14] Galletti A. M. R.; Antonetti C.; De Luise V.; Martinelli M. A. sustainable process for the production of γ-valerolactone by hydrogenation of biomass-derived levulinic acid Green Chem 14 (2012) 688-694

[15] Selva M, Gottardo M. and Perosa A. Upgrade of biomass-derived levulinic acid via Ru/C-catalyzed hydrogenation to γ‑valerolactone in aqueous−organic−ionic liquids multiphase systems ACS Sustainable Chem Eng 1 (2013) 180-189

[16] Lange J. P.; Price R.; Ayoub P. M.; Louis J.; Petrus L.; Clarke L.; Gosselink, H. Valeric biofuels: a platform of cellulosic transportation fuels Angew Chem Int Ed 49 (2010) 4479-4483

[17] Bourne R. A.; Stevens J. G.; Kie J.; Poliakoff M. Maximising opportunities in supercritical chemistry: the continuous conversion of levulinic acid to γ -Valerolactone in CO_2. Chem Commun (2007) 4632-4634

[18] Wettstein S. G .; Bond J. Q.; Alonso D. M.; Pham H.N.; Datye A. K.; Dumesic J. A. RuSn bimetallic catalysts for selective hydrogenation of levulinic acid to γ -Valerolactone Appl Catal B Environ 117 (2012) 321–329

[19] Nadgeri J. M.; Hiyoshi N.; Yamaguchi A.; Sato O.; Shirai M. Liquid phase hydrogenation of methyl levulinate over mixture of supported ruthenium catalyst and zeolite in water. Appl Catal A Gen 470 (2014) 215– 220

[20] Hengne A. M.; Rode C. V. Cu-ZrO_2 nanocomposite catalyst for selective hydrogenation of levulinic acid and its ester to γ-valerolactone Green Chem 14 (2012) 1064-1072

[21] Chia M.; Dumesic J. A. Liquid-phase catalytic transfer hydrogenation and cyclization of levulinic acid and its esters to γ -Valerolactone over metal oxide catalysts Chem Commun 47 (2011) 12233-12235

[22] Du X. L.; He L.; Zhao S.; Liu Y. M.; Cao Y.; He H. Y.; Fan K. N. Hydrogen-independent reductive transformation of carbohydrate biomass into γ -Valerolactone and pyrrolidone derivatives with supported gold catalyst Angew Chem Int Ed 50 (2011) 7815-7819

[23] Hengne A. M.; Malwadkar A. V.; Biradar N. S.; Rode C. V. Surface synergism of Ag-Ni/ZrO_2 nanocomposite for catalytic transfer hydrogenation of Bio-derived platform molecules RSC Adv 4 (2014) 9730-9736

[24] Fukumoto K.; Yoshizawa M.; Ohno H. Room temperature ionic liquids from 20 natural amino acids J Am Chem Soc 127 (2004) 2398-2399

[25] Shukla S. K.; Khupse N. D.; Kumar A. Do anions influence the polarity of protic ionic liquids? Phys Chem Chem Phys 14 (2012) 2754-2761

[26] Duan Z.; Gu Y.; Zhang J.; Zhu L.; Deng Y. Protic pyridinium ionic liquids: Synthesis, acidity determination and their performances for acid catalysis J Mol Catal A Chem 250 (2006) 163–168

[27] Yan Z-P.; Lin L. and Lu S. Synthesis of γ-valerolactone by hydrogenation of biomass-derived levulinic acid over Ru/C catalyst Energy Fuels 23 (2009) 3853-3858

Chapter 6

Conclusions and future recommendations

6.1 CONCLUSIONS

In this doctoral thesis, designing of imidazolium halide ionic liquids and trasition metal nanoparticles (of ruthenium and silver) containing ionanofluids was successfully carried out as novel fluids for heat transfer and catalysis applications. For this purpose, imidazolium cation based ILs were prepared with variation in anions such as chloride, bromide, iodide and tetrafluroborate. Thermal properties as well as density and viscosity of these fluids were investigated in detail. Main conclusions are:

- Ruthenium nanoparticles were prepared with a simple protocol without using any external stabilizing agent at room temperature and used for in-situ preparation of ionanofluids (INFs). The density and viscosity of Ru-INFs decreases with increase in mass of anions of the corresponding ILs. Thermal properties of these INFs were also found to be improved than those of base ILs.
- Silver (Ag) NPs with variable morphologies, of 1D, 2 D and 3 D directly procrred were also used for developing INFs. Silver nanoplates with 2D structure shows highest density and viscosity due to agglomeration of nanoplates during phase transformation of nanoparticles from water to IL phase. One dimentional silver nanowires has the highest thermal conductivity compared to two dimentional silver nanoplates and three dimentional silver nanospheres. Enhanced thermal conductivity, reduced viscosity of Ag-nanowires-INF make this fluid as a potential heat transfer.
- A combination of 5% Ru/C and IL, [Hmim][HSO_4] was found to be highly efficient for the selective hydrogenation of levulinic acid (LA) to γ-valerolactone (GVL) in an aqueous medium. Variation in anion and its chain length influenced the acidities of ILs as shown by Hammet acidity function. Increase in IL acidity resulted in the enhancement in both LA conversion and GVL selectivity. The optimum concentrations of both IL and Ru/C catalyst were determined to give 90% LA conversion with > 96% selectivity to

GVL. Combination of 5% Ru/C and [Hmim][HSO_4] catalyst effectively used up to four recycles with same selectivity to GVL.

6.2 FUTURE RECOMMENDATIONS

✓ Development of functionalized ILs and INFs with better thermal and flow properties, as heat transfer fluids and catalysts

✓ Development of scale up strategies of these ILs and INFS for higher scale testing for heat transfer applications.